Structural and mechanistic investigation of a proton-dependent lipid transporter involved in lipoteichoic acids biosynthesis

Inauguraldissertation

zur
Erlangung der Würde eines Doktors der Philosophie

vorgelegt der

Philosophisch-Naturwissenschaftlichen Fakultät

Der Universität Basel

von

Bing Zhang

Basel, 2020

Genehmigt von der Philosophisch-Naturwissenschaften Fakultät

auf Antrag von

Prof. Dr. Camilo Perez, Prof. Dr. Sebastian Hiller, Prof. Dr. Christine Ziegler

Basel, den 17.11.2020

Prof. Dr. Martin Spiess

Dekan

Acknowledgement

First of all, special thanks to my supervisor Camilo for offering me the opportunity to conduct this interesting project about structural and biochemical characterization on lipid transporter from a human pathogen, lighting up my Ph.D. adventure in this beautiful and lovely city Basel. The road of a new adventure is always full of unknowns, exciting peaks and horizons. To begin it, I was not only with enthusiasm but also anxiety. Thanks for your kindness and patience to guide me across the very beginning of the way. The whole exploring was impressive and will be one of the most beautiful memories of me. I not only gained a lot of expertise regarding the structural biology field but also was influenced by the spirit of being a real scientist. Furthermore, thanks for giving me the freedom to do the project at my pace and always helping me when I needed it, which served as good training that made me become an independent researcher. Due to the efforts we put together, I obtained many chances to share our findings with many colleagues, which cheered me a lot.

Thank Sebastian for being my second supervisor. Thanks for your nice suggestions regarding my project.

Thank our collaborators Prof. Jan Willem Veening and Dr. Xue Liu for the effort to make such a good story with us!

Thank our lab members who maintain a friendly environment for working together. I'm encouraged by all of you who always work hard and keep going forward. Thank Natalie and Daniel who helped me quickly get into life in Basel when I just arrived. Thank Elisabeth for the nice discussions about my project and the help in the experiments. Especially, thank you for the warm hugs when I occasionally felt down, which comforted me a lot. Thank Gonzalo for having many discussions about techniques and helping me with the usage of equipment. Thanks, Luzern, for being an atmosphere maker and cheering me up. Thank Arantza for your kindness to show me new experimental techniques. Thank Xiaochun for being a positive addition to my project, and I always felt happy to have many talks in Chinese after work. Special thanks to Firas for helping me with the improvement of my thesis.

I was impressed by many people I met during this three-year working at the biozentrum. Thank people from the IT service team and the Scicore team, Alexander, Ulrike, and Katarzyna from the proteomics core facility, Tim from the biophysics facility, Angie from the Ph.D. program, Gabi from the HR section, Susanna, Jacqueline, and Alexandra from the secretary section, who helped a lot to make my Ph.D. life go well. I was affected by the working attitude of Timm and Susan. I also obtained help from Roman, Raphael, Dominik, Florian, et al.

Thank Yusuke for having many talks with me, which comforted and encouraged me a lot. Thank Tamara for spending much of my leisure time together. Thank Daxin, Haoyue, Cheng, Chao, Guangyi, Zihe, Liang, Dongchun, Yating, Ed, Wuzhou and many other friends for spending a nice time together. Thank Tong and Yueer for many video talks and for always cheering me up. I also appreciate Chao Feng for helping me to solve many questions.

Whom I want to show special thank are my dear parents. Thank you for the unconditional trust, support and love. Thank you for being by my side just because I needed it. I will always love you and be proud of you!

In the end, thank myself for the effort I've ever put in. What I passed through makes who I am now. Know, speak to, and love myself.

Abstract

Staphylococcus aureus (*S.aureus*) is a successful opportunistic human pathogen, causing superficial infections such as skin and soft tissue infections as well as invasive fatal ones including endocarditis, pneumonia and septicemia with high mortality. It represents one of the growing public health concerns worldwide since the rapid spreading of multi-antibiotic resistant *S.aureus* strains has increased the failure of therapeutics, urgently calling for pathogenesis research and development of effective treatment strategies.

30% of the population carries *S.aureus* on the skin and mucous membranes where the pH is usually mild acidic (average 4 to 6). Managing survival under this environment is a critical step for *S.aureus* successful colonization, dissemination and infection. The cell wall, a multi-layered protective structure, plays a crucial role in maintaining *S.aureus* viability under hostile surroundings. Lipoteichoic acids (LTA) are one type of the main components of the *S.aureus* cell wall, composed of repeating glycerol phosphate units and a glycolipid anchor called diglucosyl-diacylglycerol (Glc_2-DAG) that fixes LTA polymers on the outer leaflet of the plasma membrane. Glc_2-DAG is synthesized in the cytoplasm and transferred across the plasma membrane by the integral membrane protein LtaA (lipoteichoic acid protein A). The deletion of LtaA in *S.aureus* led to the alteration of the LTA anchor from Glc_2-DAG to diacylglycerol (DAG) and attenuated virulence during animal infection.

LtaA belongs to transporters that mediate glycolipid translocation. This category is closely involved in the cell wall biosynthesis by transferring multiple precursors or molecules to satisfy the proper assembly of the cell wall. Bacteria harbor diverse glycolipid transporters, most of which are not well understood. LtaA was predicted to belong to the major facilitator superfamily (MFS), a large family of membrane proteins that are ubiquitously distributed in all kingdoms of life, transferring a broad range of substrates from sugars, peptides to ions and lipids across membranes. Research on MFS transporters involved in glycolipids transport is scarce, hindering the understanding of their flipping mechanisms.

In this study, we determined the structure of LtaA by X-ray crystallography at a resolution of 3.3 Å. LtaA presents the canonical MFS fold with 12 transmembrane helices (TMs) arranged

in two pseudo-symmetric sub-domains, N-domain (TM1-6) and C-domain (TM7-12). A striking feature is the presence of a large amphiphilic central cavity which we hypothesized to accommodate the amphiphilic substrate Glc_2-DAG. By analyzing LtaA crystal structure, along with site-direct mutagenesis and transport assays *in vitro*, we demonstrated that the di-glucosyl moiety of Glc_2-DAG is recognized by multiple conserved hydrophilic residues located in the N-terminal domain and loaded to the central cavity. We also proposed a proton-coupling mechanism where E32 undergoes protonation/deprotonation, and this extra driving force allows Glc_2-DAG to be translocated at a higher rate. By investigating LtaA function in *S.aureus*, we revealed that the proton-coupling mechanism allows LtaA to act as an environmental pH sensor and contribute to the survival of *S.aureus* under an acidic environment. Our results provided insights into the molecular basis of Glc_2-DAG flipping and made LtaA a novel target for the development of anti-*S.aureus* therapeutics.

Contents

1 Introduction

1.1 *Staphylococcus aureus*

Staphylococcus aureus (*S.aureus*) is a Gram-positive bacterium of Firmicutes phylum with a size between 0.5–1.5 μm in diameter, which forms irregular grape-like clusters[1] (Fig. 1.1). It serves as a successful opportunistic human pathogen since the first description of the staphylococcal disease in 1880[2,3]. As a commensal bacterium, it is carried by more than 30% of the population, and around 10%-20% is the persistent colonization[4,5]. Sites can be colonized by *S.aureus* including anterior nares, axilla, pharynx, gastrointestinal tract, vagina and perineum[4]. Colonized people with *S.aureus* are at a higher risk to get infected[6]. As a versatile pathogen, it invades breaches on skin or mucus membranes, causing various skin and soft tissue infections. *S.aureus* can further spread to distant organs, leading to life-threatening diseases including infective endocarditis, pleuropulmonary and septicemia[7]. *S.aureus* is highly contagious and can be transmitted to a new host through everything that can contact the skin or mucus membranes, such as clothes, smartphones or medical devices[8]. Notably, the transmission through various medical materials facilitates *S.aureus* infection as one of the leading causes of healthcare facility acquired infections including prosthetics, catheters and other implant devices related infections[9]. Invasive diseases caused by *S.aureus* are often associated with a big burden of morbidity and mortality (nearly 20% mortality), making treatments against this bacterium an unmet medical need for more than 100 years[5,10]. The occurrence and the quick spread of multiple drug resistance strains, such as methicillin-resistant *S. aureus* (MRSA) against β-lactams and vancomycin-resistant *S. aureus* (VRSA) resistant to the so-called last line medicine vancomycin[11,12], increase thereby the failure of therapeutics and health burden caused by *S.aureus* infection. In 2018, the percentage of MRAS isolates ranged from 5% to 43% in middle and south Europe[13]. It has been estimated that MRSA causes over 150,000 cases and an extra EUR 380 million costs of treatments annually in Europe[14,15]. Thus, *S.aureus* has been identified as one of ESKAPE pathogens (*Enterococcus faecium*, *S. aureus*, *Klebsiella pneumoniae*, *Acinetobacter baumannii*, *Pseudomonas aeruginosa*, *and Enterobacter species*) that are the most common causes of life-threatening infections, requiring intensive research and development of therapies with high priority[16].

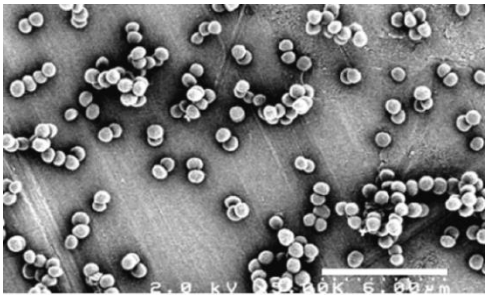

Fig. 1.1 Observation of *S. aureus* by Scanning Electron Microscopy. The scale bar indicates 6 μm. Adapted from[17]

1.2 Cell wall of *S.aureus*

To sustain its colonization, dissemination and infection of human hosts, *S.aureus* has to survive under various hostile environments. The nature reservoirs include the skin where it is dry, mildly acidic (average pH is between 4 to 6) and with a high concentration of salt, moisty and mildly acidic mucosal membranes and host macrophages where the environment is also acidic[1,5]. Besides these harsh physical conditions, *S.aureus* will also encounter anti-bacterial substances on skin and mucosal membranes as well as phagosomes and lysosomes in macrophages, which are all harmful to *S.aureus*[5]. The *S.aureus* cell wall is a multi-layered protective structure (typically 30-80 nm) that maintains the cell integrity, helps in pathogenicity and protects it from toxins, host defenses and antibiotics[18,19]. Thus, it serves as the first line of bacterial defense as it interacts directly with various environments and provides *S.aureus* high adaptability towards harmful surroundings[1]. Like the other Gram-positive bacteria, *S.aureus* presents a cell wall composed of thick peptidoglycan (PG) multilayer and long polymers called teichoic acids[19–21] (Fig. 1.2). PG consists of disaccharides cross-linked by peptide side chains, accounting for around 50% weight of the cell wall[1,5]. Teichoic acids are long polymers containing repetitive polyol phosphate subunits. The cell wall also harbors many surface proteins that process diverse functions, such as substance exchange, host interaction (adhesion, invasion, conjugation and immune evasion) and environment stimulus sensing[5,16].

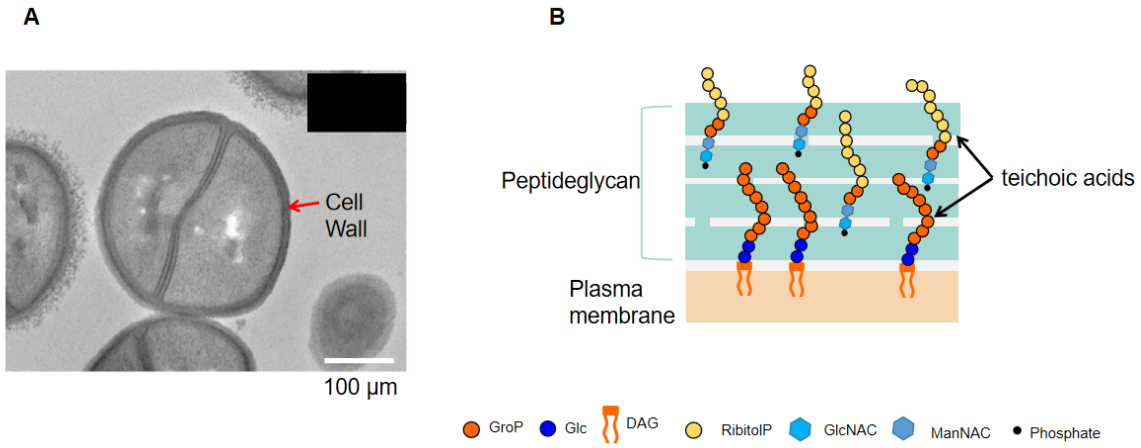

Fig. 1.2 The cell wall of *S.aureus*. A: Observation of the cell wall by Transmission Electron Microscopy. Adapted from[17]. B: Scheme of the cell wall with teichoic acids highlighted. Adapted from[2]

Due to the fundamental role of the cell wall in bacteria, it has been treated as a hotspot for antibiotics development. Many star antibiotics used in clinical target the cell wall biosynthesis pathway, especially the PG assembly pathway that is highly conserved in a broad spectrum of bacteria[22]. β-lactams are the most clinically used antibiotics containing thousands of derivatives (such as penicillin V, ampicillin, methicillin, oxacillin) since Alexander Fleming discovered that benzylpenicillin could kill staphylococci effectively in 1920s[23,24]. β-lactams bind to penicillin-binding proteins (PBPs) involved in the cross-linking step of PG synthesis, interfering with the cell wall assembly and resulting in cell rupture[23]. Another type is glycopeptides/glycolipopeptides (such as vancomycin, teicoplanin), also disrupting the cross-linking step of PG by binding to the natural substrate of PBPs, the D-alanyl-D-alanine moiety[25].

However, resistance to one or several antibiotics occurred quickly and spread worldwide[26]. *S.aureus* first developed the penicillin resistance by obtaining penicillinase that can hydrolyze the effective module of penicillin, the β-lactam ring[27]. To date, resistance to many β-lactams is also related to the updated β-lactamase of *S.aureus*[23]. Penicillin resistance led to the development of new penicillin derivatives that are insensitive to penicillinase, such as methicillin and oxacillin. However, the widespread use of penicillin derivatives led to the appearance of methicillin-resistant strains, by acquiring the major resistant-related gene *mecA* encoding a protein PBP2a or *mecC* encoding PBP2a$_{LGA}$ that display low binding affinity to the whole β-lactams[27,28]. Subsequently, vancomycin was applied to treat invasive MRSA infections in 1980s[29]. Vancomycin resistance in *S.aureus* was also observed afterward with an

enhanced minimum inhibitory concentration (MIC) from ≤2 μg/ml to > 16 μg/ml[30]. It's believed that the occurrence of VRSA is a result of acquiring multiple resistant-related genes that have not been fully characterized so far[31]. One of the major contributors to vancomycin resistance is the *van* cluster involved in the synthesis of D-alanyl-D-lactate or D-alanyl-D-serine which are the substitutions of D-alanyl-D-alanine and display low affinity to vancomycin[30]. Although the occurrence of VRSA is not as much as MRSA, VRSA poses a potential health threat, which exhorts a more detailed understanding of *S.aureus* cell wall biosynthesis and the identification of new targets for next-generation antibiotics development.

1.3 Lipoteichoic acids

Teichoic acids are crucial cell wall components identified by Baddiley and coworkers in 1958[32], who named them in reference to teīkhos which means "fortification wall" in Greek, highlighting their importance in cell protection[33]. Teichoic acids are roughly classified into two types: wall teichoic acids (WTA), which are bound to the peptidoglycan, and lipoteichoic acids (LTA), which are anchored to the cell membrane[2].

LTA molecules are composed of polymerized polyol phosphate units through phosphodiester bonds and a glycolipid anchor, being retained in all Gram-positive bacteria except some *Micrococcus* strains[34,35]. According to the difference in the chemical structure, there are five types of LTA identified[36](Fig. 1.3). *S.aureus* contains the simplest and the best-characterized type I LTA[33] composed of 1,3-linked glycerol phosphate repeating units (average 25 units[37]) which are tethered to the membrane by a glycolipid linker diglucosyl-diacylglycerol (β-glycosyl(1–6)-β-glucosyl(1–3)-diacylglycerol, Glc_2-DAG) inserted in the extracellular side of cell membrane[38] (Fig. 1.4). The terminal phosphate of polymerized units is linked to the hydroxyl group at the C6 position of the glucosyl moiety of Glc_2-DAG[38]. Hydroxyl groups at the C2 position of glycerol phosphate moieties are commonly decorated with D-alanyl or glycosyl groups[39]. LTA molecules are relatively abundant in the plasma membrane of *S.aureus*, accounting for every ninth lipid on the outer leaflet of the plasma membrane[34].

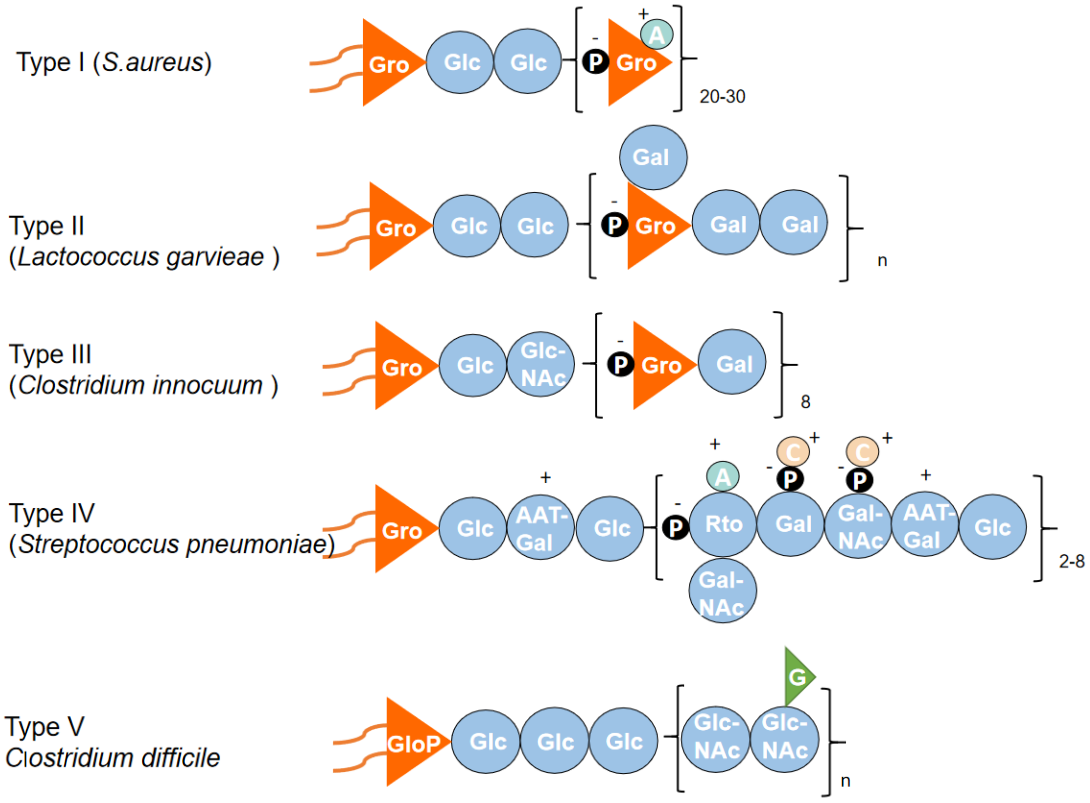

Fig. 1.3 Representative cartoon of type I-V LTA. Gro, glycerol; Glc, glucose; A, D-alanine; P: phosphate; Gal, galactose; GlcNAc, N-acetylglucosamine; C, choline; AAT-Gal, 2-acetamido-4-amino-2,4,6- trideoxy-d-galactose; GalNAc, N-acetylgalactosamine; Rto, ribitol; G: glyceric acid. Adapted from[36,40]

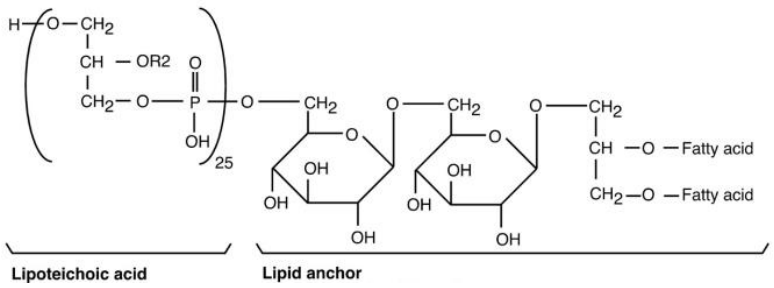

Fig. 1.4 Formula of a lipoteichoic acid molecule of *S.aureus.* R2: 60%-70% D-alanine, 15%: N-acetylglucosamine, 15% H. Percentages indicate the proportion of the substation in lipoteichoic acids. Adapted from [41].

The glycolipid anchor Glc_2-DAG is also abundant, counting 7% of the plasma membrane[42]. The lipid tail lengths vary between 14 carbons to 21 carbons, among which the richest is C15:0/C17:0[42] (Fig. 1.5). To sustain proper LTA polymer assembly in the extracellular side,

the anchor must be transferred to the outer leaflet of the cell membrane, which makes it a crucial step by determining the available anchor level for proper LTA assembly.

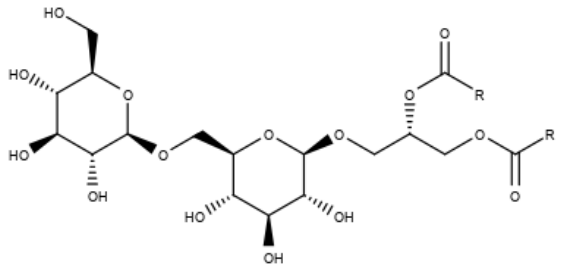

Fig. 1.5 Scheme of diglucosyl-diacylglycerol (Glc_2-DAG). R indicates the lipid tail, varying from 14-21 carbons.

1.3.1 Biosynthesis pathway of LTA

Key enzymes involved in *S.aureus* LTA biosynthesis have been identified (Fig. 1.6). The biosynthesis of LTA in *S.aureus* begins from the assembly of the glycolipid anchor Glc_2-DAG in the cytoplasm. Glucose-6-phosphate is converted into glucose-1-phosphate by an enzyme called PgcA[43]. Another enzyme GtaB catalyzes glucose-1-phosphate to its nucleotide-activated form, the uridine diphosphate glucose (UDP-Glc)[43]. The glycosyltransferase Ypfp adds two UDP-Glc units processively to DAG to form Glc_2-DAG[44,45]. Glc_2-DAG is then transferred across the cytoplasm membrane as the anchor of glycerol phosphate polymerization that happens on the extracellular side of the membrane[44,46]. This translocation step is facilitated by the putative membrane translocase LtaA[44]. LtaS then builds the polymer by iteratively adding the glycerol phosphate units originated from phosphatidylglycerol to the anchor Glc_2-DAG[47]. This step releases DAG molecules which are then converted to phosphatidic acid by DgkB as the precursor for the biosynthesis of new phosphatidylglycerol molecules[48]. The C2 hydroxyl position of glycerol groups of LTA can be decorated with D-alanine moieties (around 60%-70% depending on the strains[39]) by four concerted Dlt proteins, DltABCD[20,49] or glycosyl groups (around 15%[43]) by CsbB, GtcA and YfhO[39]. LTA molecules display a zwitterionic property because of negatively charged phosphate moieties and free amino groups of incorporated alanine moieties[20,50].

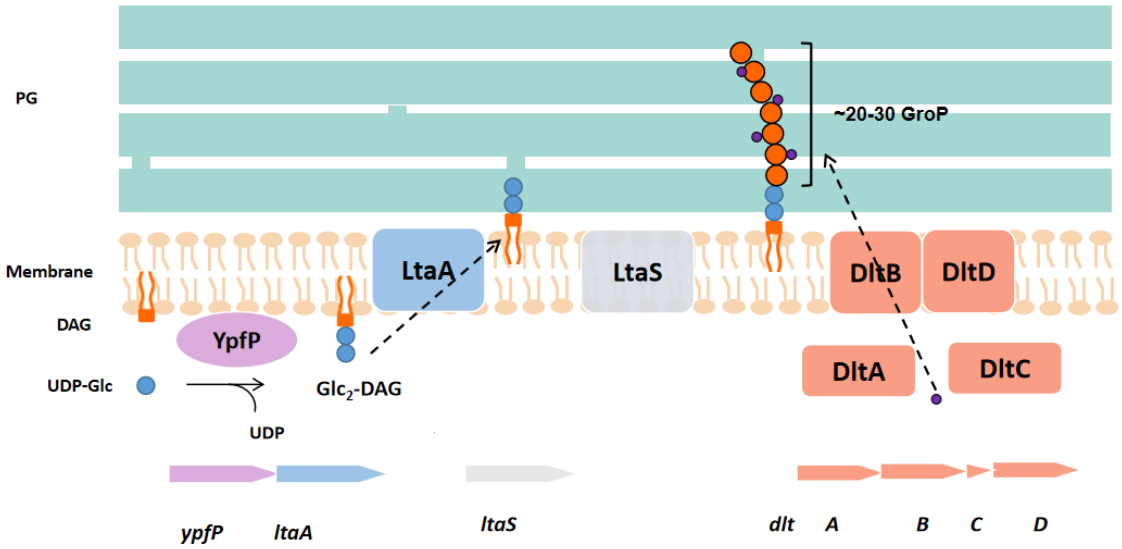

Fig. 1.6 The biosynthesis pathway of the LTA in *S.aureus*. Glc, glucose; UDP-Glc, uridine diphosphate glucose; GroP, glycerol phosphate; DAG, diacylglycerol; Glc_2-DAG, diglucosyl-diacylglycerol. Adapted from[2,51].

1.3.2 Functions of LTA

As a constituently expressed cell wall component, LTA participates in maintaining cell wall mechanic rigidity and contributes to the osmotic protection of the cell. The LTA knockout strain (*ltaS* deletion) could only survive under experimental high osmotic conditions (such as the supplement of either 7.5% NaCl or 40% sucrose in the culture medium) or lower temperature (from 37 °C to 30 °C), but with morphological defects[52,53]. Faster lysis under Triton X-100 solution was observed in the *ypfP* inactive strain[45]. It has been suggested that LTA contributed to the osmotic protection by influencing the PG layer assembly[54]. A decreased cross-linking level of the PG layer was observed in LTA depletion strain[54]. Spontaneous mutations that increased the cross-linking level of PG, such as mutations on *gdpP* which regulates the cross-linking level of PG through controlling the intracellular di-adenosine monophosphate (c-di-AMP) level[53] or on *sgtB*, a PG glycosyltransferase which directly participates in PG assembly[54], were proposed to allow the cell survival without LTA molecules.

LTA also contributes to cell division since it is deeply involved in maintaining cell wall structure. Defects in cell division, such as aberrant size, aberrant shape and aberrant positioning of division septa, were observed in *ltaS*, *ypfP* or *ltaA* deletion *S.arueus* strains[47,52,55]. These defects were attributed to the absence of LTA, which disrupts the interaction between LTA and the cell elongation and division machinery. Specifically, it was

reported that the interaction between LTA and the following proteins is disrupted, FtsZ, which allows the initiation of cell division by forming the Z-ring structure at the division site[56–58], ClpX, which was proposed to be a modulator of FtsZ[59] and autolysins which enable the separation of daughter cells[60,61]. Thus, LTA help in the localization of division machinery[58] and the regulation of the autolytic activity[47,61]. Because the autolysin activity was reported to relate to Mg^{2+} concentration[62], the regulation of autolytic activity was credited to the control of Mg^{2+} concentration through the D-alanylation level of LTA molecules[61,63,64]. Furthermore, participating in Mg^{2+} regulation renders LTA a pivotal contributor to extracellular ion homeostasis[63].

As a crucial part of the cell wall, the front line to interact with hosts, LTA molecules interact with many host receptors involved in inflammatory response, colonization and infection process. Hosts recognize pathogens and induce innate immune response via highly-conserved pattern recognition receptors (PRRs) including Toll-like receptors and C-type lectin receptors[65,66]. Toll-like receptors recognize many pathogen-associated substances and initiate proinflammatory responses to eliminate pathogens, but there is a risk for them to induce sepsis with the same mechanism[67]. LTA was proposed to interact with Toll-like receptors 2 (TLR2) expressed on epithelial as well as endothelial cells and D-alanine moieties of it play a key role in inducing immune response[68–70]. L-ficolin, a C-type lectin receptor, was documented to bind LTA, activating the complement pathway and pathogen opsonization[71]. LTA has also been documented to interact with many receptors of macrophages and monocytes, including type I macrophage scavenger receptor localized at the surface of macrophages as a part of the innate pathogen recognition system[72] and CD36 helping with the TRL2-related inflammatory signaling[69,73]. LTA was proposed to participate in the formation of biofilm[74,75],which facilitates the colonization of *S.aureus* and helps it in the resistance to harmful environments[76–78].

Of note, LTA molecules promote the resistance to anti-bacterial substances such as cationic antimicrobial peptides (CAMPs) and cationic antibiotics by their D-alanine decoration which enhances the positive charge and repels CAMPs and cationic antibiotics[64,79–82]. LTA was also demonstrated to participate in developing the resistance to daptomycin that belongs to the lipopeptide antibiotics applied as the last resort for MRSA infections[83,84].

1.3.3 LTA serve as a target to develop anti-*S.aureus* infection therapeutics

LTA molecules act as crucial cell wall components and display versatile roles in *S.aureus* pathogenesis, which make it a potential target for the development of novel anti-*S.aureus* strategies. Research on LTA-targeted treatments including developing antibiotics, conjugated antibodies and vaccines has been carried out in different labs. A small inhibitor targeting LtaS was developed named compound 1771[85]. Nevertheless, compound 1771 contains an ester moiety which might be hydrolyzed by esterase in the blood[86]. HSGN-189 was proposed to inhibit LTA biosynthesis, displaying a high MRSA killing ability (MIC= 0.25 mg/mL)[86]. Pagibaximab, a human chimeric monoclonal antibody against LTA, displayed an impressive staphylococcal killing effect, but it failed in Phase II because no significant protective effect against staphylococcal sepsis was observed in very low birth weight neonates trial[87]. Several molecules that mimic LTA structure or the epitope of LTA, such as synthetic ploy-glycerolphosphate polymers[88], a short peptide (12 amino acids)[89] or even LTA from other species[90] have been proposed to induce protective effects and ameliorate *S.aureus* infection in animal models. However, the LTA-targeted clinical usage remains largely vacant, partly owing to the fact that the molecular basis of its biosynthesis, functions and interactions with hosts are not well known. Notably, the 3D structures of many crucial proteins involved in LTA biosynthesis remain to be characterized, such as YpfP, LtaA and full-length LtaS (extracellular domain has been solved[46]). Solving the structure of these proteins will pave the way to the understanding of LTA biosynthesis and the application of LTA-derivative therapeutics.

1.4 Putative Glc_2-DAG translocase LtaA

LtaA is the putative candidate that facilitates the translocation of Glc_2-DAG across the plasma membrane, identified by Angelika Gründling and Olaf Schneewind in 2006[44]. Gene MU50 (locus tag SAV1016, Uniport ID: Q99V76) was denoted to *ltaA*, whose predicted start overlaps to the end of the *ypfP* coding sequence, and it could be found in all close-related species of *S.aureus* (such as *Staphylococcus epidermidis*, *Staphylococcus haemolyticus* and *Staphylococcus saprophyticus*)[44]. As the translocase of the anchor of LTA, LtaA plays an essential role in proper LTA assembly. The knockout of *ltaA* gene in *S.aureus* abolished the flip of Glc_2-DAG and led to the assembly of LTA on DAG[44]. The change of the anchor influenced the distribution of LTA because more LTA molecules were released to the

supernatant[44]. This change also led to the reduction of virulence during animal infection[44]. More recently, LtaA has been proposed to involve in developing daptomycin resistance which is influenced by the Glc_2-DAG level of LTA[83]. More questions in-depth, such as how does LtaA conduct the Glc_2-DAG translocation, how does the anchor flipping coordinate to the LTA biosynthesis and what is the regulatory mechanism remain unknown. Solving the structure of LtaA will facilitate tackling these questions and promoting the application of LtaA-targeted anti-*S.aureus* therapeutics.

1.5 Transport systems

The cell membrane is mainly composed of a phospholipid bilayer, forming a two-dimensional semipermeable barrier. It defines the boundary of the organism and its environment, regulating many exchanges of essential substances with the environment[91]. Except for a few small molecules that can diffuse freely across the lipid bilayer, and some bulky substances (such as pathogens and dead cells) can be exchanged by the endocytosis and exocytosis process, the transmembrane transport of most solutes is mediated by transport protein systems[92]. Transport proteins allow the uptake of nutrients and ions, excretion the deleterious and communication between the cell and the environment, serving the cell in many aspects, including cell growth and cell division, metabolism and signal transduction[92].

Two major types of transport proteins are channels and transporters[93] (Fig. 1.7). Channels can open the cytoplasmic side and the extracellular side simultaneously, while transporters can only open one side at the same time[93]. Open both sides when activated only allows channels to transfer the substrates downhill their electrochemical gradients. Thus, translocation against the substrate electrochemical gradient relies on the transporters.

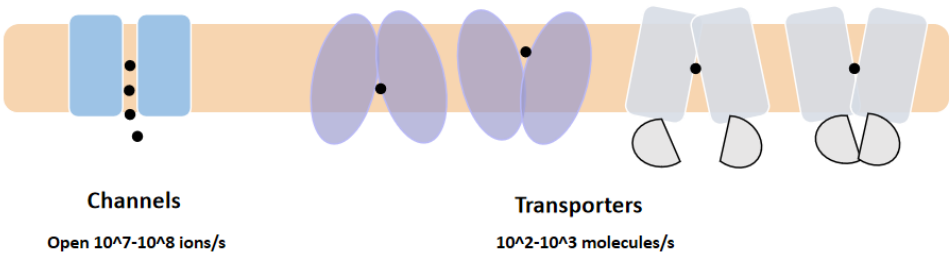

Fig. 1.7 Scheme of channels and transporters. Adapted from[94]

According to the transport mode and energy coupling, transporters are mainly divided into three groups: facilitators, primary active transporters and secondary active transporters[93]. Facilitators, also known as uniporters, belong to passive transporters. Energetically similar to channels, they transport targets only downhill the electrochemical gradient. Primary active transporters are driven by the energy from photons or chemical reactions such as the adenosine triphosphate (ATP) hydrolysis[95]. Primary active transporters contribute to generating an electrochemical potential across membranes by transporting charged molecules[96]. This electrochemical potential can act as the energy source of secondary active transporters to mediate the transport of substances across the membrane[97]. According to the relative movement direction, secondary active transporters are divided into symporters and antiporters. Symporters transfer the substrate and the driving solute in the same direction while antiporters transfer the two in a different direction[98] (Fig. 1. 8). Further classification of transporters is determined by their structure fold, function, mechanism and substrate[93].

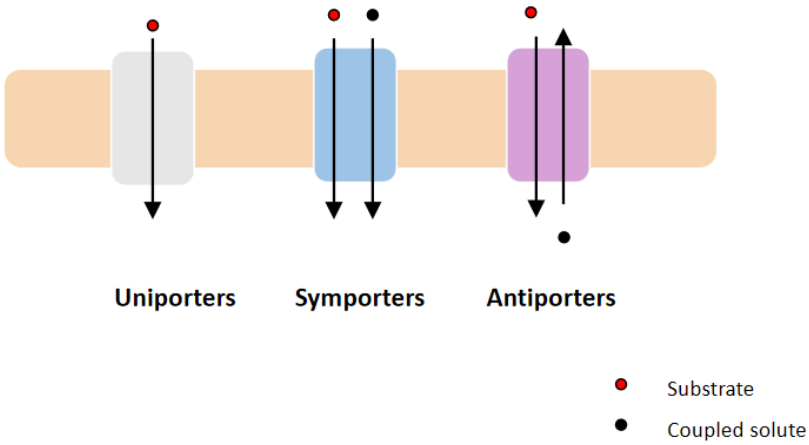

Fig. 1.8 Scheme of uniporters, symporters and antiporters. Adapted from[98]

1.6 Glycolipid transporters

Lipids and their conjugates are indispensable for living organisms, forming the cell membranes, serving as the energy storage source and participating in various signal transduction and metabolism[99]. Among all lipid conjugates, glycolipid, a ubiquitous and important component of the cell envelop of bacteria, has critical functions in maintaining cell integrity and contributing to the invasion and immune evasion from hosts[100]. They are generally synthesized from nucleotide-activated sugar precursors and lipid acceptors, followed

by the export process by specific transporters to participate in the building of PG, TA, capsular polysaccharide (CPS), lipopolysaccharide (LPS), etc.[100] The flip-flop of glycolipids with large and polar head groups is energetic unfavorable and serves as the rate-limiting step for transport[101]. To support the physiological requirement, it's well accepted that the transmembrane transport of glycolipids is mediated by transporters[101]. A common type of glycolipid transporters is ATP-binding cassette (ABC) transporters. ABC transporters are primary active transporters with a broad range of substances, from small ions to large macromolecule[102]. Four structures of ABC transporters that mediate glycolipids transport have been solved so far including MsbA responsible for the lipid A translocation for LPS synthesis[103], PglK that transports the lipids-linked glycan donor for protein N-glycosylation[104], Wzm–Wzt that mediates the transport of the O-antigen for LPS bsynthesis[105,106] and TarGH involved in WTA biosynthesis[107]. Both MsbA and PglK are type I ABC exporters consisting of two transmembrane domains (TMDs) forming the transport cavity and two cytoplasmic nucleotide-binding domains (NBDs) that perform ATP hydrolysis to energize the transport activity[100,103,104] (Figure 1.9). In addition, PglK displays two unique short α-helices at the periplasmatic side running parallel to the membrane and might contribute to the interaction with its substrate[104]. Although they display similar structural distributions, two distinct transport mechanisms have been demonstrated. MsbA was proposed to take an "alternating access" mechanism where the substrate fully enters the binding pocket, and this is called a "trap and flip" model[108,109] (Fig. 1.10 A). In contrast, an outward-only mechanism was proposed to PglK[104] (Fig. 1.10 B). Outward-facing PglK recognizes the undecaprenyl moiety of undecaprenyl pyrophosphate (Und-PP) lipid carriers, whereas the hydrophilic headgroup is transported to the outward-open cavity[104]. Then ATP hydrolysis drives NBDs apart and TMDs together, squeezing the headgroup out of the binding pocket[104]. Wzm-Wzt presents a type II exporter fold, with channel-forming TMDs in an open conformation and closed nucleotide-free NBDs[106](Figure 1.9). Wzm-Wzt was assumed to recognize the pyrophosphate group of Und-PP together with the first sugar through the interface of NBD and its corresponding carbohydrate-binding domain (CBD)[105,106], followed by the headgroup insertion and its spontaneously re-orientation to the periplasmic side, while the lipid tails probably remain in the membrane[106] (Fig. 1.10 C). The translocation was possibly facilitated by multiple rounds of ATP binding and hydrolysis[106]. TarGH also displays a type II exporter fold similar to that of Wzm-Wzt[107] (Figure 1.9). But TarGH was implicated to first interact with the pyrophosphate group of Und-PP only[107]. The flipping mechanism for TarGH is similar to that

of Wzm–Wzt[107].

Another type of glycolipid transporters is from the polysaccharide transport (PST) family, the multidrug/oligosaccharidyl-lipid/polysaccharide (MOP) superfamily of secondary transporters, such as Wzx for the O-antigen flipping[110]. However, no structure is available in this category. But the structure of MurJ from a close-related family to the PST family has been solved, providing some hints for glycolipid translocation by secondary transporters. MurJ is a lipid II (Und-PP-MurNAc-pentapeptide-GlcNAc) flippase involved in PG synthesis[111]. It contains 14 TMs divided into two lobes, TM1-6 and TM 7-14 respectively (Fig. 1.11). A Na^+ interaction site and membrane potential were demonstrated to be essential for MurJ's function[112,113]. The lipid moiety was also proposed to stay in the membrane during the translocation[112].

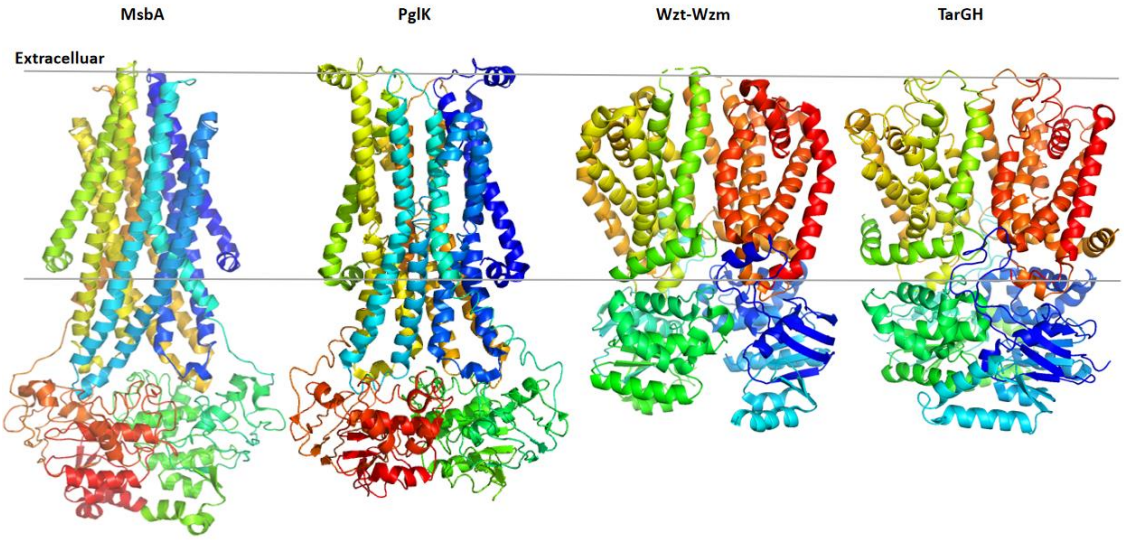

Fig. 1.9 Representative structures of ABC transporters. From the left to the right: MsbA with ADP-vanadate (PDB: 5TTP); Outward-facing PglK with ATPgammaS bound (PDB: 6HRC); Wzt-Wzm (PDB: 6OIH) and TarGH in inward-facing conformation (PDB: 6JBH). Transporters are colored in rainbow.

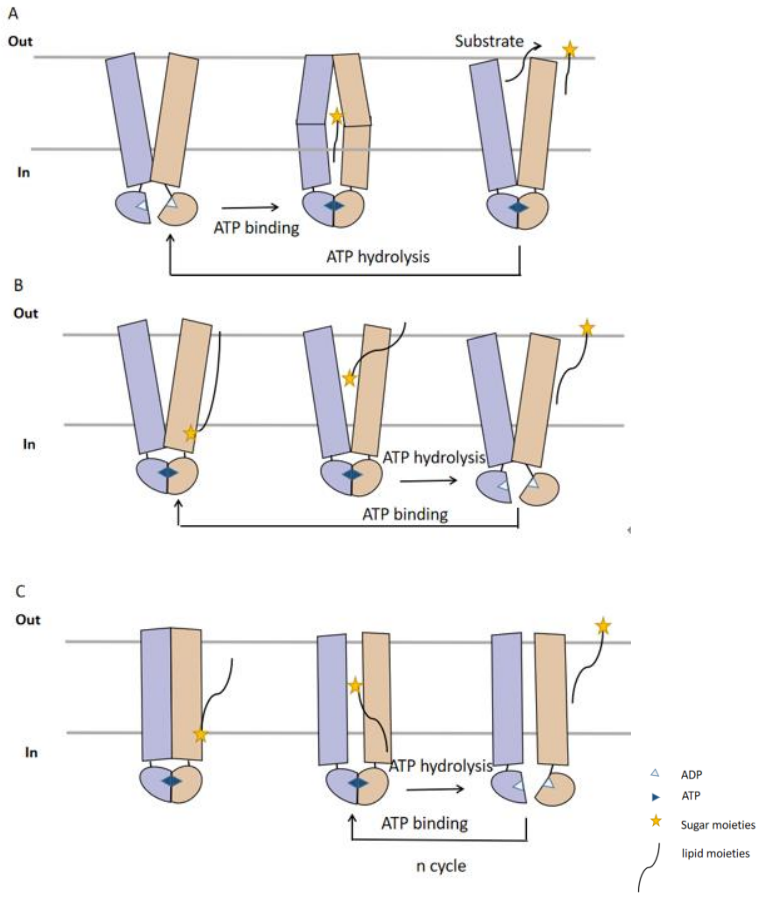

Fig. 1.10 Schematic illustration of translocation mechanisms of ABC flippases. A. Classical "alternating access" mechanism of MsbA. B. Outward-only mechanism of PglK. C. The flipping mechanism of Wzt-Wzm. The translocation of the polysaccharides might be facilitated by repeat cycles of ATP binding and hydrolysis. Adapted from[104,108,114]

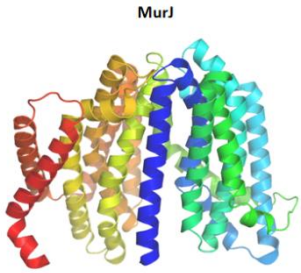

Fig. 1.11 Representative structure of MOP transporters. Inward-facing MurJ (PDB: 5T77) and lipid II. Transporters are colored in rainbow.

LtaA was predicted to belong to the major facilitator superfamily (MFS) which displays distinct structural architecture from the PST transporters or ABC transporters[44,115]. The flipping mechanism was also expected to be different. The diversity of overall architectures and flipping mechanisms of glycolipid transporters indicates the complexity and significance

of glycolipid translocation in nature.

Since the substrate recognition, binding and flipping mechanism of LtaA were expected to be more similar to MFS transporters than ABC transporters mediating glycolipid translocation, a brief introduction of MFS transporters regarding their overall structural fold, substrate binding and flipping mechanisms will be shown in the next section.

1.7 Major facilitator superfamily

1.7.1 General features of MFS transporters

The major facilitator superfamily (MFS) of transporters (TCDB classification: #2.A.1, http://www.tcdb.org/) is the largest group of secondary transporters, which is ubiquitous in all kingdoms of life. It consists of more than 15,000 sequenced proteins, a number still growing rapidly thanks to genome sequencing[116]. In 1993, the bioinformatics researchers have already established the term of major facilitator superfamily that contained transporters mediating sugar (oligosaccharides) transfer, multidrug efflux, metabolites up-taken as well as organic and inorganic phosphate exchange[117–119]. Later, the major facilitator superfamily quickly expanded to 82 families. In addition to the substrates above, MFS transporters mediate the transport of amino acids and short peptides, organic and inorganic cations and anions, lipids, nucleobases and nucleotides[119–121]. Many MFS transporters are involved in diseases and are considered as important drug targets[122]. However, there is still a large amount of MFS transporters identified only by bioinformatic tools, and very little is known regarding their mechanism, such as the ones involved in glycolipid transport.

Phylogeny and sequence analysis showed that MFS transporters generally consist of 400-600 amino acids and share transmembrane topology similarities by dividing into 12 transmembrane α helices, but the number of TMs can be extended to 14 or 24[119,123,124]. 12 TMs are connected by hydrophilic loops, and the N termini and C termini are located on the cytoplasmic side[121,125]. These 12 TMs are organized into two sub-domains, the N-domain (TM1-6) and the C-domain (TM7-12)[125]. Transporters from different families usually display low sequence similarity[125]. Although with low primary sequence similarity, three highly

conserved signature sequence motifs (Motif A-C) have been identified to be shared along MFS transporters[126]. The Motif-A ("G(X)3DRXGRR") at the loop that joins TM2 to TM3 together with a motif-A-like sequence presented at the equivalent loop connecting TM8 and TM9 serves as one of the most conserved regions of MFS symporters and antiporters[127]. Other conserved regions include Motif-B "R(X)2QG" in TM4 and Motif-C "G(X)8G(X)3GP(X)2GG" in TM5[127–129]. Not all three motifs are present in all MFS transporters.

1.7.2 Structural characterizations of MFS transporters

In 2003, the first structure of an MFS transporter, the lactose permease LacY from *E.coli*, was solved by X-ray crystallography, paving a way for understanding its transport mechanism as well as the general working mechanism of MFS transporters[130]. Later the same year, the structure of an sn-glycerol-3-phosphate/phosphate antiporter (GlpT) from *E.coli* was also elucidated[131]. Until now there are 27 unique MFS transporters known of 3D structure from six different families. Except for LacY, there are ten more involved in saccharides translocation, four of which are from bacteria and six are from eukaryotes, including *E.coli* fucose transporter FucP (with mutant N162A)[132], melibiose/ Na^+ symporter MelB from *Salmonella typhimurium*[133], *E.coli* xylose/H^+ symporter XylE[134], *Staphylococcus epidermidis* glucose/H^+ symporter GlcP[135], human glucose transporter GLUT1[136], human glucose transporter (with mutant N45T) GLUT3[137], fructose transporter GLUT5 from *Bos Taurus* and *Rattus norvegicus*[138], sugar transport 10 from *Arabidopsis thaliana*[139] and a hexose transporter from *Plasmodium falciparum*[140]. Seven of them are short peptide transporters from bacteria: oligopeptide/H^+ symporter $PepT_{So}$ from *Shewanella oneidensis*[141], oligopeptide/H^+ symporter $PepT_{St}$ from *Streptococcus thermophilus*[142], a proton-dependent oligopeptide transporter from *Geobacillus kaustophilus*[143], *E.coli* peptide transport YgbH[144], *Yersinia enterocolitica* dipeptide transporter[145], *Xanthomonas campestris* peptide transporter $PepT_{Xc}$[146] and *Staphylococcus hominis* S-Cys-Gly-3M3SH transporter $PepT_{Sh}$[147]. The others are three related to multidrug efflux, EmrD ,YajR and MdfA from *E.coli*[127,148,149]; one deals with phosphate transfer from eukaryote *Piriformospora indica*[150]; three mediate nitrate exchange, including NarU[151] and NarK[152] from *E.coli* and NRT1.1 from eukaryote *Arabidopsis thaliana*[153]; one ferroprotein (FPN) Fe^{2+} transporter from *Bdellovibrio bacteriovarus*[154]. The details of structures solved MFS transporters are listed below (Table 1.1).

Table 1-1 All structure solved MFS transporters

Name	Description	Organism	PDB code	Resolution limit
LacY	Lactose:proton symporter	*E.coli*	1PV6, 1PV7, 2CFP, 2CFQ, 2V8N, 2Y5Y，4OAA，4ZYR，5GXB，6C9W	2.95
GlpT	Glycerol-3-phosphate: Pi antiporter	*E.coli*	1PW4	3.3
EmrD	Mutidrug transporter	*E.coli*	2GFP	3.5
FucP	L-Fucose:proton symporter	*E.coli*	3O7Q, 3O7P	3.1
$PepT_{so}$	Peptide: proton symporter	*S. oneidensis*	4TPH,4TPG,4TPJ, 4UVM, 6JI1,6JKD, 6JKC	3.0
$PepT_{st}$	Peptide: proton symporter	*S.thermophilus*	4APS, 4XNJ, 4XNI ,5OXl, 5OXK, 5OXM, 5OXN, 6EIA, 5OXQ, 5OXP, 5OXO	1.95
GkPOT	Peptide: proton symporter	*G.kaustophilus*	4IKV, 4IKW, 4IKX, 4IKY, 4IKZ	2.0
XylE	D-Xylose:proton symporter	*E.coli*	4GBY, 4GBZ, 4GC0, 4JA3, 4JA4, 4QIQ	2.6
GlcP	Glucose:proton symporter	*S.epidermidis*	4LDS	3.2
PiPT	Phosphate:proton transporter	*P.indica* (E)	4J05	2.9
NarU	Nitrate transporter	*E.coli*	4IU9, 4IU8	3.01
NarK	Nitrate transporter	*E.coli*	4JR9, 4JRE, 4U4V, 4U4T, 4U4W	2.35
YajR	Drug efflux:proton transporter	*E.coli*	3WDO	3.15
MelB	Melibiose:sodium symporter	*S.typhimurium*	4M64	3.35
YbgH	Peptide: proton symporter	*E.coli*	4Q65	3.4
NRT1.1	Nitrate transporter	*A.thaliana* (E)	5A2N, 5A2O, 4OH3	3.25
GLUT1	Glucose transporter	*Homo sapiens*	4PYP, 5EQI, 5EQG, 5EQH	3.0
YePEPT	Peptide: proton symporter	*Y.enterocolitica*	4W6V	3.02

Continued table 1-1 All solved structure of MFS transporters

Name	Description	Organism	PDB code	Resolution limit
MdfA	Multidrug resistance transporter	*E.coli*	4ZP0, 4ZOW, 4ZP2	2.0
GLUT3	Glucose transporter	*Homo sapiens*	4ZW9, 4ZWB, 4ZWC	1.5
BbFPN	Hepcidin (Fe2+) transporter	*B.bacteriovarus*	5AYN, 5AYM, 5AYO	2.2
GLUT5	Fructose transporter	*Bos Taurus* (E)	4YB9	3.2
GLUT5	Fructose transporter	*Rattus norvegicus* (E)	4YBQ	3.27
$PepT_{Xc}$	Peptide: proton symporter	*X.campestris*	6EI3	2.1
$PepT_{Sh}$	S-Cys-Gly-3M3SH transporter	*S.hominis*	6EXS	2.5
STP10	Glucose:protein symporter	*A.thaliana* (E)	6H7D	2.4
PfHT1	Hexose transporter	*P.falciparum* (E)	6RW3	3.65

(E) indicates the protein originated from Eukaryote

The overall structure of these transporters displays the classic MFS fold, presenting 12 TMs except transporters from the proton-dependent oligopeptide transporter (POT) family with 14 TMs, such as $PepT_{So}$[141]. These 12TMs are divided into two discretely folded domains (N-domain and C-domain), related by a twofold pseudosymmetry axis perpendicular to the membrane plane (Fig. 1.12, Fig. 1.13 **A**). Previous bioinformatic evidence suggested that 12 TMs are originated by a duplication of 3 TMs to 6 TMs and another duplication to 12 TMs[119,155], which is supported by structural features. TM4, TM5 and TM6 can be related to TM1, TM2 and TM3 by rotating around the axis parallel to the membrane bilayer; TM7, TM8, TM9 and TM10, TM11, TM12 can be related to each other in the same way[121]. Every first TM helices of the 3-TMs bundle, TM1, TM4, TM7 and TM10, are placed in the center of the transporter (Fig. 1.13), defining the interface of the substrate-binding pocket which is generally located in the half-way of the transporter[120]. TM3, TM6, TM9 and TM12 are positioned on the periphery of the TM1, TM4, TM7 and TM10 group (Fig. 1.13), and these are believed to be important for structural rigidity[120]. TM2, TM5, TM8 and TM11 sit on the sides of the transporter, mediating the interactions between the two sub-domains[120](Fig. 1.13). The linking loops of the two domains are relatively long, some of which present a short α

helix[121].

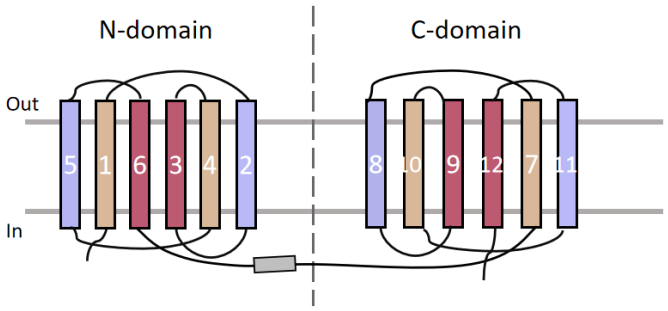

Fig. 1.12 Topology diagram of the MFS fold. TM 1,4,7,10 are colored in wheat; TM 2,5,8,11 are in light purple; TM 3,6,9,12 are shown in rose-red color. The loops are depicted in black. The short α helix in the connecting loop is in gray. Adapted from[156]

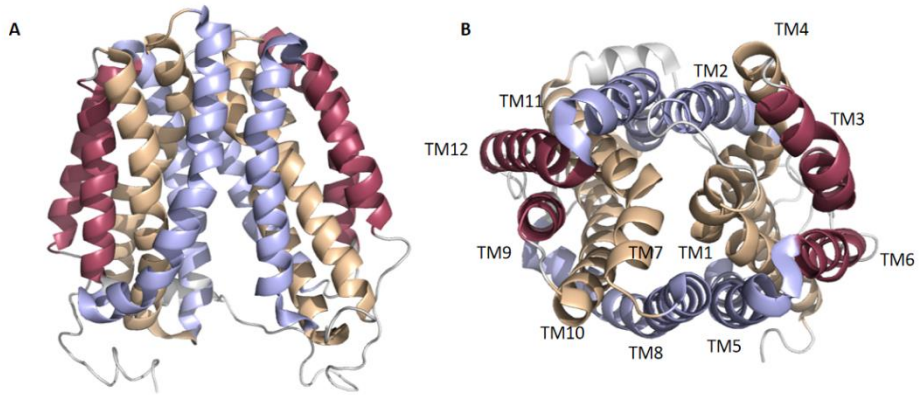

Fig. 1.13 The overall architecture of a classical MFS transporter LacY. A: Inward-facing apo LacY (PDB code: 2CFQ). B: Top view of LacY. TM 1,4,7,10 are colored in wheat; TM 2,5,8,11 are in light purple; TM 3,6,9,12 are shown in rose-red color. The loops are depicted in gray.

1.7.3 Substrate binding

All MFS transporters contain a single substrate-binding pocket formed by residues from the N-domain and the C-domain[120]. The first ligand-bound MFS transporter structure XylE was obtained in 2012, shedding the light on transporter-substrate interaction from the structural standpoint[134]. Nowadays, there are six more solved substrate-bound structures from four families, including $PepT_{So}$ with tri-peptides[157], $PepT_{St}$ with di-peptides[158], nitrite or nitrate bound NarK[152,159], nitrite bound NRT1.1[153], multidrug resistance transporter MdfA with chloramphenicol[160] and BbFPN with Fe^{2+} [154]. Two general features of the ligand-binding pocket have been proposed: 1) only a few residues are involved in the interaction with the

substrate. 2) The two domains contribute asymmetrically to the interaction with the substrate[120]. Meanwhile, the binding pocket can be highly adaptable towards the nature of a specific substrate. A single Lys314 located in the binding pocket of YePEPT is crucial for the preference of negatively charged di-peptides, while its substitution to negatively charged Glu contributes to binding positively charged di-peptides instead[145]. Other residues located outside the binding pocket can also contribute to substrate recognition, which is often related to a specific physiological function. For instance, pfHT1 is a hexose transporter of malaria parasites that transports many hexoses besides glucose, while GLUT3 is a highly specific glucose transporter of humans[137,140]. pfHT1 was proposed to achieve its sugar promiscuity by coordinating with residues located in TM1-TM7b[140]. This sugar promiscuity was hypothesized to reduce the dependence on glucose after the parasite infects human red blood cells[140].

1.7.4 Proton Coupling

Some MFS transporters are coupled with a second driving solute or several solutes to transfer their natural substrates. The coupled solutes can be Na^+, H^+, phosphate, etc.[94] The ones coupled with protons can make use of the electrochemical energy called proton motive force generated by a gradient of H^+ across the membrane ($\Delta\mu H^+$)[156]. The proton motive force is often utilized by bacteria to transfer substances against their concentration[156]. The movement of the substrate and the coupled proton can be in the same or the opposite direction, known as proton-coupled symporters and proton-coupled antiporters respectively[156]. Symporters are generally for substance (such as sugars, short peptides) up-taken and antiporters for effluxion (such as drugs)[146,160–162].

Some similarities of the proton coupling were proposed among different families including both proton-coupled symporters and antiporters[146]. A striking one is that the coupling sites are conserved within a family, generally happening in Glu, His and Asp located close to or inside the binding pocket[127,130,132,135,146,149,161,163]. These residues can undergo pKa changes during the conformational changes of the transporter and present the protonation and deprotonation process[120]. One of the fundamental questions regarding the proton coupling mechanism is how the proton coupling coordinates to the substrate binding and the conformational change. Researchers have intensively investigated these questions in the proton/lactose symporter LacY. The proton was hypothesized to transfer from Glu269 to His322, both of which

participate in the substrate binding[164,165], and further, to Glu325[164]. Glu325 was identified to involve exclusively in protonation/deprotonation with a pKa 10.5, and its protonation was required for the binding of the substrate[166]. Arg306 was proposed to be essential to the deprotonation of Glu325[167]. The proton motive force was demonstrated to change the rate-limiting step of the transport from deprotonation to opening the apo LacY [167].

1.7.5 Alternating access

MFS transporters achieve their substrate translocation through the membrane by the "alternating access" mechanism, namely the binding site is made accessible from one side of the membrane to another or in a reverse order[168]. MFS transporters generally adopt one of the alternating access models called the "Rocker switch" mechanism where the chronological opening is achieved by the conformational change between two sub-domains that transfers from the V-shape like outward-facing state to an inverted V-shape like inward-facing state[168]. Between the outward-facing and the inward-facing state is the intermediate occlude state[168]. Due to the structural asymmetry, namely, the asymmetrical contribution of two domains to the interaction with the substrate, transporter states can be further divided into the outward-occluded or the inward-occluded conformation[120,121]. Accompanied by the conformational shifts, the substrate enters from one side of the transporter and is released from the other side (Fig. 1.14).

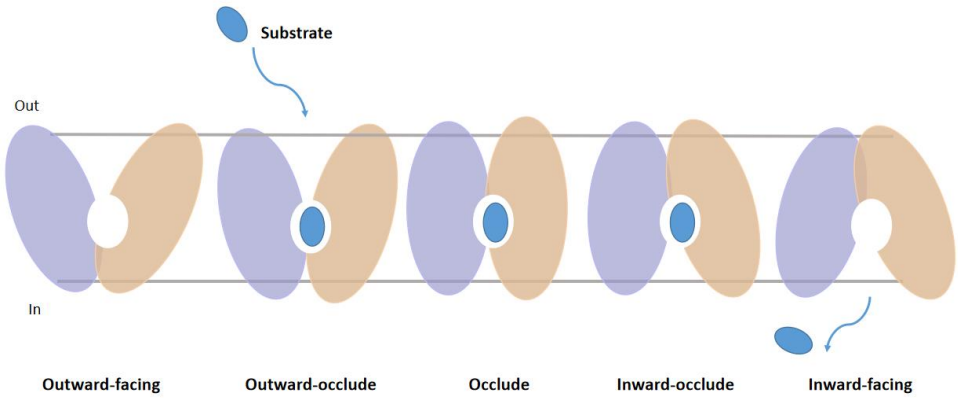

Fig. 1.14 The conformational change and the substrate translocation of MFS transporters. Adapted from[120]

Multiple conformational states of some MFS transporters have been elucidated, providing insights into understanding the conformational change and the "Rocker switch" model. LacY

serves as the most intensively studied prototype of MFS transporters, being elucidated the outward-facing, the inward-facing and the occlude state[169–172]. The other two sugar transporters, XylE[173,174]and GLUT5[138] were known the outward-facing structure and the inward-facing structure. Besides sugar transporters, transporters that mediate short peptides[141,142], exchange nitrite/nitrate[151,152] and transfer Fe^{2+}[154] have been characterized in more than one conformation. With the limited structural information, we have already proposed that the conformational change originates from both the rigid body movement, namely the overall domain rotation, and the local position rearrangement of the residues from TMs, especially from the TM1,4,7,10 which display more discontinuities compared to other TMs to satisfy a larger movement[120,168]. The rotation of the rigid body and rearrangement of local residues generally require the breakage and the re-formation of interactions (such as salt bridges and/or polar interactions) between gating residues which can seal the cytoplasmic side or the extracellular side of transporters during the transport cycle[98,131,168,174]. The binding and the release of the substrate were announced to encourage this breakage and re-formation, thus promoting the conformational change[98,132,164]. Coupling with driven solutes was also assumed to facilitate the substrate binding and conformational change[135,161,175,176]. Nevertheless, how are substrate binding and/or ion coupling involved in conformational change is still not well understood.

1.8 Aims of this work

S.aureus infection represents a threatening global health burden facilitated by its high adaptability to various harsh environments, notably, to the clinical usage of diverse antibiotics. LTA serves as a crucial component of the cell wall and plays a pivotal role in helping with *S.aureus*' adaptation and antibiotic resistance. LtaA is an MFS flippase involved in the flipping of the glycolipid anchor Glc_2-DAG which is a key brick of LTA assembly. No structure involved in glycolipid transporters belonging to MFS transporters is available. The molecular basis of LtaA function and mechanism remains largely unknown. Thus, solving the structure of LtaA will greatly promote the understanding of its substrate recognition and the flipping mechanism, establishing a framework for understanding MFS glycolipid transporters.

Therefore, the primary goal of my project was to perform a structural study on LtaA, followed by its functional characterization *in vitro* and *in vivo*, to elucidate the translocation mechanism

of Glc_2-DAG.

2 Stabilization and crystallization of a membrane protein involved in lipid transport

Bing Zhang[1], Camilo Perez[1†]

[1]Biozentrum, University of Basel, 4056 Basel, Switzerland.

Author Contribution:

I carried out the experimental part and contributed to manuscript writing.

Chapter 19

Stabilization and Crystallization of a Membrane Protein Involved in Lipid Transport

Bing Zhang and Camilo Perez

Abstract

Lipoteichoic acids (LTA) are ubiquitous cell wall components of Gram-positive bacteria. In *Staphylococcus aureus* LTA are composed of a polymer with 1,3-linked glycerol phosphate repeating units anchored to the plasma membrane. The anchor molecule is a lipid-linked disaccharide (anchor-LLD) synthesized at the cytoplasmic leaflet of the membrane. The anchor lipid becomes accessible at the outer leaflet of the membrane after the flippase LtaA catalyzes translocation. Recently we have elucidated the structure of LtaA using vapor diffusion X-ray crystallography and in situ annealing. We were able to obtain LtaA crystals after optimization of purification protocols that led to stabilization of LtaA isolated in detergent micelles. Here we report a protocol that describes the purification, stabilization, crystallization, and data collection strategies carried out to determine the structure of LtaA. We highlight key points that can be used to determine crystal structures of other membrane proteins.

Key words Membrane protein, Lipid flippases, X-ray crystallography, In situ annealing, TEV protease, Protein purification, Detergent micelles

1 Introduction

Gram-positive bacteria such as *S. aureus* are coated with an essential cell envelope composed of a thick peptidoglycan multilayer, in which teichoic acids (TAs) are embedded. TAs are long anionic polymers composed of repeating glycerol phosphate or ribitol phosphate units [1]. TAs are divided into two subtypes: lipoteichoic acids (LTA), which are anchored to the cell membrane, and wall teichoic acids (WTA), which are bound to the peptidoglycan layer [2]. LTA and WTA are both essential to resist antibacterial agents, localize the cell wall elongation and division machinery, contribute to immune evasion, and prevent recognition and opsonization by antibodies, and have been shown to be important for adhesion, colonization, and biofilm formation [3–12].

S. aureus LTA are composed of a polymer of 1,3-glycerol-phosphate repeat units attached to C-6 of the nonreducing glucosyl

Camilo Perez and Timm Maier (eds.), *Expression, Purification, and Structural Biology of Membrane Proteins*, Methods in Molecular Biology, vol. 2127, https://doi.org/10.1007/978-1-0716-0373-4_19,

of the disaccharide moiety of a gentiobiosyl-diacylglycerol anchor lipid (anchor-LLD). The anchor-LLD is found embedded in the extracellular leaflet of the plasma membrane [1, 2, 13–16], but its synthesis is carried out at the cytoplasmic leaflet by the action of the processive glycosyltransferase YpfP [17]. The anchor-LLD is translocated to the outer leaflet of the membrane by the flippase LtaA. Thus, LtaA regulates LTA synthesis by adjusting the extracellular concentration of anchor-LLD available for the polymerization reaction to happen [18].

LtaA is a 44 kDa monomeric membrane protein without prominent soluble domains. Thus, elucidation of a high-resolution structure of LtaA using cryo-electron microscopy (cryo-EM) methods is rather challenging at the current level of development of the technique. X-ray crystallography has shown to be successful in the determination of structures of membrane proteins with similar characteristics to LtaA in the past. However, obtaining well-diffracting crystals depends on several parameters including purity of the protein sample, stability of the protein in detergent micelles, presence of flexible regions that could preclude formation of well-ordered lattice structures, conformational diversity, surface properties that will dictate the formation of crystal contacts, stability of the protein at high concentrations, suitable cryo-protection strategies, etc. In this chapter we describe the experimental approaches that we used for the purification, stabilization, and crystallization of LtaA. We also describe the in situ annealing methodology used to increase the resolution of X-ray diffraction of LtaA crystals from 7 to 3.3 Å. We highlight important steps that could be applied to crystallographic studies of other membrane proteins.

2 Materials

2.1 Protein Expression

1. *E. coli* BL21-Gold (DE3) competent cells (Stratagene).
2. pET-19b expression vector (Novagen) carrying LtaA sequence: The vector contains an N-terminal His10 affinity tag followed by a Tobacco etch virus (TEV) protease site.
3. 1 M Ampicillin stock, dissolved in filtered ultrapure water: Store at −20 °C.
4. Terrific broth medium with 1% glucose (TB glucose) containing 100 μg/ml ampicillin.
5. Luria broth (LB) medium containing 100 μg/ml ampicillin.
6. LB agar plate containing 100 μg/ml ampicillin.
7. 1 M Isopropyl β-D-1-thiogalactopyranoside (IPTG) in filtered ultrapure water.
8. Miniprep DNA purification kit.

2.2 Protein Purification

1. Membrane preparation buffer (MP buffer), 50 mM Tris–HCl pH 8.0, 500 mM NaCl, 0.5 mM phenylmethylsulfonyl fluoride (PMSF), 5 mM β-mercaptoethanol (β-Me).
2. Membrane resuspension buffer (MR buffer), 50 mM Tris–HCl pH 8.0, 500 mM NaCl, 5 mM β-Me.
3. Nickel-nitrilotriacetic acid agarose matrix (Ni-NTA) for immobilized metal affinity chromatography (IMAC).
4. Superdex 200 Increase 10/300 GL column for size-exclusion chromatography (SEC) (GE Healthcare).
5. PD-10 desalting column (GE Healthcare).
6. Tobacco etch virus (TEV) protease: Self-preparation [19].
7. Solubilization buffer (Sol. buffer), 50 mM Tris–HCl pH 8.0, 200 mM NaCl, 15% glycerol, 1% lauryl maltose neopentyl glycol (LMNG, Anatrace), 1% *n*-dodecyl-β-D-maltoside (DDM, Anatrace), 5 mM β-Me. Detergents and β-Me are added freshly from stock solutions before usage.
8. Equilibration buffer (Eq. buffer), 50 mM Tris–HCl pH 8.0, 200 mM NaCl, 10% glycerol, 20 mM imidazole, 0.02% LMNG, 0.02% DDM, 5 mM β-Me.
9. Wash buffer-1, 50 mM Tris–HCl pH 8.0, 200 mM NaCl, 10% glycerol, 50 mM imidazole, 0.02% LMNG, 0.02% DDM, 5 mM β-Me.
10. Wash buffer-2, 50 mM Tris–HCl pH 8.0, 200 mM NaCl, 10% glycerol, 50 mM imidazole, 0.02% LMNG, 5 mM β-Me.
11. Elution buffer (Elu. buffer), 50 mM Tris–HCl pH 8.0, 200 mM NaCl, 10% glycerol, 200 mM imidazole, 0.02% LMNG, 5 mM β-Me.
12. Size-exclusion chromatography buffer (SEC buffer), 10 mM Tris–HCl pH 8.0, 150 mM NaCl, 0.02% LMNG.
13. Desalting buffer, 10 mM Tris–HCl pH 8.0, 150 mM NaCl, 0.1% Cymal-7 (Anatrace).
14. 30 kDa MWCO Vivaspin™ 20 concentrator (GE Healthcare).
15. Nanodrop (Thermo Fisher).

2.3 Protein Crystallization

1. MRC 96-well and MRC Maxi 48-well plates.
2. Stock solutions for crystallization: 1 M Magnesium acetate, 1 M glycine pH 9.5, 50% (v/v) polyethylene glycol 300 (PEG 300).
3. Cryo-buffers: (**1**) 15 mM Magnesium acetate, 150 mM NaCl, 10 mM Tris–HCl pH 8.0, 15 mM glycine pH 9.5, 0.1% Cymal-7, 26% PEG 300; (**2**) and (**3**) same composition as cryo-buffer (1) but containing 31% and 36% PEG 300, respectively.
4. Liquid nitrogen.
5. Cryoloops.

2.4 In Situ Annealing

1. X-ray beamline: X06SA-PXI at the SLS, Paul Scherrer Institut (PSI), provides fast and stable energy (wavelength) selection in the range from 5.7 to 17.5 keV (0.7–2.2 Å). Beamline X06SA-PXI is optimized for micro-focusing applications and features a beam down to $2 \times 1\ \mu m^2$. Beam size can be varied to match the dimensions of the crystal, thereby maximizing the diffraction signal.
2. Single-photon counting hybrid pixel area EIGER 16M (Dectris) detector [20]: The EIGER 16M at X06SA-PXI is a fast detector that allows collection of datasets at high speed. It has pixel-array detectors with low noise, fast frame rate, and negligible dead time.
3. Data collection software: The software suite developed at the SLS allows for fast scanning of crystals, automated data collection, and data processing [21–24].
4. Thin film to block nitrogen-gas stream.

3 Methods

3.1 Protein Expression

This protocol for LtaA expression comprises transformation of *E. coli* BL21-Gold (DE3) competent cells with recombinant vector carrying LtaA gene, cell culturing, and LtaA expression induction (*see* **Note 1**).

1. Thaw 50 µl of *E. coli* BL21-Gold (DE3) competent cell on ice, add 1 µl of pET19b-LtaA plasmid (approximately 30 ng), mix, and incubate on ice for 30 min.
2. Apply heat shock at 42 °C for 45 s followed by incubation on ice for 2 min.
3. Add 450 µl of pre-warmed LB medium and incubate for 1 h at 37 °C with mild shaking.
4. Centrifuge at 2000 × *g* for 4 min, discard 400 µl of supernatant, resuspend the pellet gently, and spread on LB agar plate containing 100 µg/ml ampicillin. Leave incubating at 37 °C for about 16 h.
5. Inoculate a single colony in 100 ml of TB glucose medium containing 100 µg/ml ampicillin. Grow cells at 37 °C shaking at 200 rpm for about 16 h.
6. Inoculate the main culture (10 L of fresh TB glucose media containing 100 µg/ml ampicillin) to have initial $OD_{600} = 0.05$. Grow cells at 37 °C shaking at 130 rpm for about 3–4 h.
7. Add 0.2 mM IPTG and induce LtaA expression for 1 h.

8. Harvest cells by centrifugation at 10,000 × *g* at 4 °C for 15 min.
9. Weight pellet and store them at −80 °C.

3.2 Protein Purification

This protocol includes preparation of membrane vesicles, solubilization of membranes, and purification of LtaA by affinity chromatography and size-exclusion chromatography. All steps are carried out at 4 °C unless stated otherwise (*see* **Notes 2–5**).

3.2.1 Membrane Vesicle Preparation

1. Thaw cell pellets and resuspend on ice-cold MP buffer. Keep a proportion of 8 ml MP buffer for 1 g of dry cells.
2. Stir until a homogeneous suspension is obtained.
3. Disrupt the cells in a M-110L microfluidizer (Microfluidics) at 10,000 p.s.i.
4. Remove unbroken cells by centrifugation at 4400 × *g* for 30 min. Harvest membranes by ultracentrifugation at 140,000 × *g* for 30 min. Tubes used for centrifugation should be ice-chilled.
5. Resuspend pellet of membrane vesicles in MR buffer using Dounce homogenizer. Maintain a ratio of 1 ml MP buffer for every 1 g dry cells. Store homogenized membranes at −80 °C.

3.2.2 Purification and Stabilization

1. Solubilize membranes in ice-cold Sol. buffer for 2 h (*see* **Note 2**).
2. Centrifuge at 30,000 × *g* for 30 min using ice-chilled tubes.
3. Load supernatant onto pre-equilibrated Ni-NTA superflow affinity column.
4. Wash away nonspecific bound proteins by passing through buffer 1 and buffer 2 sequentially (*see* **Note 3**).
5. Elute LtaA from the column using elution buffer.
6. Equilibrate a PD-10 column or a HiPrep™ 26/10 desalting column with SEC buffer and exchange the buffer of the eluted protein.
7. Measure the concentration of eluted protein by nanodrop and add TEV protease at 1:5 (w:w) ratio to remove His10 affinity tag. Incubate for 16 h.
8. Remove TEV protease by passing through equilibrated Ni-NTA affinity column and collect the flow through (*see* **Note 4**) (*see* Fig. 1).
9. Concentrate eluted LtaA using a pre-chilled 30 kDa MWCO Vivaspin™ 20 concentrator.
10. Run LtaA sample on a pre-equilibrated Superdex 200 Increase 10/300 GL SEC column with a flow rate of 0.5 ml/min (*see* Fig. 1).

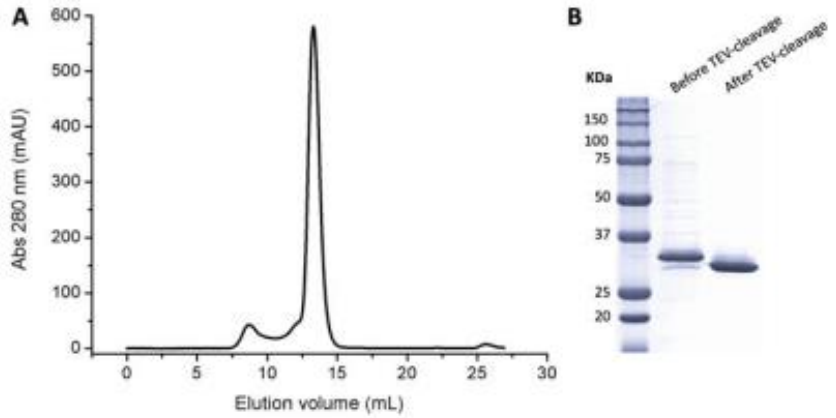

Fig. 1 LtaA purification. (**a**) Size-exclusion chromatography profile of purified LtaA. Superdex 200 Increase 10/300 GL. Void volume = 8.0 ml. (**b**) SDS-PAGE of purified LtaA before and after His-tag cleavage by TEV protease

11. Collect the main peak and change the buffer using a PD-10 column equilibrated in desalting buffer (*see* **Note 5**).
12. Collect eluate from PD-10 desalting column and measure concentration using a nanodrop.

3.3 Vapor Diffusion Crystallization

All steps are carried out at 4 °C unless stated otherwise (*see* **Notes 6** and 7).

1. Use the online "Make tray" tool of Hampton research (https://hamptonresearch.com/make_tray.aspx) to prepare a 8 × 6 crystallization screen, where the concentrations of components are varied: 30–50 mM magnesium acetate, 95–130 mM glycine pH 9.5, and 29–32% PEG 300.
2. Concentrate the protein using a 30 kDa MWCO Vivaspin™ 20 concentrator until the concentration reaches 6.0 mg/ml (*see* **Note 6**).
3. Centrifuge the concentrated protein at 20,000 × *g* for 5–15 min to remove heavy particles. Transfer protein to a new tube and keep it on ice.
4. Fill up the MRC Maxi 48-well plates with premade crystallization conditions (**step 1**).
5. Set up sitting-drop crystallization of LtaA by mixing drops of protein and reservoir solutions at 2:1 (1 μl:0.5 μl) ratios.
6. Seal the crystallization trays tightly with tape and carefully place them at 16 °C for crystals to grow.
7. Prepare cryo-protection buffers containing increasing concentrations of PEG 300 (up to 30% PEG 300).

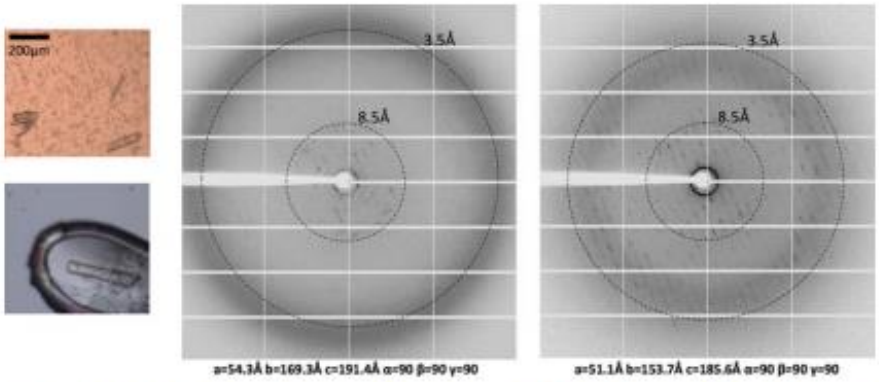

Fig. 2 Representative LtaA crystals and X-ray diffraction images before in situ annealing (*left*) and after in situ annealing (*right*). The difference in unit cell dimensions before and after in situ annealing demonstrates shrinking of the unit cell

8. Harvest LtaA crystals when they are fully grown in 1 week (*see* Fig. 2).
9. Perform sequential exchange of drop buffer and cryoprotection buffers under a light microscope. Let the solution to equilibrate for about 1 min every time the PEG 300 concentration is raised.
10. Harvest crystals using cryoloops and flash freeze them by immersion in liquid nitrogen.

3.4 In Situ Annealing and X-Ray Diffraction

1. Mount the crystal on goniometer at the beamline.
2. Perform in situ annealing by blocking the nitrogen-gas stream with a thin film for about 30 s while the crystal is still mounted on the goniometer [25]. It is important to not retract the cryojet and to observe that the flash-cooled drop turns slightly opaque (*see* **Note 7**) (*see* Fig. 2).
3. Expose the crystal to X-rays and collect datasets rotating the goniometer head 360° (*see* Fig. 2).

4 Notes

1. Optimizing expression conditions is an essential part of a crystallography project. Often large amounts of purified protein are necessary for screening crystallization conditions. We suggest carrying out screening of homologs, types of media, cell culture temperatures, and concentration of induction agents. A useful strategy for quick screening of homologs is to generate GFP fusion constructs and use in-gel fluorescence and fluorescence size-exclusion chromatography (FSEC).

2. As soon as a reliable expression protocol has been established, we recommend to use a GFP fusion construct to screen multiple detergents and buffer conditions in combination with in-gel fluorescence and FSEC to establish optimal solubilization parameters. Detergents that form small micelles promote formation of better crystal contacts; however in most cases they do not extract membrane proteins in high yields. Therefore, we recommend to screen for detergents that form large micelles and exchange them at a later point during purification for detergents that form small micelles.
3. A two-step washing strategy was applied to perform gently detergent exchange. Buffer 1 contains the same detergents as the solubilization buffer, whereas buffer 2 contains a different detergent (or mixture). Detergent exchange by using more than two buffers or by using concentration gradients can also be tested.
4. We recommend to test whether removing the affinity tag can have an impact on the stability and crystallization of the protein. In the case of LtaA, we noticed that removal of the tag was important to avoid aggregation during concentration (*see* Fig. 3).
5. We recommend to perform detergent exchange during SEC or after by using a PD-10 desalting column. In this particular case, exchanging to a detergent that forms small micelles was essential to obtain better protein crystals.
6. We recommend to test multiple protein concentrations and protein:mother-liquor ratios during early steps of crystallization screening experiments.
7. Flash-cooling and/or manipulation of protein crystals during flash-cooling can potentially cause lattice disorder. This is enhanced in crystals with high solvent content or with few intermolecular crystal contacts, as it is usually the case for membrane protein crystals. Lattice disorder results in increased mosaicity and reduced X-ray diffraction resolution. One potential way to resolve this issue is to use annealing techniques that involve warming the flash-cooled crystal and flash-cooling it again before data collection. In the case of LtaA crystals, the highest X-ray diffraction resolution achieved before annealing was 6–7 Å. We optimized a method for in situ annealing that included testing multiple annealing times, different thicknesses of films used to block the nitrogen-gas stream, and varying the distance of the cryo-stream to the crystal. The X-ray diffraction resolution achieved after crystal annealing was around 3.3–3.8 Å (*see* Fig. 2).

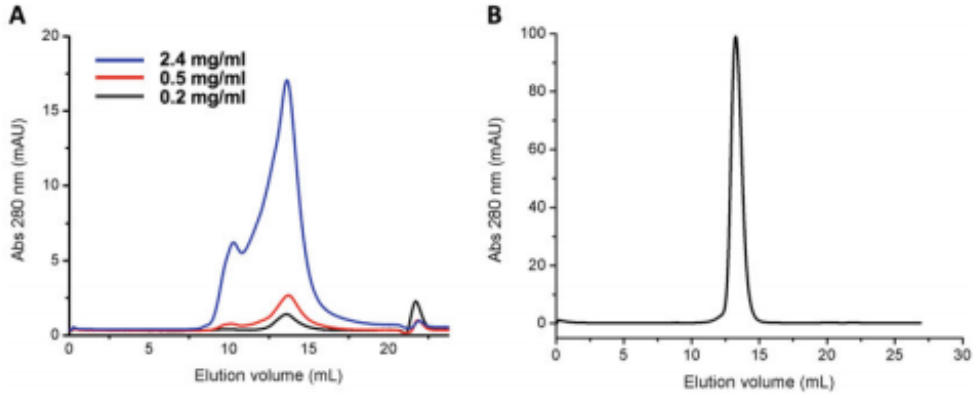

Fig. 3 Impact of His-tag removal on LtaA stability during concentration. (**a**) Size-exclusion chromatography profile of purified His_{10}-LtaA at different concentrations. (**b**) Size-exclusion chromatography profile of purified His-tag-less LtaA at 6 mg/ml. Superdex 200 Increase 10/300 GL. Void volume = 8.0 ml

Acknowledgments

We thank the staff at the PX beamline of the Swiss Light Source, Switzerland. This work was supported by the Swiss National Science Foundation (SNSF) (PP00P3_170607).

References

1. Neuhaus FC, Baddiley J (2003) A continuum of anionic charge: structures and functions of D-alanyl-teichoic acids in gram-positive bacteria. Microbiol Mol Biol Rev 67(4):686–723
2. Xia G, Kohler T, Peschel A (2010) The wall teichoic acid and lipoteichoic acid polymers of Staphylococcus aureus. Int J Med Microbiol 300(2–3):148–154. https://doi.org/10.1016/j.ijmm.2009.10.001
3. Saar-Dover R, Bitler A, Nezer R, Shmuel-Galia L, Firon A, Shimoni E, Trieu-Cuot P, Shai Y (2012) D-alanylation of lipoteichoic acids confers resistance to cationic peptides in group B streptococcus by increasing the cell wall density. PLoS Pathog 8(9):e1002891. https://doi.org/10.1371/journal.ppat.1002891
4. Fritz G, Mascher T (2014) A balancing act times two: sensing and regulating cell envelope homeostasis in Bacillus subtilis. Mol Microbiol 94(6):1201–1207. https://doi.org/10.1111/mmi.12848
5. Reichmann NT, Picarra Cassona C, Monteiro JM, Bottomley AL, Corrigan RM, Foster SJ, Pinho MG, Grundling A (2014) Differential localization of LTA synthesis proteins and their interaction with the cell division machinery in Staphylococcus aureus. Mol Microbiol 92(2):273–286. https://doi.org/10.1111/mmi.12551
6. Sewell EW, Brown ED (2014) Taking aim at wall teichoic acid synthesis: new biology and new leads for antibiotics. J Antibiot 67(1):43–51. https://doi.org/10.1038/ja.2013.100
7. Lee JH, Kim NH, Winstel V, Kurokawa K, Larsen J, An JH, Khan A, Seong MY, Lee MJ, Andersen PS, Peschel A, Lee BL (2015) Surface glycopolymers are crucial for in vitro antiwall teichoic acid IgG-mediated complement activation and opsonophagocytosis of Staphylococcus aureus. Infect Immun 83(11):4247–4255. https://doi.org/10.1128/IAI.00767-15
8. Gautam S, Kim T, Lester E, Deep D, Spiegel DA (2016) Wall teichoic acids prevent antibody binding to epitopes within the cell wall of Staphylococcus aureus. ACS Chem Biol 11(1):25–30
9. Abachin E, Poyart C, Pellegrini E, Milohanic E, Fiedler F, Berche P, Trieu-Cuot P (2002) Formation of D-alanyl-lipoteichoic

acid is required for adhesion and virulence of Listeria monocytogenes. Mol Microbiol 43 (1):1–14

10. Bucher T, Oppenheimer-Shaanan Y, Savidor A, Bloom-Ackermann Z, Kolodkin-Gal I (2015) Disturbance of the bacterial cell wall specifically interferes with biofilm formation. Environ Microbiol Rep 7:990. https://doi.org/10.1111/1758-2229.12346
11. Peschel A, Otto M, Jack RW, Kalbacher H, Jung G, Gotz F (1999) Inactivation of the dlt operon in Staphylococcus aureus confers sensitivity to defensins, protegrins, and other antimicrobial peptides. J Biol Chem 274 (13):8405–8410. https://doi.org/10.1074/jbc.274.13.8405
12. Campbell J, Singh AK, Santa Maria JP Jr, Kim Y, Brown S, Swoboda JG, Mylonakis E, Wilkinson BJ, Walker S (2011) Synthetic lethal compound combinations reveal a fundamental connection between wall teichoic acid and peptidoglycan biosyntheses in Staphylococcus aureus. ACS Chem Biol 6(1):106–116. https://doi.org/10.1021/cb100269f
13. Percy MG, Grundling A (2014) Lipoteichoic acid synthesis and function in gram-positive bacteria. Annu Rev Microbiol 68:81–100. https://doi.org/10.1146/annurev-micro-091213-112949
14. Fischer W (1993) Molecular analysis of lipid macroamphiphiles by hydrophobic interaction chromatography, exemplified with lipoteichoic acids. Anal Biochem 208(1):49–56. https://doi.org/10.1006/abio.1993.1007
15. Fischer W, Koch HU, Rosel P, Fiedler F, Schmuck L (1980) Structural requirements of lipoteichoic acid carrier for recognition by the poly(ribitol phosphate) polymerase from Staphylococcus aureus H. A study of various lipoteichoic acids, derivatives, and related compounds. J Biol Chem 255(10):4550–4556
16. Brown S, Santa Maria JP Jr, Walker S (2013) Wall teichoic acids of gram-positive bacteria. Annu Rev Microbiol 67:313–336. https://doi.org/10.1146/annurev-micro-092412-155620
17. Kiriukhin MY, Debabov DV, Shinabarger DL, Neuhaus FC (2001) Biosynthesis of the glycolipid anchor in lipoteichoic acid of Staphylococcus aureus RN4220: role of YpfP, the diglucosyldiacylglycerol synthase. J Bacteriol 183(11):3506–3514. https://doi.org/10.1128/JB.183.11.3506-3514.2001
18. Lu D, Wormann ME, Zhang X, Schneewind O, Grundling A, Freemont PS (2009) Structure-based mechanism of lipoteichoic acid synthesis by Staphylococcus aureus LtaS. Proc Natl Acad Sci U S A 106(5):1584–1589. https://doi.org/10.1073/pnas.0809020106
19. Tropea JE, Cherry S, Waugh DS (2009) Expression and purification of soluble His(6)-tagged TEV protease. Methods Mol Biol 498:297–307. https://doi.org/10.1007/978-1-59745-196-3_19
20. Casanas A, Warshamanage R, Finke AD, Panepucci E, Olieric V, Noll A, Tampe R, Brandstetter S, Forster A, Mueller M, Schulze-Briese C, Bunk O, Wang M (2016) EIGER detector: application in macromolecular crystallography. Acta Crystallogr D Struct Biol 72(Pt 9):1036–1048. https://doi.org/10.1107/S2059798316012304
21. Wojdyla JA, Panepucci E, Martiel I, Ebner S, Huang CY, Caffrey M, Bunk O, Wang M (2016) Fast two-dimensional grid and transmission X-ray microscopy scanning methods for visualizing and characterizing protein crystals. J Appl Crystallogr 49(Pt 3):944–952. https://doi.org/10.1107/S1600576716006233
22. Huang CY, Olieric V, Howe N, Warshamanage R, Weinert T, Panepucci E, Vogeley L, Basu S, Diederichs K, Caffrey M, Wang M (2018) In situ serial crystallography for rapid de novo membrane protein structure determination. Commun Biol 1:124. https://doi.org/10.1038/s42003-018-0123-6
23. Wojdyla JA, Kaminski JW, Panepucci E, Ebner S, Wang X, Gabadinho J, Wang M (2018) DA+ data acquisition and analysis software at the Swiss Light Source macromolecular crystallography beamlines. J Synchrotron Radiat 25(Pt 1):293–303. https://doi.org/10.1107/S1600577517014503
24. Basu S, Kaminski JW, Panepucci E, Huang C-Y, Warshamanage R, Wang M, Wojdyla JA (2019) Automated data collection and real-time data analysis suite for serial synchrotron crystallography. J Synchrotron Radiat 26 (1):244–252. https://doi.org/10.1107/S1600577518016570
25. Heras B, Martin JL (2005) Post-crystallization treatments for improving diffraction quality of protein crystals. Acta Crystallogr D Biol Crystallogr 61(Pt 9):1173–1180. https://doi.org/10.1107/S0907444905019451

3 Structure of a proton-dependent lipid transporter involved in lipoteichoic acids biosynthesis

Bing Zhang[1*], Xue Liu[2*], Elisabeth Lambert[1*], Guillaume Mas[1], Sebastian Hiller[1], Jan-Willem Veening[2], Camilo Perez[1†]

[1]Biozentrum, University of Basel, 4056 Basel, Switzerland.

[2]Department of Fundamental Microbiology, Faculty of Biology and Medicine, University of Lausanne, 1015 Lausanne, Switzerland.

[*]These authors contributed equally to this work

Author Contribution:

I carried out the expression, purification and crystallization of LtaA. I collected, processed diffraction datasets, and solved the LtaA structure with the aid of Camilo Perez.
I performed the synthesis of Glc_2-DAG, and did partial identification of the product.
I also conducted the *in vitro* flipping assays, and analyzed the data.
I measured the expression level of WT LtaA and six LtaA mutants in *S.aureus*.
I also contributed to the manuscript preparation.

nature structural & molecular biology

ARTICLES

https://doi.org/10.1038/s41594-020-0425-5

Check for updates

Structure of a proton-dependent lipid transporter involved in lipoteichoic acids biosynthesis

Bing Zhang[1,3], Xue Liu[2,3], Elisabeth Lambert[1,3], Guillaume Mas[1], Sebastian Hiller[1], Jan-Willem Veening[2] and Camilo Perez[1]✉

Lipoteichoic acids (LTAs) are essential cell-wall components in Gram-positive bacteria, including the human pathogen *Staphylococcus aureus*, contributing to cell adhesion, cell division and antibiotic resistance. Genetic evidence has suggested that LtaA is the flippase that mediates the translocation of the lipid-linked disaccharide that anchors LTA to the cell membrane, a rate-limiting step in *S. aureus* LTA biogenesis. Here, we present the structure of LtaA, describe its flipping mechanism and show its functional relevance for *S. aureus* fitness. We demonstrate that LtaA is a proton-coupled antiporter flippase that contributes to *S. aureus* survival under physiological acidic conditions. Our results provide foundations for the development of new strategies to counteract *S. aureus* infections.

The Gram-positive pathogen *S. aureus* is one of the leading causes of nosocomial infections around the globe[1,2]. Multiple strains have acquired resistance to clinically used antibiotics[1,2], and methicillin-resistant *S. aureus* (MRSA) is one of the most successful modern pathogens[1–4]. The cell wall of Gram-positive bacteria is primarily composed of peptidoglycan, wall-associated proteins, capsular polysaccharide and teichoic acids (TA)[5,6]. TA are divided in LTA and wall-teichoic acids (WTAs)[5–7], both of which are necessary for proper localization of the cell-wall elongation and division machinery, contribute to immune evasion by concealing cell-wall epitopes, prevent recognition and opsonization by antibodies and have been shown to be important for adhesion, colonization and biofilm formation[8–12]. By altering TA composition, Gram-positive bacteria are able to resist the action of hydrophobic antibacterial agents, cationic antimicrobial peptides, β-lactam and glycopeptide antibiotics[7,13,14].

From the five types of LTA known to date[5,15], the best characterized is type I LTA from *S. aureus*, which is recognized by Toll-like receptor 2 and has been associated with various inflammatory diseases ranging from minor skin diseases to severe sepsis[16,17]. *S. aureus* LTA are composed of a polymer of 1,3-glycerol-phosphate repeat units attached to C-6 of the non-reducing glucosyl of the anchor lipid-linked-disaccharide gentiobiosyl-diacylglycerol (anchor-LLD) embedded in the extracellular side of the plasma membrane[5–7,18]. Synthesis of the anchor-LLD occurs at the cytoplasmic leaflet of the membrane[19–22]. Thus, translocation of anchor-LLD across the plasma membrane is a requisite for extracellular assembly of LTA[7,19,23] (Fig. 1a), thus constituting a rate-limiting step in LTA synthesis since it regulates the pool of precursor anchor-LLD available. This translocation reaction is presumed to be catalyzed by the flippase LtaA, although its flippase activity has not been demonstrated. LtaA is found in all known *S. aureus* strains and also in closely related *Staphylococcus* species[19]. Deletion of the *ltaA* gene in *S. aureus* leads to attenuated virulence during animal infection and alterations in LTA composition, such as anchoring to phosphatidylglycerol and longer polymer length[7,19]. Despite the clear relevance of LtaA in LTA biogenesis, remarkably little is known about its mechanism and function, in part owing to the lack of structural information and the absence of comprehensive functional characterization in vitro and in vivo.

LtaA is a member of the major facilitator superfamily (MFS) of transporters[19]. The MFS superfamily, ubiquitously distributed across all kingdoms of life, consists of 74 families classified on the basis of their type of substrate[24]. In bacteria, MFS transporters are mainly used for the uptake of nutrients and extrusion of deleterious compounds. Whereas in humans, they are implicated in the transport of a wide range of toxins and drugs, and their malfunction leads to multiple diseases[25–27]. Currently, only six different MFS families have been structurally characterized[28–34]. However, there are no reports that describe the structure of flippases in any of the 74 MFS families.

To elucidate the mechanism of LtaA-catalyzed anchor-LLD flipping, we determined the structure of *S. aureus* LtaA, characterized its transport properties by in vitro flipping assays, and investigated its function and relevance in live *S. aureus* cells. The structure of LtaA revealed a 12 transmembrane helices (TM) MFS fold and displays an outward-facing conformation. The central cavity of LtaA shows a unique amphiphilic architecture never seen before in any of the structurally characterized MFS transporters. We show that LtaA is an antiporter flippase that couples anchor-LLD translocation to proton antiport, which confers LtaA pH-sensing properties used by *S. aureus* to cope with the acidic stress found under normal physiological conditions.

Results

LtaA displays in vitro flipping activity. To characterize the flipping mechanism of LtaA in vitro, it is essential to establish reliable measurements of lipid translocation activity of wild-type (WT) LtaA and variants. Lipid translocation has been investigated for other lipid transporters using fluorescently labelled substrates that, when exposed on the outer leaflet of proteoliposomes, are quenched by sodium dithionite, a membrane-impermeable reducing agent[35–37]. Because a suitable fluorescently labeled lipid substrate was so far not available for LtaA at the time of our study, we performed the chemoenzymatic synthesis of a nitrobenzoxadiazole (NBD)-labeled anchor-LLD (NBD-anchor-LLD) using recombinantly expressed

[1]Biozentrum, University of Basel, Basel, Switzerland. [2]Department of Fundamental Microbiology, Faculty of Biology and Medicine, University of Lausanne, Lausanne, Switzerland. [3]These authors contributed equally: Bing Zhang, Xue Liu, Elisabeth Lambert. ✉e-mail: camilo.perez@unibas.ch

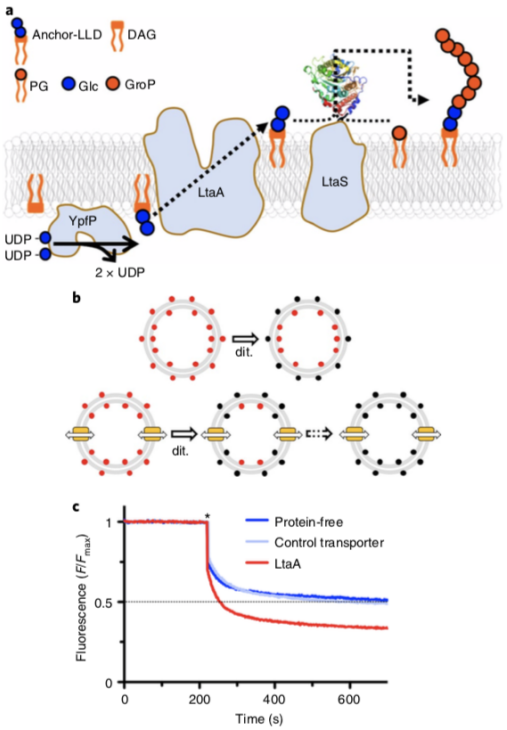

Fig. 1 | LtaA-catalyzed anchor-LLD flipping. a, LTA-synthesis pathway in *S. aureus*[5]. YpfP synthesizes the LTA anchor-LLD on the cytoplasmic leaflet of the membrane, and LtaA performs anchor-LLD flipping towards the extracellular side of the membrane, where the LtaS polymerase assembles the 1,3-glycerol-phosphate polymer on anchor-LLD. The structure of the periplasmic domain of LtaS (PDB: 4UOO)[22] is shown. PG, phosphatidylglycerol; DAG, diacylglycerol; Glc, glucose; GroP, glycerol-phosphate; anchor-LLD, gentiobiosyl-diacylglycerol. Figure adapted from Percy and Gründling[5]. **b**, Scheme of flipping assay. NBD-anchor-LLD lipids (red spheres) are irreversibly reduced (black spheres) by dithionite (dit.). In protein-free liposomes, only outer-leaflet fluorophores are reduced. In proteoliposomes containing LtaA (yellow boxes), a larger proportion of the fluorophores are reduced owing to exchange. Full fluorescence quenching will be achieved after prolonged incubation (dashed arrow). **c**, Flipping of NBD-anchor-LLD by LtaA. Representative traces shown are from protein-free liposomes and proteoliposomes containing either LtaA or a functionally unrelated transporter (bacterial choline transporter) ($n \geq 3$). Asterisk marks addition of dithionite. *F* corresponds to the fluorescence intensity measured for each time point. F_{max} is the average fluorescence measured during the first 200 seconds.

and purified YpfP[20,21]. In *S. aureus*, YpfP synthesizes the native LtaA substrate during LTA assembly (Fig. 1a). In an in vitro reaction, purified YpfP catalyzed the reaction between UDP-Glc and NBD-labeled diacylglycerol (NBD-DAG) to produce NBD-anchor-LLD. Tandem mass spectrometry (MS/MS), parallel-reaction monitoring (PRM), high-resolution liquid chromatography–mass spectrometry (HPLC–MS) and one-dimensional proton nuclear magnetic resonance (1D ^{1}H NMR) spectroscopy confirmed the presence of NBD-anchor-LLD in enriched extracts (Supplementary Figs. 1–8 and Supplementary Tables 1–6).

For the functional flipping assay, we incorporated NBD-anchor-LLD into protein-free liposomes or into LtaA proteoliposomes. Upon the addition of dithionite, the fluorescence of protein-free liposomes plateaus at about 50% of the total fluorescence (Fig. 1b,c), consistent with the expectation that NBD-anchor-LLD distributes symmetrically between the two leaflets and that it does not show spontaneous transbilayer diffusion, owing to its prominent hydrophilic disaccharide headgroup. In contrast, in LtaA-proteoliposomes, the NBD-anchor-LLD fluorescence plateaus at about 35% of the initial intensity, clearly demonstrating that LtaA possesses NBD-anchor-LLD flipping activity (Fig. 1b,c).

To verify that the flipping activity detected was LtaA-specific, we performed the same type of experiment but with a functionally unrelated protein (choline transporter) reconstituted in proteoliposomes (Fig. 1c). In this experiment, quenching by dithionite led to a fluorescence plateau of 50%, validating that the flipping activity observed in LtaA proteoliposomes is catalyzed by LtaA. Furthermore, control experiments with protein-free liposomes containing the precursor molecule NBD-DAG plateau at about 30% (Extended Data Fig. 1), consistent with spontaneous transbilayer diffusion of NBD-DAG due to its prominent hydrophobicity. Together, these experiments demonstrate that LtaA displays anchor-LLD flippase activity.

Structure of *S. aureus* LtaA. We determined the structure of LtaA from *S. aureus* at 3.3 Å resolution (Fig. 2a,b, Extended Data Figs. 2–4 and Table 1). Experimental phases were determined by single-wavelength anomalous diffraction (SAD) from selenomethionine (SeMet)-derivative crystals. The register of the resulting model was confirmed by the anomalous densities of 16 SeMet residues along the polypeptide chain (Extended Data Fig. 4). LtaA crystals commonly diffracted X-rays up to 7 Å resolution; however, by optimizing in situ annealing conditions[38], we were able to increase the diffraction resolution up to 3.3 Å, accompanied by an up to 18% reduction of the unit cell volume (Extended Data Fig. 2c).

LtaA displays the fold of MFS transporters, which consists of 12 TM divided into two 6TM domains (amino- and carboxy-terminal domains) related by a pseudo-rotational two-fold symmetry axis perpendicular to the plane of the membrane (Fig. 2a and Extended Data Fig. 5a). The fold of both domains is similar, showing an r.m.s. deviation (r.m.s.d.) of 3.2 Å upon secondary-structure superposition. Both domains are connected through a cytoplasmic helical loop, a structural feature observed in many other MFS fold transporters[39,40]. The LtaA structure displays an outward-facing state with two prominent lateral hydrophobic entrances (Fig. 2a and Extended Data Fig. 5b). One of the entrances is flanked by TMs 2 and 11, whereas TMs 5 and 8 flank the entrance on the opposite side. TM11 delimiting one of the hydrophobic entrances displays the antiporter motif[41] G ($G^{345}(X)_6G(X)_3GP(X)_2GG^{363}$), whereas on the opposite entrance, TM5 displays a similar motif-G-like sequence at the same position (Extended Data Fig. 5c). Access to the central cavity from the cytoplasmic face is sealed off by multiple interactions between TMs 2, 4 and 5 from the N-terminal domain, and TMs 8, 10 and 11 from the C-terminal domain, and cytoplasmic loops connecting TMs 4–5 and TMs 10–11 (Extended Data Fig. 5d).

One striking structural feature of LtaA architecture is the presence of a large amphiphilic central cavity whose hydrophilic part is harbored by the N-terminal domain of the flippase with the participation of residues E32, R35, D68, W127 and W150, located in TMs 1, 2, 4 and 5 (Fig. 2a,c). On the other hand, the hydrophobic part of the cavity is harbored by the C-terminal domain of the flippase with the participation of 8 hydrophobic residues located in TMs 7, 8, 9 and 10 (Fig. 2a,c). Such an amphiphilic cavity has

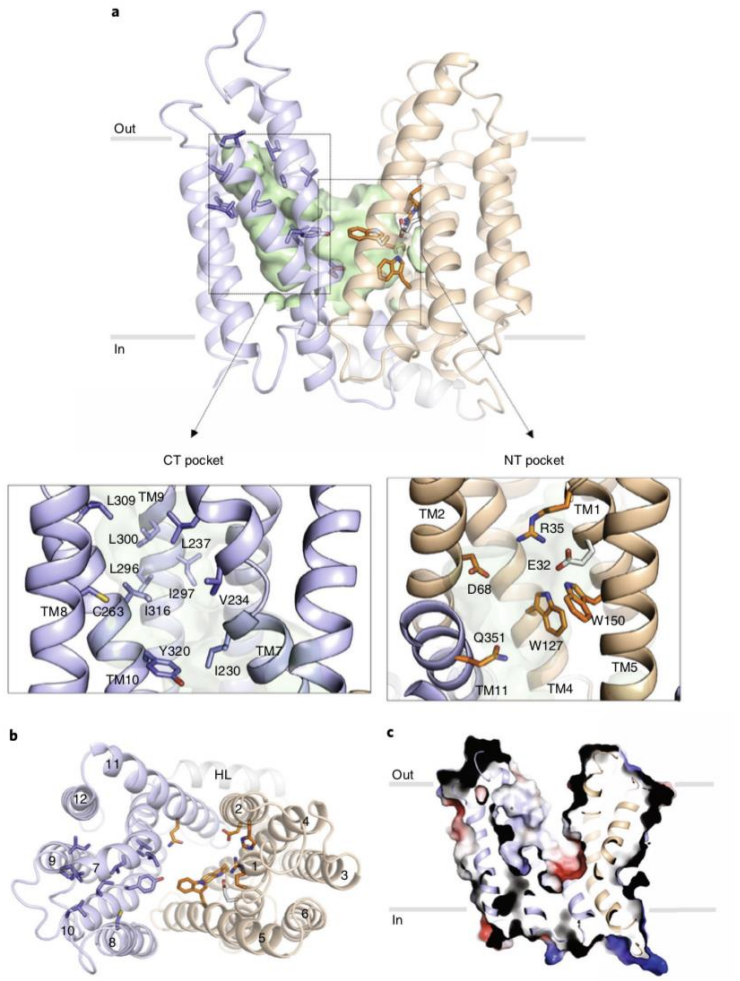

Fig. 2 | *S. aureus* LtaA structure. a, Structure of LtaA showing its central cavity (green surface). CT, C-terminal, NT, N-terminal. The N-terminal domain is shown in light orange, and the C-terminal domain is shown in light blue. Residues forming the hydrophobic C-terminal pocket and the hydrophilic N-terminal pocket are shown. **b**, Top view of LtaA. Residues in sticks participate in the formation of the amphiphilic cavity. TM segments are numbered. HL, helical loop. **c**, Vacuum electrostatic surface representation of LtaA, showing the internal cavity.

not been observed in any other MFS fold transporter described to date. Sequence-conservation analysis revealed that residues forming the N-terminal hydrophilic pocket are highly conserved among LtaA homologues found in other *Staphylococcus* species or further Gram-positive bacteria, whereas residues forming the C-terminal hydrophobic pocket are less conserved, although their positions are prominently occupied by amino acids with aliphatic side chains (Extended Data Fig. 6 and Supplementary Fig. 9).

LtaA displays high selectivity towards the headgroup of its substrate. We used computational docking to test whether the binding of anchor-LLD to outward-facing LtaA was feasible. The ligand-docking analysis suggests that the gentiobiosyl headgroup of the anchor-LLD is preferentially accommodated in the N-terminal hydrophilic pocket, whereas the diacylglycerol aliphatic tails are docked with one or both chains in the C-terminal hydrophobic pocket in multiple conformations (Fig. 3a and Extended Data Fig. 7a). This, together with the high sequence conservation of the residues forming the hydrophilic pocket, led us to hypothesize that LtaA might display high selectivity towards the anchor-LLD headgroup. To test this hypothesis, we assessed flipping activity in the presence of different disaccharide compounds (Fig. 3b–c and Extended Data Fig. 7b). If LtaA displays high selectivity towards the disaccharide headgroup of its substrate, one would expect to see

Table 1 | Data collection and refinement statistics

	LtaA (SeMet)[a] (PDB 6S7V)
Data collection	
Space group	$C222_1$
Cell dimensions	
a, *b*, *c* (Å)	51.39, 162.47, 191.05
α, β, γ (°)	90, 90, 90
Resolution (Å)	20–3.3 (3.4–3.3)[b]
R_{meas} (%)	13.5 (153.7) [22.1 (414.8)][c]
$I/\sigma(I)$	12.76 (1.64) [6.93 (1.36)]
$CC_{1/2}$ (%)	99.9 (94.4) [100 (86.8)]
Completeness (%)	83.37 (32.3) [98.37 (97.55)]
Redundancy	40 (39)
Refinement	
Resolution (Å)	20–3.3 (3.4–3.3)
No. reflections	12,387 [19,539]
R_{work} / R_{free} (%)	27.05/28.94
No. atoms	
Protein	3,001
B factors	
Protein	84
R.m.s. deviations	
Bond lengths (Å)	0.006
Bond angles (°)	0.987

[a]Data are from one crystal. [b]Values in parentheses are for highest-resolution shell. [c]Values in square brackets are before anisotropic truncation.

reduced flipping activity in the presence of an excess of gentiobiose (β-D-Glc-(1,6)-D-Glc), a disaccharide with the same chemical composition and conformation as the anchor-LLD headgroup. Indeed, we found that increasing concentrations of gentiobiose inhibit LtaA-catalyzed flipping activity, whereas other disaccharides, that is lactose (β-D-Gal-(1,4)-D-Glc), sucrose (α-D-Glc-(1,2)-β-D-Fru) and trehalose (α-D-Glc-(1,1)-α-D-Glc) showed no inhibitory effect at a similar concentration (Fig. 3c). These results indirectly but strongly suggest that LtaA displays high selectivity towards the headgroup of its substrate.

LtaA N-terminal hydrophilic pocket is crucial for flipping activity. Next, we assessed the functional role of residues in the highly conserved N-terminal hydrophilic pocket. According to our docking model, this pocket might accommodate the anchor-LLD headgroup. First, we constructed a *S. aureus* NCTC8325 Δ*ltaA* mutant, which we then complemented with an ectopic copy of the *ltaA* gene carrying single point mutations, and evaluated growth on agar plates at 37 °C and in the presence of 5% CO_2 (Fig. 3d). Strikingly, although *ltaA* was shown not to be essential under laboratory conditions[19], we found that non-complemented Δ*ltaA* mutants are non-viable in the presence of 5% CO_2, demonstrating that LtaA is crucial for *S. aureus* fitness. Mutants Y320A and Q351A rescued the growth defect of the Δ*ltaA* strain, whereas mutants E32A, R35A, D68A, W127A and W150A did not. Notably, under overexpression conditions, the mutants R35A, D68A, W127A and W150A, but not E32A, rescued the growth defect (Extended Data Figs. 8 and 9), indicating that E32 has a key role in LtaA activity.

Next, for several of the mutants tested for their ability to rescue Δ*ltaA*, we examined for the capacity to perform flipping of NBD-anchor-LLD. In vitro flipping assays with LtaA double mutants, which combine the five mutations that showed the stronger impact on *S. aureus* growth, revealed that the mutant R35A/D68A is not active and that the relative activity of mutants E32A/D68A and D68A/W150A is about half that of LtaA-WT (Fig. 3e,f). This agrees with our in vivo assays that revealed that the mutants E32A, R35A, D68A, W127A and W150A display a strong growth defect of the Δ*ltaA* strain (Fig. 3d). Taken together, these results indicate that slight modifications of the activity of LtaA are sufficient to perturb the assembly line of LTA, and in consequence, the fitness of *S. aureus*.

LtaA is a proton-coupled antiporter flippase. Charged residues located in substrate-binding sites of secondary transporters have been frequently associated with proton coupling because they may undergo pKa shifts as a consequence of structural changes during the transport cycle[39,42]. LtaA possesses three candidates for such pH-coupling residues, E32, R35 and D68, which are all located in the N-terminal hydrophilic part of the central amphiphilic cavity (Fig. 2a). We therefore explored whether anchor-LLD flipping could be energized by a proton-gradient by measuring LtaA catalyzed NBD-anchor-LLD flipping in proteoliposomes (Fig. 4a and Extended Data Fig. 10). In the absence of a proton gradient, quenching of the NBD-anchor-LLD reached a plateau at about 35% of the total fluorescence. Strikingly, if we imposed an inward proton gradient (low pH_{out}/high pH_{in}), larger quenching of NBD-anchor-LLD was observed. On the contrary, if we imposed an outward proton gradient (high pH_{out}/low pH_{in}), less quenching of NBD-anchor-LLD was observed, relative to no gradient conditions (Fig. 4a). As controls, we carried out the same type of experiment but with protein-free liposomes (Fig. 4b) and with a functionally unrelated protein reconstituted in proteoliposomes (Extended Data Fig. 10a); the result was that NBD-anchor-LLD quenching plateaued at about the same fluorescence level, independent of the pH gradient. In summary, these results reveal that LtaA performs vectorial flipping of anchor-LLD opposite to the direction of the proton gradient.

Protons transport mediated by LtaA was demonstrated using a fluorescence assay[43] in which proteoliposomes loaded with 100 mM KCl (pH 7.3) were diluted 20-fold into an assay buffer containing 10 mM KCl (pH 7.3). Under these conditions, if LtaA performs H^+ transport, the addition of the K^+-selective ionophore valinomycin will drive H^+ influx and cause quenching of the fluorophore 9-amino-6-chloro-2-methoxyacridine (ACMA). The robust fluorescence decrease observed upon the addition of valinomycin reflects H^+ influx into the proteoliposomes driven by the membrane potential (Fig. 4c). A control experiment with protein-free liposomes showed little fluorescence change (Fig. 4c).

We performed flipping assays and proton-transport assays with the single-point-mutant LtaA-E32A reconstituted in proteoliposomes (Fig. 4b,c). This residue was selected as the best candidate to undergo protonation and deprotonation because of its theoretical pKa-value of 7.8 in the current outward-facing structure, compared to residues R35 and D68 with pK_a values of 14 and 3.4, respectively. Our results show that the E32A mutation is insensitive to transmembrane proton gradients, maintaining basal activity (Fig. 4b). Consistent with this is the observed decrease of H^+ influx driven by the membrane potential (Fig. 4c). In summary, these data establish that LtaA works as a proton-coupled antiporter flippase, and that residue E32 plays a crucial role in proton coupling, presumably by being involved in proton transport. The importance of proton coupling for LtaA function in vivo becomes evident as pointed out by the strong growth defect of the *S. aureus* Δ*ltaA* strain expressing LtaA-E32A (Fig. 3d and Extended Data Fig. 9a).

LtaA is essential to combat acid stress. In *S. aureus* cells, synthesis of anchor-LLD by the glycosyltransferase YpfP occurs at the cytoplasmic leaflet without interruption as long as the levels of DAG

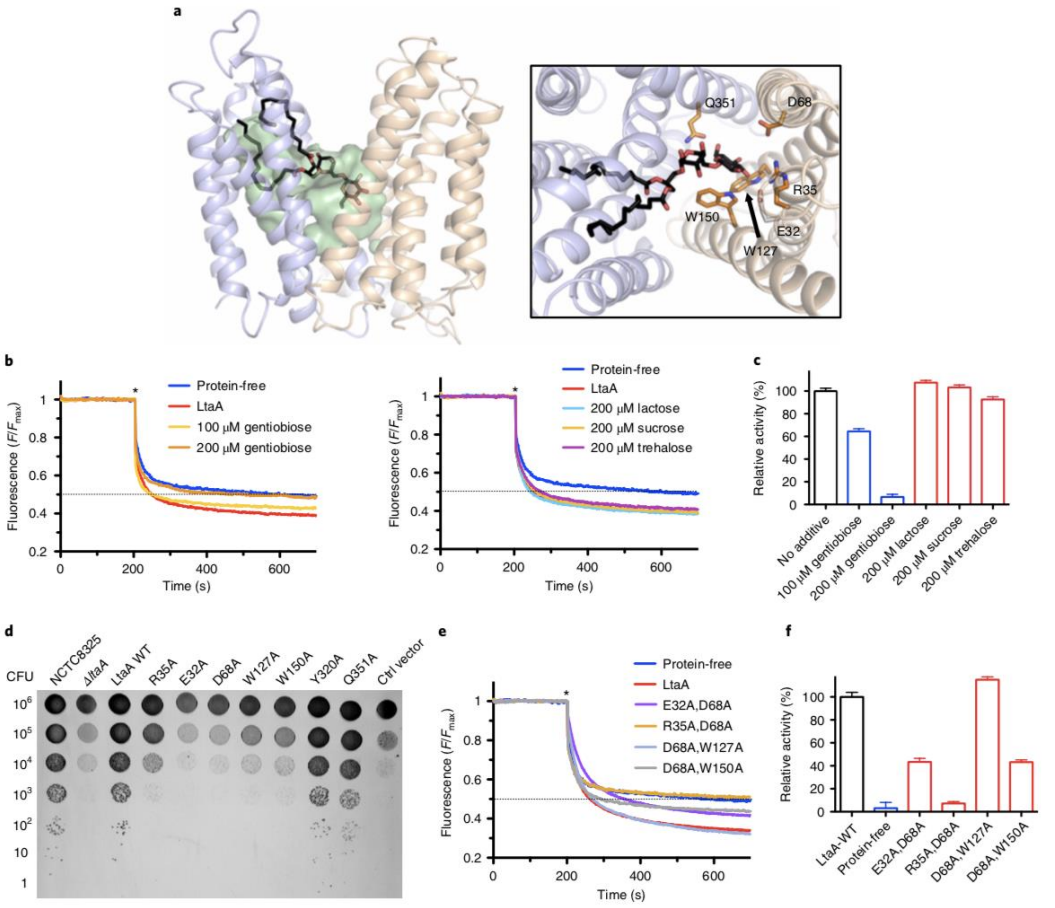

Fig. 3 | Amphiphilic cavity characterization. a, A model of lipid-linked-disaccharide docked into the amphiphilic cavity of LtaA (see also Extended Data Fig. 7a). The lipid tail length corresponds to C_{16} chains[19]. Right inset, top view of anchor-LLD binding pocket and residues coordinating its gentiobiosyl headgroup. **b**, Representative traces of LtaA-catalyzed flipping in the presence of different disaccharides at given concentrations ($n \geq 3$). **c**. Relative flipping activity of assays shown in **b**. Error bars indicate the s.d. of technical replicates, $n \geq 3$. **d**, Cell growth on IPTG-free C + Y agar plates at 37 °C and in the presence of 5% CO_2. Δ*ltaA* represents the *S. aureus* NCTC8325 Δ*ltaA* mutant; LtaA WT represents the Δ*ltaA* mutant complemented with WT *ltaA* on a multicopy vector (pLOW); Ctrl vector indicates the Δ*ltaA* mutant complemented with pLOW carrying a nonrelated gene (*dcas9*); the other labels represent the Δ*ltaA* mutant complemented with *ltaA* with corresponding point mutations. **e**, Representative traces of flipping activity of LtaA-WT and variants. **f**, Relative flipping activity of assays shown in **e**. Asterisk marks addition of dithionite. Error bars indicate the s.d. of technical replicates, $n \geq 3$. *F* corresponds to the fluorescence intensity measured for each time point. F_{max} is the average fluorescence measured during the first 200 seconds.

and UDP-Glc in the cell are preserved[20,21]. Under these conditions, healthy *S. aureus* displays an outward anchor-LLD gradient that would suffice to drive LtaA-facilitated flipping. Thus, we wondered whether the proton-coupling activity of LtaA could play an important role in the survival of *S. aureus* under physiological conditions encountered at the human nasopharynx and mucous membranes and on the skin, which present mild acidic environments ($5.0 < pH < 6.5$)[44–46].

To evaluate this hypothesis, we investigated the growth characteristics of *S. aureus* NCTC8325 Δ*ltaA* on plates at 37 °C under different pH conditions in the absence of CO_2 (ambient conditions) (Fig. 4d). We found that at high pH, the Δ*ltaA* mutant does not show a growth defect compared with WT or *ltaA*-complemented *S. aureus*, in line with previous findings[19]. However, very strong growth retardation was observed in the Δ*ltaA* mutant at low pH, while complementation with *ltaA*-WT restored normal growth. Alternatively, the presence of 5% CO_2, which acidifies the medium to about pH 6.0 owing to CO_2/HCO_3 equilibria, equivalently suffices to promote a strong growth defect of the Δ*ltaA* mutant (Fig. 4d). In the same way, point mutations of the proton-coupling E32 residue and others forming the N-terminal hydrophilic pocket showed a strong growth defect at low pH (Fig. 4e), consistent with their important role in

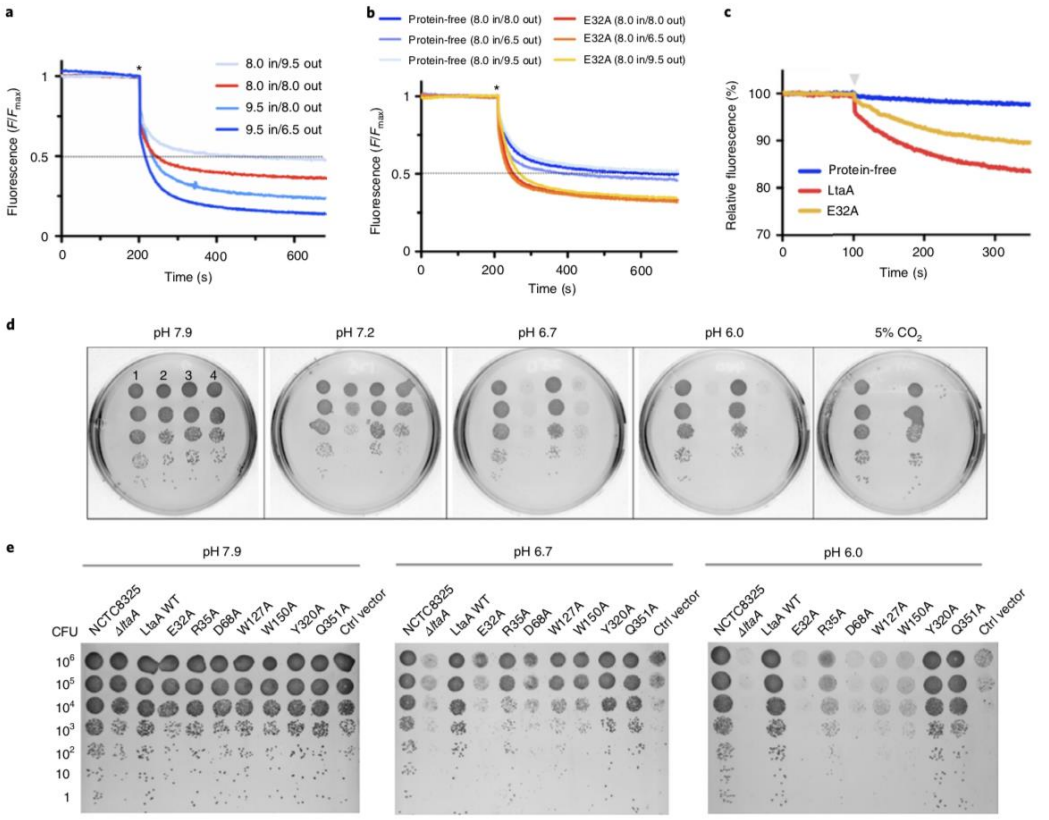

Fig. 4 | LtaA proton coupling and *S. aureus* Δ*ltaA* growth under acidic conditions. a,**b**, Representative traces of flipping assays with protein-free liposomes, LtaA-WT and LtaA-E32A, in the presence of different proton gradients; in and out denote the pH of the buffer inside and outside of liposomes, respectively ($n \geq 3$). Asterisk marks addition of dithionite. Traces in (**a**) are for LtaA-WT proteoliposomes. *F* correspond to the fluorescence intensity measured for each time point. F_{max} is the average fluorescence measured during the first 200 seconds. **c**, Proton-transport assay. Representative time courses are shown ($n \geq 3$). Proteoliposomes and protein-free liposomes containing 100 mM KCl were diluted in buffer containing 10 mM KCl and 9-amino-6-chloro-2-methoxyacridine (ACMA). H^+ influx was initiated by establishing a membrane potential by addition of the potassium ionophore valinomycin (gray triangle). **d**, Cell growth in IPTG-free C + Y agar plates under different pH conditions at 37 °C in the absence of CO_2 (ambient condition) or in the presence of 5% CO_2 (initial pH 7.9). 1 indicates *S. aureus* NCTC8325 WT, 2 indicates the Δ*ltaA* mutant, 3 indicates the Δ*ltaA* mutant complemented with WT *ltaA* on a multicopy vector (pLOW) and 4 indicates the Δ*ltaA* mutant complemented with pLOW carrying a functionally unrelated gene (*dcas9*). **e**, *S. aureus* NCTC8325 Δ*ltaA* mutant complemented with *ltaA* carrying corresponding point mutations. Shown is cell growth on IPTG-free C + Y agar plates under different pH conditions at 37 °C. LtaA WT represents Δ*ltaA* mutant complemented with wild type *ltaA*; Ctrl vector indicates Δ*ltaA* mutant complemented with a functionally unrelated gene (*dcas9*).

the coordination of the anchor-LLD headgroup and E32 essential role in proton transport, as shown above. The E32A mutant does not recover the growth defect at low pH even under overexpression conditions (Extended Data Fig. 9b). Fluorescence microscopy and transmission electron microscopy (TEM) of *S. aureus* NCTC8325 WT and Δ*ltaA* grown at 37 °C in LB medium at pH 6.5 or grown in the presence of 5% CO_2 (medium pH 6.5) showed that the *ltaA* deletion mutant displays aberrant cell morphologies, including enlarged cells, defects in the formation and localization of the division septum and abnormal cell-wall shape (Fig. 5a,b and Extended Data Fig. 9c).

Our results attribute an essential role to LtaA in the survival of *S. aureus* under acidic conditions. This is highly relevant because such conditions are encountered in the most common niches of this bacteria in the human body[44–47]. Thus, the development of drugs targeting LtaA might lead to new therapies for the treatment of *S. aureus* infections.

Discussion

Taken together, our biochemical and structural studies suggest a functional cycle in which LtaA performs anchor-LLD translocation energized by proton antiport (Fig. 6). The mechanism probably follows in its structural conformations the classic antiporter alternating-access cycle[48,49]. However, owing to the amphiphilic nature of the substrate, the conformational and energy landscape of lipid flipping by LtaA might look very different than that of canonical

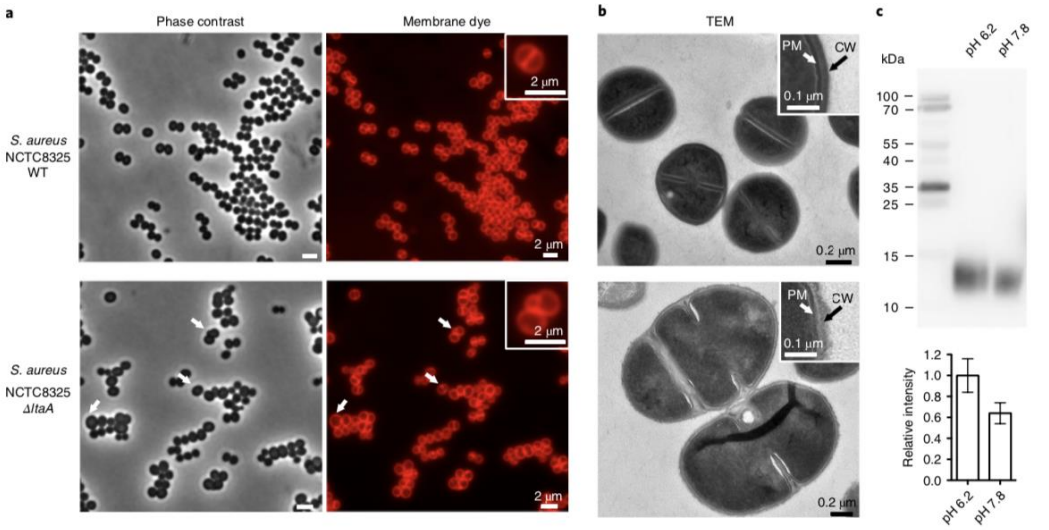

Fig. 5 | Morphology of *S. aureus* NCTC8325 WT and Δ*ltaA* mutant, and LTA abundance. a, Phase contrast and fluorescence images. Bacteria were grown to mid-exponential phase in LB medium at 37 °C with 5% CO_2, causing acidification of the medium. The membrane dye used was Nile red. White arrows point to cells with aberrant morphology. **b**, Transmission electron microscopy (TEM) images. PM indicates plasma membrane. CW indicates cell wall. Low-magnification images are shown in Extended Data Fig. 9c. **c**, Detection of LTA by immunoblotting. *S. aureus* NCT8325 was cultured in LB medium buffered with PBS to different pH (6.2 and 7.8) levels. Cell lysates were normalized on the basis of optical density. Samples were separated by 12% SDS–polyacrylamide gel electrophoresis and LTA was detected by an LTA (polyglycerolphosphate)-specific primary antibody. Histogram shows the relative amounts of LTA determined from band intensities ($n = 4$). Error bars indicate s.d. of technical replicates.

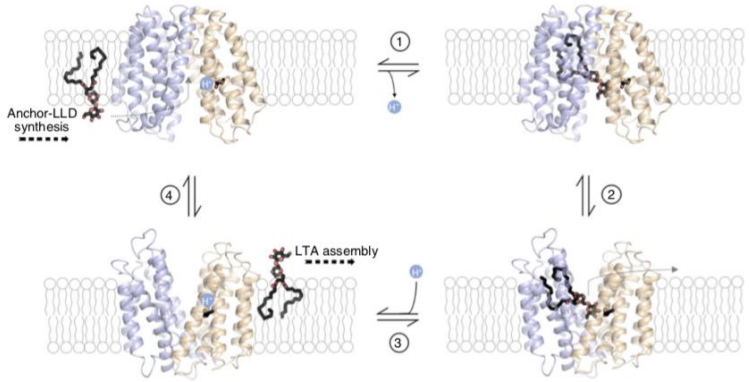

Fig. 6 | LtaA anchor-LLD flipping mechanism. 1, Binding of lipid-linked-disaccharide (black and red sticks) in the central cavity of LtaA in the inward-facing conformation (modeled conformation) and deprotonation of E32. 2, Transition to outward-facing state (structure determined in this study). 3, Substrate release into the membrane and protonation of E32. 4, Transition to inward-facing state (modeled conformation). The N-terminal domain is shown in light orange, and the C-terminal domain is shown in light blue. The inward-facing model of LtaA was constructed by rigid body alignment of the N-terminal domain (TM1–6) and the C-terminal domain (TM7–12) to those of inward-facing LacY (PDB: 2CFQ)[60].

transporters of water-soluble substrates. Specifically, substrate recognition, loading into the central cavity and release are expected to entail different mechanisms. In a first step, deprotonated LtaA in an inward-facing conformation recognizes and binds the anchor-LLD in its central cavity, positioning the lipid tails at the C-terminal hydrophobic pocket and the disaccharide headgroup at the N-terminal hydrophilic pocket. Recognition and extraction of the anchor-LLD from the pool of surrounding lipids are facilitated by specific binding of the gentiobiosyl headgroup, which allows extraction of the lipid out of the membrane. Subsequently, LtaA will change its conformation to an outward-facing state promoting substrate release into the membrane. We suggest that the prominent lateral entrances observed in

the crystal structure might facilitate the toppling of the anchor-LLD back into the bilayer. After substrate release in the outward-facing state, residue E32 will become protonated, facilitating the transition to an inward-facing state, where it will then undergo deprotonation. This mechanism explains the stimulation of transport by a proton gradient, and while in the absence of it, LtaA performs antiport driven by the outward directed anchor-LLD gradient maintained by the activity of YpfP in *S. aureus* cells. In the absence of a proton gradient, anchor-LLD translocation will happen at a slower rate in the cell, in full agreement with our in vitro flipping assays.

The LtaA flipping mechanism proposed here has certain similarities to the flipping mechanism proposed for the lipid-II flippase MurJ[50,51]. MurJ belongs to the multidrug/oligosaccharyl-lipid/polysaccharide (MOP) family of transporters, and plays an important role in peptidoglycan assembly[52]. Similar to the C-terminal hydrophobic pocket observed in LtaA, in MurJ, a hydrophobic groove formed by C-terminal TM helices 13 and 14 contributes to binding of the undecaprenyl lipid tail of lipid-II. These similarities suggest that secondary transporter flippases might share a mechanism wherein part of the internal cavity specializes in binding specific lipid moieties, facilitating in this way loading and translocation of amphiphilic molecules. Thus, the amphiphilic cavities observed in LtaA and MurJ might constitute a general structural signature that may contribute to the identification of other flippases in silico. The architecture of the outward-open LtaA structure provides the basis to understand anchor-LLD recognition, binding and release into the membrane. These results, together with the apparent high selectivity of LtaA for the anchor-LLD headgroup and inhibition of the flipping activity by gentiobiose, provide the structural basis to design inhibitors targeting LTA assembly.

The mechanism by which LtaA contributes to *S. aureus* survival under acidic conditions is intimately related to its capacity to couple anchor-LLD flipping to proton transport. This mechanism makes LtaA a 'pH sensing' flippase that, by increasing anchor-LLD transport under low pH conditions, enlarges the population of LTA at the outer leaflet of the plasma membrane (Fig. 5c). Besides the already-known important functions of LTA for cell division and protection against environmental threats[5,7–9], we hypothesize that increased amounts of LTA in the cell wall will probably provide an efficient way to buffer against acidification thanks to the high negative charge of the LTA backbone polymer. Notably, the description of a pH-sensing mechanism in a lipid transporter represents a fundamental conceptual advance in the field of lipid transport.

Membrane transport proteins performing unidirectional active translocation of lipids (flipping) generate membrane asymmetry[50,51,53–57]. On the other hand, membrane proteins that perform passive bidirectional translocation of lipids (scrambling) disrupt the membrane asymmetry[36,37,58]. Lipid flipping energized by ATP hydrolysis has been well characterized for multiple protein families[53,55–57]. Our results identify LtaA as a new class of flippase that energizes lipid translocation by coupling to a transmembrane proton gradient. These findings will potentiate the search of other ion-coupled flippases, not only in Gram-positive bacteria but in all prokaryotes. For example, it has been shown that the lipid-II flippase MurJ requires a membrane potential for its function[59]. In this case, in addition to driving export of lipid-II due to its intrinsic net negative charge, a membrane potential might drive lipid-II flipping by transport of a coupling ion, but this remains to be shown.

Online content

Any methods, additional references, Nature Research reporting summaries, source data, extended data, supplementary information, acknowledgements, peer review information; details of author contributions and competing interests; and statements of data and code availability are available at https://doi.org/10.1038/s41594-020-0425-5.

Received: 11 September 2019; Accepted: 30 March 2020;
Published online: 4 May 2020

References

1. Rivera, A. M. & Boucher, H. W. Current concepts in antimicrobial therapy against select Gram-positive organisms: methicillin-resistant Staphylococcus aureus, penicillin-resistant pneumococci, and vancomycin-resistant enterococci. *Mayo Clin. Proc.* **86**, 1230–1243 (2011).
2. Cosgrove, S. E. et al. The impact of methicillin resistance in *Staphylococcus aureus* bacteremia on patient outcomes: mortality, length of stay, and hospital charges. *Infect. Control Hosp. Epidemiol.* **26**, 166–174 (2005).
3. Turner, N. A. et al. Methicillin-resistant *Staphylococcus aureus*: an overview of basic and clinical research. *Nat. Rev. Microbiol.* **17**, 203–218 (2019).
4. Brown, S. et al. Methicillin resistance in *Staphylococcus aureus* requires glycosylated wall teichoic acids. *Proc. Natl Acad. Sci. USA* **109**, 18909–18914 (2012).
5. Percy, M. G. & Grundling, A. Lipoteichoic acid synthesis and function in Gram-positive bacteria. *Annu. Rev. Microbiol.* **68**, 81–100 (2014).
6. Brown, S., Santa Maria, J. P. Jr. & Walker, S. Wall teichoic acids of Gram-positive bacteria. *Annu. Rev. Microbiol.* **67**, 313–336 (2013).
7. Xia, G., Kohler, T. & Peschel, A. The wall teichoic acid and lipoteichoic acid polymers of *Staphylococcus aureus*. *Int. J. Med. Microbiol.* **300**, 148–154 (2010).
8. Reichmann, N. T. et al. Differential localization of LTA synthesis proteins and their interaction with the cell division machinery in *Staphylococcus aureus*. *Mol. Microbiol.* **92**, 273–286 (2014).
9. Sewell, E. W. & Brown, E. D. Taking aim at wall teichoic acid synthesis: new biology and new leads for antibiotics. *J. Antibiot. (Tokyo)* **67**, 43–51 (2014).
10. Lee, J. H. et al. Surface glycopolymers are crucial for in vitro anti-wall teichoic acid IgG-mediated complement activation and opsonophagocytosis of *Staphylococcus aureus*. *Infect. Immun.* **83**, 4247–4255 (2015).
11. Gautam, S., Kim, T., Lester, E., Deep, D. & Spiegel, D. A. Wall teichoic acids prevent antibody binding to epitopes within the cell wall of *Staphylococcus aureus*. *ACS Chem. Biol.* **11**, 25–30 (2016).
12. Bucher, T., Oppenheimer-Shaanan, Y., Savidor, A., Bloom-Ackermann, Z. & Kolodkin-Gal, I. Disturbance of the bacterial cell wall specifically interferes with biofilm formation. *Environ. Microbiol. Rep.* **7**, 990–1004 (2015).
13. Campbell, J. et al. Synthetic lethal compound combinations reveal a fundamental connection between wall teichoic acid and peptidoglycan biosyntheses in *Staphylococcus aureus*. *ACS Chem. Biol.* **6**, 106–116 (2011).
14. Peschel, A. et al. Inactivation of the *dlt* operon in *Staphylococcus aureus* confers sensitivity to defensins, protegrins, and other antimicrobial peptides. *J. Biol. Chem.* **274**, 8405–8410 (1999).
15. Reichmann, N. T. & Grundling, A. Location, synthesis and function of glycolipids and polyglycerolphosphate lipoteichoic acid in Gram-positive bacteria of the phylum Firmicutes. *FEMS Microbiol. Lett.* **319**, 97–105 (2011).
16. Hong, S. W. et al. Lipoteichoic acid of Streptococcus mutans interacts with Toll-like receptor 2 through the lipid moiety for induction of inflammatory mediators in murine macrophages. *Mol. Immunol.* **57**, 284–291 (2014).
17. Kang, S.-S., Sim, J.-R., Yun, C.-H. & Han, S. H. Lipoteichoic acids as a major virulence factor causing inflammatory responses via Toll-like receptor 2. *Arch. Pharm. Res.* **39**, 1519–1529 (2016).
18. Fischer, W., Koch, H. U., Rosel, P., Fiedler, F. & Schmuck, L. Structural requirements of lipoteichoic acid carrier for recognition by the poly(ribitol phosphate) polymerase from *Staphylococcus aureus* H. A study of various lipoteichoic acids, derivatives, and related compounds. *J. Biol. Chem.* **255**, 4550–4556 (1980).
19. Grundling, A. & Schneewind, O. Genes required for glycolipid synthesis and lipoteichoic acid anchoring in *Staphylococcus aureus*. *J. Bacteriol.* **189**, 2521–2530 (2007).
20. Jorasch, P., Wolter, F. P., Zahringer, U. & Heinz, E. A UDP glucosyltransferase from *Bacillus subtilis* successively transfers up to four glucose residues to 1,2-diacylglycerol: expression of *ypfP* in *Escherichia coli* and structural analysis of its reaction products. *Mol. Microbiol.* **29**, 419–430 (1998).
21. Kiriukhin, M. Y., Debabov, D. V., Shinabarger, D. L. & Neuhaus, F. C. Biosynthesis of the glycolipid anchor in lipoteichoic acid of *Staphylococcus aureus* RN4220: role of YpfP, the diglucosyldiacylglycerol synthase. *J. Bacteriol.* **183**, 3506–3514 (2001).
22. Grundling, A. & Schneewind, O. Synthesis of glycerol phosphate lipoteichoic acid in *Staphylococcus aureus*. *Proc. Natl Acad. Sci. USA* **104**, 8478–8483 (2007).
23. Lu, D. et al. Structure-based mechanism of lipoteichoic acid synthesis by *Staphylococcus aureus* LtaS. *Proc. Natl Acad. Sci. USA* **106**, 1584–1589 (2009).
24. Reddy, V. S., Shlykov, M. A., Castillo, R., Sun, E. I. & Saier, M. H. Jr. The major facilitator superfamily (MFS) revisited. *FEBS J.* **279**, 2022–2035 (2012).
25. Cura, A. J. & Carruthers, A. Role of monosaccharide transport proteins in carbohydrate assimilation, distribution, metabolism, and homeostasis. *Compr. Physiol.* **2**, 863–914 (2012).
26. Smith, D. E., Clemencon, B. & Hediger, M. A. Proton-coupled oligopeptide transporter family SLC15: physiological, pharmacological and pathological implications. *Mol. Aspects Med.* **34**, 323–336 (2013).

27. Quistgaard, E. M., Low, C., Guettou, F. & Nordlund, P. Understanding transport by the major facilitator superfamily (MFS): structures pave the way. *Nat. Rev. Mol. Cell Biol.* **17**, 123–132 (2016).
28. Iancu, C. V., Zamoon, J., Woo, S. B., Aleshin, A. & Choe, J.-Y. Crystal structure of a glucose/H^+ symporter and its mechanism of action. *Proc. Natl Acad. Sci. USA* **110**, 17862–17867 (2013).
29. Deng, D. et al. Molecular basis of ligand recognition and transport by glucose transporters. *Nature* **526**, 391–396 (2015).
30. Sun, L. et al. Crystal structure of a bacterial homologue of glucose transporters GLUT1–4. *Nature* **490**, 361–366 (2012).
31. Pedersen, B. P. et al. Crystal structure of a eukaryotic phosphate transporter. *Nature* **496**, 533–536 (2013).
32. Zheng, H., Wisedchaisri, G. & Gonen, T. Crystal structure of a nitrate/nitrite exchanger. *Nature* **497**, 647–651 (2013).
33. Yan, H. et al. Structure and mechanism of a nitrate transporter. *Cell Rep.* **3**, 716–723 (2013).
34. Newstead, S. et al. Crystal structure of a prokaryotic homologue of the mammalian oligopeptide-proton symporters, PepT1 and PepT2. *EMBO J.* **30**, 417–426 (2011).
35. Menon, I. et al. Opsin is a phospholipid flippase. *Curr. Biol.* **21**, 149–153 (2011).
36. Brunner, J. D., Lim, N. K., Schenck, S., Duerst, A. & Dutzler, R. X-ray structure of a calcium-activated TMEM16 lipid scramblase. *Nature* **516**, 207–212 (2014).
37. Malvezzi, M. et al. Ca^{2+}-dependent phospholipid scrambling by a reconstituted TMEM16 ion channel. *Nat .Commun.* **4**, 2367 (2013).
38. Hanson, B. L. & Bunick, G. J. Annealing macromolecular crystals. *Methods Mol. Biol.* **364**, 31–42 (2007).
39. Nagarathinam, K. et al. Outward open conformation of a major facilitator superfamily multidrug/H^+ antiporter provides insights into switching mechanism. *Nat. Commun.* **9**, 4005 (2018).
40. Bibi, E. & Kaback, H. R. In vivo expression of the *lacY* gene in two segments leads to functional lac permease. *Proc. Natl Acad. Sci. USA* **87**, 4325–4329 (1990).
41. Varela, M. F., Sansom, C. E. & Griffith, J. K. Mutational analysis and molecular modelling of an amino acid sequence motif conserved in antiporters but not symporters in a transporter superfamily. *Mol. Membr. Biol.* **12**, 313–319 (1995).
42. Smirnova, I. N., Kasho, V. & Kaback, H. R. Protonation and sugar binding to LacY. *Proc. Natl Acad. Sci. USA* **105**, 8896–8901 (2008).
43. Feng, L., Campbell, E. B. & MacKinnon, R. Molecular mechanism of proton transport in CLC Cl^-/H^+ exchange transporters. *Proc. Natl Acad. Sci. USA* **109**, 11699–11704 (2012).
44. du Plessis, J. L., Stefaniak, A. B. & Wilhelm, K. P. Measurement of skin surface pH. *Curr. Probl. Dermatol.* **54**, 19–25 (2018).
45. Frank, D. N. et al. The human nasal microbiota and Staphylococcus aureus carriage. *PLoS ONE* **5**, e10598 (2010).
46. Harell, M., Mover-Lev, H., Levy, D. & Sade, J. Gas composition of the human nose and nasopharyngeal space. *Acta Otolaryngol.* **116**, 82–84 (1996).
47. Williams, M. R., Nakatsuji, T. & Gallo, R. L. *Staphylococcus aureus*: master manipulator of the skin. *Cell Host Microbe* **22**, 579–581 (2017).
48. Law, C. J., Maloney, P. C. & Wang, D. N. Ins and outs of major facilitator superfamily antiporters. *Annu. Rev. Microbiol.* **62**, 289–305 (2008).
49. Jardetzky, O. Simple allosteric model for membrane pumps. *Nature* **211**, 969–970 (1966).
50. Kuk, A. C., Mashalidis, E. H. & Lee, S.-Y. Crystal structure of the MOP flippase MurJ in an inward-facing conformation. *Nat. Struct. Mol. Biol.* **24**, 171–176 (2017).
51. Zheng, S. et al. Structure and mutagenic analysis of the lipid II flippase MurJ from *Escherichia coli*. *Proc. Natl Acad. Sci. USA* **115**, 6709–6714 (2018).
52. Sham, L. T. et al. Bacterial cell wall. MurJ is the flippase of lipid-linked precursors for peptidoglycan biogenesis. *Science* **345**, 220–222 (2014).
53. Timcenko, M. et al. Structure and autoregulation of a P4-ATPase lipid flippase. *Nature* **571**, 366–370 (2019).
54. Hiraizumi, M., Yamashita, K., Nishizawa, T. & Nureki, O. Cryo-EM structures capture the transport cycle of the P4-ATPase flippase. *Science* **365**, 1149–1155 (2019).
55. Perez, C. et al. Structure and mechanism of an active lipid-linked oligosaccharide flippase. *Nature* **524**, 433–438 (2015).
56. Mi, W. et al. Structural basis of MsbA-mediated lipopolysaccharide transport. *Nature* **549**, 233–237 (2017).
57. Bi, Y., Mann, E., Whitfield, C. & Zimmer, J. Architecture of a channel-forming O-antigen polysaccharide ABC transporter. *Nature* **553**, 361–365 (2018).
58. Kalienkova, V. et al. Stepwise activation mechanism of the scramblase nhTMEM16 revealed by cryo-EM. *Elife* **8**, e44364 (2019).
59. Rubino, F. A., Kumar, S., Ruiz, N., Walker, S. & Kahne, D. E. Membrane potential is required for MurJ function. *J. Am. Chem. Soc.* **140**, 4481–4484 (2018).
60. Mirza, O., Guan, L., Verner, G., Iwata, S. & Kaback, H. R. Structural evidence for induced fit and a mechanism for sugar/H^+ symport in LacY. *EMBO J.* **25**, 1177–1183 (2006).

Methods

LtaA expression and purification. LtaA was overexpressed in *E. coli* BL21-Gold (DE3) (Stratagene) cells. Cells were transformed with a modified pET-19b vector (Novagen) carrying the gene encoding *S. aureus* LtaA with an N-terminal histidine 10 (His10) affinity tag. Cells were grown at 37 °C in Terrific Broth medium supplemented with 1% glucose (wt/vol) and induced with 0.2 mM IPTG. Cells were collected and resuspended in 50 mM Tris-HCl, pH 8.0; 500 mM NaCl; 5 mM β-mercaptoethanol; and 0.5 mM PMSF, disrupted and membranes were collected by ultracentrifugation. Membranes containing LtaA were solubilized in 50 mM Tris-HCl, pH 8.0; 200 mM NaCl; 20 mM Imidazole; 15% glycerol (vol/vol); 5 mM β-mercaptoethanol; 1% lauryl maltose neopentyl glycol (wt/vol) (LMNG, Anatrace); 1% N-dodecyl-*β*-D-maltopyranoside (wt/vol) (DDM, Anatrace) for 2 h at 4 °C. After centrifugation, the supernatant was loaded onto a Ni-NTA superflow affinity column (Qiagen), washed with 50 mM Tris-HCl, pH 8.0; 200 mM NaCl; 50 mM imidazole; 10% glycerol (vol/vol); 5 mM β-mercaptoethanol; 0.02% LMNG and 0.02% DDM and then washed a second time with the in the same buffer containing 200 mM Imidazole. Imidazole was removed by desalting using a PD-10 column (GE Healthcare). The His10 affinity tag was removed by overnight treatment with tobacco etch virus (TEV) protease. TEV protease was later removed by passing through Ni-NTA affinity column. LtaA was further purified by size exclusion chromatography (SEC) in buffer 10 mM Tris-HCl pH 8.0, 150 mM NaCl, 0.02% LMNG (Superdex 200 Increase 10/300 GL, GE Healthcare). The main peak was collected and the buffer exchanged to 10 mM Tris-HCl pH 8.0, 150 mM NaCl, 0.1% Cymal-7 (Anatrace) using a PD-10 desalting column[61].

SeMet derivative production. *E. coli* BL21-Gold (DE3) (Stratagene) cells carrying the LtaA expression vector were grown in TB-glucose medium at 37 °C until an optical density at 600 nm (OD_{600}) of 0.5–1.0 was reached. These were then used to inoculate a preculture of M9 medium supplemented with vitamin B1 hydrochloride. Cells were then grown until OD_{600} was 0.5 and were used to inoculate 2 L of M9 medium supplemented with vitamin B1 hydrochloride. Cells were grown overnight at 37 °C until OD_{600} was ~0.9, followed by the addition of an amino acids/SeMet cocktail and incubation for 30 min. SeMet-LtaA expression was induced with 0.2 mM IPTG and 90 min incubation.

LtaA crystallization. LtaA was concentrated up to 6.0 mg per mL using a 30-kDa MWCO Vivaspin 20 concentrator (GE healthcare). After extensive optimization of crystallization conditions, LtaA crystals were obtained at 16 °C using sitting-drop vapor diffusion. Plate-shaped crystals were obtained in reservoir conditions containing 30–70 mM magnesium acetate, 80–120 mM glycine pH 9.5 and 30–34% PEG 300. Crystals appeared after 3–4 d and matured to full size within 1 week. Crystals were dehydrated and cryoprotected by gently increasing PEG 300 concentration in the drop followed by flash freezing by immersion in liquid nitrogen[61].

In situ annealing and data collection. LtaA crystals diffracted X-rays up to about 6–7 Å resolution in general. Performing in situ annealing led to X-rays diffraction to higher resolution (3.8 Å to 3.3 Å, depending on the crystal)[61]. In situ annealing was performed by blocking the cold nitrogen stream with a thin film while the crystal was mounted on the goniometer. Annealing time, thickness of the film and distance of the cryo-stream to the crystal were critical parameters to optimize. The X-ray diffraction patterns displayed in Extended Data Fig. 2c show an example of diffraction before and after annealing. Enhancement in X-rays diffraction resolution was accompanied by a 10% to 18% reduction of the unit cell volume. The best datasets were collected from crystals exposed to X-rays only after annealing. An annealing time of about 10 s produced the best results. Three datasets collected from one LtaA crystal were merged and used to determine the structure. This LtaA crystal showed anisotropic diffraction up to 3.3 Å and belonged to the space group $C222_1$, with unit cell constants $a = 51.39$ Å, $b = 162.47$ Å and $c = 191.05$ Å, and $\alpha = 90°$, $\beta = 90°$ and $\gamma = 90°$ (Table 1). Data were processed and merged with XDS[62] and anisotropic scaling/ellipsoid truncation was performed. Resolution limits after ellipsoid truncation were $a^* = 3.0$ Å, $b^* = 4.0$ Å and $c^* = 3.5$ Å. We used a Karplus CC* (Pearson correlation coefficient)-based data-cutoff approach to determine the usable resolution of the datasets[63]. The resolution limit was set taking into account a $CC_{1/2} > \sim 40\%$ based on data-merging statistics and a CC* analysis against unmerged intensities in Phenix package[64] satisfying Karplus CC* against CC_{work} and CC_{free} criteria, as well as R_{free} of the highest-resolution shell against the refined structure being less than or equal to ~50% (Table 1). A second criterion for limiting the resolution was the overall completeness percentage observed after anisotropic ellipsoid truncation, which was kept above 80%. Diffraction data were collected at the beamline X06SA at the Swiss Light Source (SLS, Villigen).

Structure determination. The structure of LtaA was solved by single-wavelength anomalous diffraction (SAD). SeMet positions were found using SHELX[65] and refined using CCP4i2 programs[66], CRANK2 (ref. [67]) and PHASER[68]. Solvent flattening and density modification were performed using PARROT[69]. The resulting phases and electron-density maps were used to build an initial model. The anomalous densities of 16 SeMet residues along the polypeptide chain aided in tracing the correct amino acids register in the resulting model (Extended Data Fig. 4). Tracing of TM helices was facilitated by placing fractions of a LtaA homology model generated by Swissmodel[70] using as reference model the structure of the MFS transporter YajR[71] (PDB: 3WDO). Model building was performed in Coot[72]. Subsequently, multiple rounds of molecular replacement combined with single-wavelength anomalous diffraction (MR-SAD) in CRANK2 (ref. [67]) contributed to further improvement of the initial phases and electron-density maps, facilitating the improvement of the model. Multiple rounds of refinement and model building were then performed using Phenix[64] and Coot[72]. Map sharpening was used to facilitate model building. X-ray data and refinement statistics are given in Table 1. The final refined structure has $R_{work} = 27.05\%$ and $R_{free} = 28.94\%$, with 93.35% of residues in the Ramachandran-favored region; 6.38% in Ramachandran allowed; and 0.27% as Ramachandran outliers. Molecular graphics were created in PyMOL[73]. Surface electrostatics were calculated with the APBS PyMOL plugin.

YpfP expression and purification. YpfP with an N-terminal His10 affinity tag was overexpressed in *E. coli* BL21-Gold (DE3) (Stratagene) cells by IPTG induction. Cells were disrupted by sonication, and YpfP was purified using affinity chromatography. YpfP was desalted in buffer 50 mM Tris-HCl pH 8.0, 200 mM NaCl, 10 % glycerol, concentrated to 2.4 mg per ml, flash frozen in liquid nitrogen and stored at −80 °C.

Synthesis of NBD-anchor-LLD. Synthesis of fluorescently labeled NBD-anchor-LLD was performed following a modification of the protocol described by Jorasch et al.[20] and Kiriukhin et. al.[21] and . Purified YpfP was incubated with 2 mM UDP-glucose (Sigma) and 2mM l-NBD-decanoyl-2-decanoyl-sn-glycerol (Cayman) at 30 °C for about 16 h. The reaction product was separated using thin-layer chromatography (TLC) in a solvent mixture consisting of chloroform:methanol:water (65:25:4, vol/vol/vol)[19] (Supplementary Fig. 1). NBD-lipids were visualized in a fluorescence scanner (Amersham Typhoon Imaging System). The main product was extracted from the silica using a 50:50 mixture of chloroform:methanol, followed by evaporation of solvents. The extracted product was resuspended in buffer 50 mM Tris-HCl pH 8.0, 200 mM NaCl, 3% glycerol.

HPLC–MS product analysis. Samples of NBD-DAG (Cayman), completed reaction, and extracted product from preparative TLC (NBD-DAG-Glc_2) were subjected to HPLC–MS analysis using a ReproSil-Pur ODS-3 column (Dr. Maisch) and a flow rate of 1 mL per min with a solvent gradient elution of 0.1% acetic acid (Eluent A) against acetonitrile with 0.1% formic acid (Eluent B). The gradient consisted of 95% of eluent A to 95% of eluent B over a range of 22 min. The eluted species were analysed on a Bruker microTOF electrospray ionization mass spectrometer (Bruker Daltonics) in positive-ion mode with the following settings: capillary voltage, 4,500 V; nebulizer pressure, 2 bar; drying gas, 9 L per min at 220 °C; mass range, 50–2000 *m/z*.

MS/MS and PRM LC–MS analysis. Pure NBD-DAG (Cayman) and extracted NBD-DAG-Glc_2 (10 pmol per µL in 30% acetonitrile/69.9% water/0.1% formic acid) were prepared and analyzed by high-resolution mass spectrometry on a Q-Exactive mass spectrometer equipped with a heated electrospray ionization (HESI-II) probe (both Thermo Fisher Scientific) with direct infusion. For both molecules, full and tandem mass spectra were acquired at a resolution of 140,000 FWHM (at 200 *m/z*). The three most intense fragment ions were manually selected for quantitative parallel-reaction monitoring (PRM) MS analysis[74]. The setup of the µRPLC-MS system was as described previously[75]. The extracted ion chromatograms (XICs) were obtained using the most intense fragments selected before and employed for quantification (Supplementary Notes).

NMR product analysis. NBD-DAG and DGDG were dissolved in $CDCl_3$ at a concentration of 100 µM and 75 µM, respectively. NBD-anchor-LLD was extracted from TLC plates and dissolved in $CDCl_3$ for NMR analysis. The experiments were recorded at 298 K on a Bruker Ascend 600 MHz spectrometer running Topspin 3.2 equipped with a cryogenically cooled triple-resonance probe, using a 16 ppm spectral width, 30° flip angle, 1.5 -s relaxation delay and 2.7-s acquisition time. All data were processed with Bruker TOPSPIN-NMR software (version 3.2, Bruker).

Formation of LtaA proteoliposomes. We reconstituted LtaA in unilamellar liposomes prepared by extrusion through polycarbonate filters (400-nm pore size) from a 3:1 (wt:wt) mixture of *E. coli* polar lipids and L-α-phosphatidylcholine (Avanti). Liposomes were diluted in buffer containing 20 mM Tris-HCl pH 8.0, 150 mM NaCl and 2 mM β-mercaptoethanol. After saturation with DDM (Anatrace), liposomes were mixed with purified protein at a 50:1 (wt/wt) lipid/protein ratio. Removal of detergent was performed by incubation with BioBeads (Biorad). Proteoliposomes containing a final concentration of 20 mg per mL lipids; 7.8 µM LtaA were centrifuged, washed and resuspended before being used for NBD-anchor-LLD reconstitution or stored at −80 °C after being frozen in liquid nitrogen. Before flipping assays, proteoliposomes were thawed and β-mercaptoethanol was removed by freeze/thaw cycles and washing upon

ultracentrifugation. NBD-anchor-LLD was then incorporated into proteoliposomes performing freeze/thaw cycles and extrusion through a polycarbonate filter (400-nm pore size). LtaA/NBD-anchor-LLD proteoliposomes were then immediately used for flipping assays. Protein-free proteoliposomes were prepared in the same way, but without the addition of protein.

In vitro flipping assay. LtaA/NBD-anchor-LLD proteoliposomes, protein-free NBD-anchor-LLD liposomes and control transporter NBD-anchor-LLD proteoliposomes were diluted in buffer 20 mM Tris-HCl pH8.0, 150 mM NaCl before extrusion through polycarbonate filters (400-nm pore size). For sodium- and pH-gradient experiments, proteoliposomes were subjected to freeze/thaw cycles and resuspended in two steps: (1) in 200 µL of the same 'internal buffer' before extrusion; and (2) dilution in 800 µL of 'external buffer' before starting fluorescence recording. This was performed in order to minimize the effect of pH equilibration inside and outside proteoliposomes. Internal and external buffer compositions were 20 mM of either Tris pH 8.0, MES pH 6.5 or glycine pH 9.5, together with 150 mM NaCl or 150 mM KCl. Flipping of the NBD-anchor-LLD was measured by determining the percentage of NBD-fluorescence that is quenched by 5 mM sodium dithionite (Sigma) added after 200 s of starting fluorescence recording. At 100 s before data recording was finished, 0.5% Triton X100 was applied to permeabilize the liposomes, making all NBD-anchor-LLD molecules accessible to dithionite reduction. Fluorescence was recorded at 20 °C using a Jasco Fluorimeter. Excitation and emission wavelengths were 470 and 535 nm, respectively. For analysis, the fluorescence intensity was normalized to F/F_{max}. Relative flipping activities were calculated as follows: relative activity = $100 \times ((F/F_{max})_i - (F/F_{max})_{liposomes}) / ((F/F_{max})_{wt} - (F/F_{max})_{liposomes})$, where i corresponds to each respective treatment/mutants, liposomes corresponds to liposomes without protein, wt corresponds to WT LtaA proteoliposomes and F/F_{max} values correspond to the observed plateau for each recording. Curves were plotted using GraphPad Prism 5. Time courses of the dithionite-induced fluorescence decay in liposomes were repeated at least three times for each individual experiment.

Proton-transport assay. Purified LtaA WT or the variant LtaA-E32A were reconstituted into POPE:POPG (3:1) liposomes at a protein to lipid ratio of 1:50 (wt/wt). Synthetic anchor-LLD, produced from 1,2-dimyristoyl-sn-glycerol (Avanti) and 2 mM UDP-glucose, as described above, was incorporated into proteoliposomes after freeze/thaw cycles were performed. Proteoliposomes and protein-free liposomes were resuspended in 5 mM Tris-HCl/HEPES pH 7.3, 100 mM KCl and extruded through a polycarbonate filter (400-nm pore size). After a brief sonication, proteoliposomes were 20-fold diluted in buffer containing 5 mM Tris-HCl/HEPES pH 7.3, 10 mM KCl, 90 mM NaCl and 0.5 µM 9-amino-6-chloro-2-methoxyacridine (ACMA). Fluorescence was measured at 20 °C using a Jasco Fluorimeter. Excitation and emission wavelengths were 410 nm and 480 nm, respectively. After the fluorescence signal was stable, H^+ influx was initiated by establishing a membrane potential by the addition of the potassium ionophore valinomycin (5 nM). Time courses of the proton-transport assays were repeated at least three times for each individual experiment.

Mutagenesis. LtaA mutants were generated using Q5 Site-Directed Mutagenesis Kit (NEB). The sequence of the resulting constructs was confirmed by DNA sequencing (Microsynth).

Sequence-conservation analysis. The sequence conservation analysis shown in Extended Data Fig. 6 and Supplementary Fig. 9 were computed using the ConSurf server[76]. Briefly, 76 LtaA homologues found in related *Staphylococcus* species or other Gram-positive bacteria were selected from a protein sequence BLAST search on the NCBI public database using *S. aureus* LtaA protein sequence as a query. We then generated a multiple-sequence alignment using the HHMER algorithm provided by ConSurf, with conservation scores plotted in PyMOL[73].

Docking of anchor-LLD. Docking of anchor-LLD (1,2-dihexadecanoic-3-O-(β-D-glucopyranosyl-1 → 6-O-β-D-glucopyranosyl-sn-glycerol)) to the LtaA structure was done with Autodock Vina[77]. Initial anchor-LLD coordinates were generated from two-dimensional geometry in Phenix (eLBOW)[64], and stereochemistry was corrected in Phenix (REEL)[64], with reference to the X-ray crystal structures of ligands PDB: 6GB and PDB: DDR. Docking was carried out over a search space of 60 × 54 × 36 Å covering the entire amphiphilic central cavity.

Construction of mutants in *Staphylococcus aureus* NCTC8325. Strains, plasmids and oligonucleotides used in this study are listed in Supplementary Table 7. A vector for efficient allelic replacement, pMAD[78], was used for knockout of ltaA in *Staphylococcus aureus* NCTC8325. Specifically, the upstream and downstream regions of the ltaA-coding region were amplified from genomic DNA by primer pairs OVL2253-OVL 2254 and OVL2255-OVL2256, respectively. A spectinomycin-resistance cassette was amplified with oligonucleotides OVL2257 and OVL2258 from plasmid pMAD-int2-luc-spc-gfp[79]. Then the three fragments were assembled by gibson assembly to produce the fragment upstream-spectinomycin-downstream. The gibson assembly product was then used as template for amplification of the ltaA replacement fragment with oligonucleotides OVL2259 and OVL2260 containing NcoI and BamHI sites. The ltaA replacement fragment and vector pMAD-int2-luc-spc-gfp were both ligated to produce the ltaA knockout plasmid pMAD-Δ*ltaA* construct, followed by transformation into *E. coli* strain IM08B[80]. The previously described gene-deletion method for the temperature-sensitive vector pMAD[78] was used for the construction of the *ltaA* deletion strain in NCTC8325 with pMAD-Δ*ltaA*. The final Δ*ltaA* genotype of the mutant was confirmed by both PCR and Sanger sequencing.

***S. aureus* phenotypic assay.** Bacteria cells were grown in 3 mL of LB medium at 37 °C, with 200 rpm shaking to $OD_{600} = 0.3$. For the complementary strains with pLOW vector, a final concentration of 5 µg/ml of erythromycin was added to the medium. The bacterial culture was then serially diluted. 10 µl of the original and its serial dilutions were spotted onto C + Y (casitone + yeast extract) agar plates at different pH, without or complemented with 0.1 mM IPTG. In the absence of IPTG, the pLOW vector provides a mild protein expression level[79], as indicated by growth restoration of the Δ*ltaA* mutant by ltaA-WT and single point mutants in absence of IPTG, whereas in the presence of IPTG it provides protein overexpression[79]. The plates were incubated at 37 °C with or without 5% CO_2 overnight. The images of the plates were captured by BioRad Gel Doc XR + imaging system.

***S. aureus* complementation assays.** The pLOW vector was used for the construction of *ltaA* complementary strains. The *ltaA* fragment was amplified from genomic DNA with oligonucleotides OVL2243 and OVL2244 containing SalI and NotI digestion sites (Supplementary Table 7). The amplified ltaA fragment was cloned into the vector pLOW-dCas9 (ref. [79]) to produce pLOW-ltaA. This was then transformed into *E. coli* IM08B. Point mutations were introduced by PCR mutagenesis (Supplementary Table 7). Later *ltaA* variants were cloned into pLOW with the same method described above. The pLOW vector carrying *ltaA* or variants were then introduced into NCTC8325 Δ*ltaA* strain by electroporation transformation with erythromycin selection (5 µg per mL) on LBA plates as described above (Supplementary Notes).

***S. aureus* fluorescent microscopy.** LB medium pre-warmed at 37 °C in the presence of 5% CO_2 overnight (causing acidification to about pH 6.5) or LB medium with low pH (adjusted by dissolving LB medium powder in PBS pH 6.5) were used to grow cells for fluorescence microscopy experiments. Fluorescence microscopy was performed using a Leica DMi8 microscope with a ×100 phase contrast objective (NA 1.40) with a SOLA Light Engine (Lumencor) light source. A chroma cube nr (Quad = Chroma 89000, mCT_LP = 49017) was used. For nile red staining, light was filtered through external excitation filter 545/25 nm (Chroma ET545/×25), and the external filter ET605/70 nm was used for emission. An exposure time of 800 ms with 100% of light from SOLA Light Engine was used for capturing images. The images were obtained with LasX software (Leica) and processed with ImageJ (https://imagej.nih.gov) (Supplementary Notes).

***S. aureus* transmission electronic microscopy.** The same bacterial cells for fluorescent microscopy were used for transmission electronic microscopy. Ultrathin sections (50 nm) of cells fixed in agarose were cut on a Leica Ultracut (Leica Mikrosysteme) and picked up on a copper slot grid (2 × 1 mm) coated with a polystyrene film. Sections were poststained with 4% uranyl acetate. Micrographs were collected with a transmission electron microscope Philips CM100 (Thermo Fisher Scientific) at an acceleration voltage of 80 kV with a TVIPS TemCam-F416 digital camera (TVIPS). The final images were processed with ImageJ (https://imagej.nih.gov) (see Supplementary Notes).

Immunoblotting detection of LTA in *Staphylococcus aureus* NCTC8325 at different pH. LB media with differing pH were prepared by dissolving LB powder (Difco LB medium, BD) in PBS followed by pH adjustment, and then sterilized by filtering with 0.2-µM membranes. The sample preparation and western blotting of LTA were performed based on the previous studies of Gründling et al.[19,22]. Briefly, *S. aureus* cells were cultured in LB at 37°, collected and resuspended in 500 µL of TBS buffer (20 mM Tris-Cl, pH 7.4, 150 mM NaCl). Bacteria were lysed by bead beater in 4 runs of 30 s per cycle with 6 m s^{-1}. The cell lysate was separated on 12% SDS–PAGE, followed by western blot analysis. LTA was detected with LTA (poly glycerolphosphate)-specific primary antibody (clone 55, HyCult Biotechnology) and antimouse IgG (H + L) HRP antibody (Promega) as the secondary antibody. The blots were developed with SuperSignal west pico plus chemiluminescent substrate (Thermo Fisher Scientific), and the images were obtained with a Fusion FX7 imaging system (Witec). The relative amount of LTA was determined from the band intensities of western blots ($n = 4$) using ImageJ (https://imagej.nih.gov).

Preparation of *S. aureus* membranes for LC–MS analysis. *S. aureus* cells were grown in 4 mL of LB medium at 37 °C and 200 r.p.m. shaking to $OD_{600} = 0.4$. For the complementary strains with pLOW vector, a final concentration of 5 µg mL^{-1} of erythromycin and 0.1 mM IPTG were added to the medium. Cells were collected by centrifugation and resuspended in 10 mM Tris-HCl pH 8.0, 1 mM EDTA with lysostaphin, followed by a 0.5 h incubation at 37 °C. Cells were then further subjected to sonication. Membranes were isolated and resuspended in 100 mM Tris-HCl pH 8.5, 5% SDS and 10 mM tris(2-carboxyethyl) phosphine (TECP).

Samples were incubated at 37 °C for 1 h after the addition of chloroacetamide to reduce and alkylate disulfides. Samples were then loaded on an S-Trap Micro Spin column (Protifi). On-column peptide digestion was performed by adding trypsin and incubated at 47 °C for 1 h. Digested peptides were collected by passing 50 mM triethylammonium bicarbonate (TEAB) buffer, 0.2 % formic acid (wt/vol) in distilled water, and 0.2 % formic acid (wt/vol) in 50% acetonitrile (vol/vol) through the column and dried in a SpeedVac (Labconco). Dried peptides were re-suspended in 0.1% formic acid (wt/vol) with iRT normalization peptide mix (Biognosys) and stored at −20 °C.

Targeted PRM LC–MS analysis of LtaA and variants in *S. aureus* membranes. In the first step, PRM assays[74] for all possible peptides of LtaA being 6 to 25 amino acids long comprising double- and triple-charged precursor ions were generated. In total, five peptides were found to match the length criteria, leading to a total of ten PRM assays. These were applied to identify LtaA in membrane fractions of wild-type *S. aureus*. The setup of the µRPLC-MS system was as described previously[75]. Mass spectrometry analysis was performed on a Q-Exactive mass spectrometer equipped with a nanoelectrospray ion source (both Thermo Fisher Scientific). Each MS1 scan was followed by high-collision-dissociation (HCD) of the 10 LtaA precursor ions in PRM mode using a global isolation mass list. Using strict identification criteria, three peptides ions of LtaA, LTNYNTRPVK (2^+ and 3^+ ion) and MQDSSLNNYANHK (2^+) could be confidently identified, and were used for label-free PRM quantification. To control for variation in sample amounts, the total ion chromatogram (only comprising peptide ions with two or more charges) of each sample was determined by label-free quantification using Progenesis QI (version 2.0, Waters) and used for normalization. The integrated peak areas of the three peptide ions quantified by PRM were summed and employed for LtaA quantification (Supplementary Notes).

Reporting Summary. Further information on research design is available in the Nature Research Reporting Summary linked to this article.

Data availability

Atomic coordinates have been deposited in the Protein Data Bank under accession code PDB 6S7V. Source data for Figs. 1c, 3b,c,e,f, 4a–c and 5c and Extended Fig. 1 are available with the paper online.

References

61. Zhang, B. & Perez, C. Stabilization and crystallization of a membrane protein involved in lipid transport. *Methods Mol. Biol.* **2127**, 283–292 (2020).
62. Kabsch, W. Xds. *Acta Crystallogr. D Biol. Crystallogr.* **66**, 125–132 (2010).
63. Karplus, P. A. & Diederichs, K. Linking crystallographic model and data quality. *Science* **336**, 1030–1033 (2012).
64. Adams, P. D. et al. PHENIX: a comprehensive Python-based system for macromolecular structure solution. *Acta Crystallogr. D Biol. Crystallogr,* **66**, 213–221 (2010).
65. Sheldrick, G. M. A short history of SHELX. *Acta Crystallogr. A Found. Adv.* **64**, 112–122 (2008).
66. Collaborative Computational Project, Number 4. The CCP4 suite: programs for protein crystallography. *Acta Crystallogr. D Biol. Crystallogr.* **50**, 760–763 (1994).
67. Skubak, P. et al. A new MR-SAD algorithm for the automatic building of protein models from low-resolution X-ray data and a poor starting model. *IUCrJ* **5**, 166–171 (2018).
68. McCoy, A. J. et al. Phaser crystallographic software. *J. Appl. Crystallogr.* **40**, 658–674 (2007).
69. Cowtan, K. Recent developments in classical density modification. *Acta Crystallogr. D Biol. Crystallogr.* **66**, 470–478 (2010).
70. Waterhouse, A. et al. SWISS-MODEL: homology modelling of protein structures and complexes. *Nucleic Acids Res.* **46**, W296–W303 (2018).
71. Jiang, D. et al. Structure of the YajR transporter suggests a transport mechanism based on the conserved motif A. *Proc. Natl Acad. Sci. USA* **110**, 14664–14669 (2013).
72. Emsley, P., Lohkamp, B., Scott, W. G. & Cowtan, K. Features and development of Coot. *Acta Crystallogr. D Biol. Crystallogr.* **66**, 486–501 (2010).
73. Fratamico, P. M. et al. *Escherichia coli* serogroup O2 and O28ac O-antigen gene cluster sequences and detection of pathogenic *E. coli* O2 and O28ac by PCR. *Can. J. Microbiol.* **56**, 308–316 (2010).
74. Peterson, A. C., Russell, J. D., Bailey, D. J., Westphall, M. S. & Coon, J. J. Parallel reaction monitoring for high resolution and high mass accuracy quantitative, targeted proteomics. *Mol. Cell Proteomics* **11**, 1475–1488 (2012).
75. Ahrne, E. et al. Evaluation and improvement of quantification accuracy in isobaric mass tag-based protein quantification experiments. *J. Proteome Res.* **15**, 2537–2547 (2016).
76. Ashkenazy, H. et al. ConSurf 2016: an improved methodology to estimate and visualize evolutionary conservation in macromolecules. *Nucleic Acids Res.* **44**, W344–W350 (2016).
77. Trott, O. & Olson, A. J. AutoDock Vina: improving the speed and accuracy of docking with a new scoring function, efficient optimization, and multithreading. *J. Comput. Chem.* **31**, 455–461 (2010).
78. Arnaud, M., Chastanet, A. & Debarbouille, M. New vector for efficient allelic replacement in naturally nontransformable, low-GC-content, Gram-positive bacteria. *Appl Environ. Microbiol.* **70**, 6887–6891 (2004).
79. Stamsas, G.A. et al. CozEa and CozEb play overlapping and essential roles in controlling cell division in *Staphylococcus aureus*. *Mol. Microbiol.* **109**, 615–632 (2018).
80. Monk, I. R., Tree, J. J., Howden, B. P., Stinear, T. P. & Foster, T. J. Complete bypass of restriction systems for major *Staphylococcus aureus lineages*. *MBio* **6**, e00308–e00315 (2015).

Acknowledgements

We thank the staff at the PX beamline of the Swiss Light Source, Switzerland. We thank G. Cebrero and N. Bärland for providing a control transporter sample. We thank J. Daraspe and M. Rengifo for contributing to TEM images acquisition. We thank U. Lanner, A. Schmidt and T. Müntener for contributing to HPLC–MS and PRM MS studies. This work was supported by the Swiss National Science Foundation (SNSF) (PP00P3_170607 to C.P and 31003A_172861 to J.W.V.). Further funding came from a JPIAMR grant (40AR40_185533 to J.W.V.) and ERC consolidator grant 771534-PneumoCaTChER (to J.W.V). E.L. was funded by the Biozentrum International PhD Program.

Author contributions

B.Z. performed purification and crystallization of LtaA. C.P. assisted B.Z. during data collection, structure determination and docking analysis. B.Z., E.L. and C.P. established and performed in vitro flipping assays. C.P., B.Z. and E.L. analyzed the structural and in vitro functional data. E.L. performed reaction products characterization. X.L. and E.L. performed experiments in live cells. X.L, E.L, C.P. and J.W.-V. analyzed in vivo data. G.M. and S.H. performed NMR analysis. C.P. conceived the project and wrote the manuscript with input from all authors.

Competing interests

The authors declare no competing interests.

Additional information

Supplementary information is available for this paper at https://doi.org/10.1038/s41594-020-0425-5.

Correspondence and requests for materials should be addressed to C.P.

Peer review information Katarzyna Marcinkiewicz was the primary editor on this article and managed its editorial process and peer review in collaboration with the rest of the editorial team.

Reprints and permissions information is available at www.nature.com/reprints.

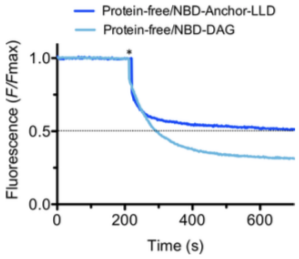

Extended Data Fig. 1 | Fluorescence quenching analysis of protein-free liposomes. Representative traces of quenching of liposomes containing NBD-anchor-LLD or NBD-DAG ($n \geq 3$). Asterisk marks addition of dithionite. Source data are available with the paper online. *F* correspond to the fluorescence intensity measured for each time point. F_{max} is the average fluorescence measured during the first 200 seconds.

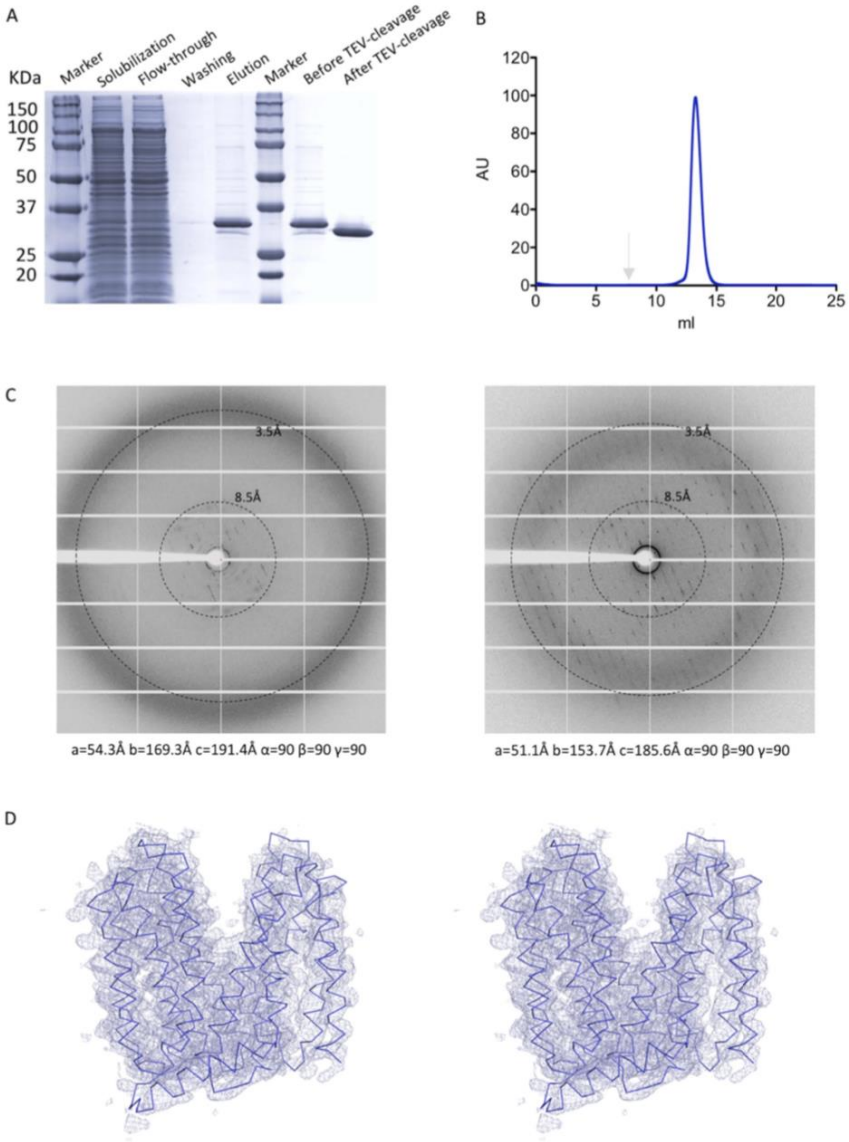

Extended Data Fig. 2 | S. aureus LtaA crystallization. a, SDS-PAGE of samples from different steps of a LtaA purification experiment. Purified protein after cleavage of the His_{10}-tag was used for crystallization. **b**, Size exclusion chromatography profile of purified LtaA (Superdex 200 10/300 Increase). Gray arrow indicates column void. **c**, Representative X-ray diffraction images of a LtaA crystal before *insitu* annealing (*left*) and after *insitu* annealing (*right*). The difference in unit cell dimensions before and after *insitu* annealing demonstrate shrinking of the unit cell. **d**, Stereo view (wall-eyed) of the *2Fo-Fc* electron density map of the 3.3Å structure of LtaA at 1.0σ level.

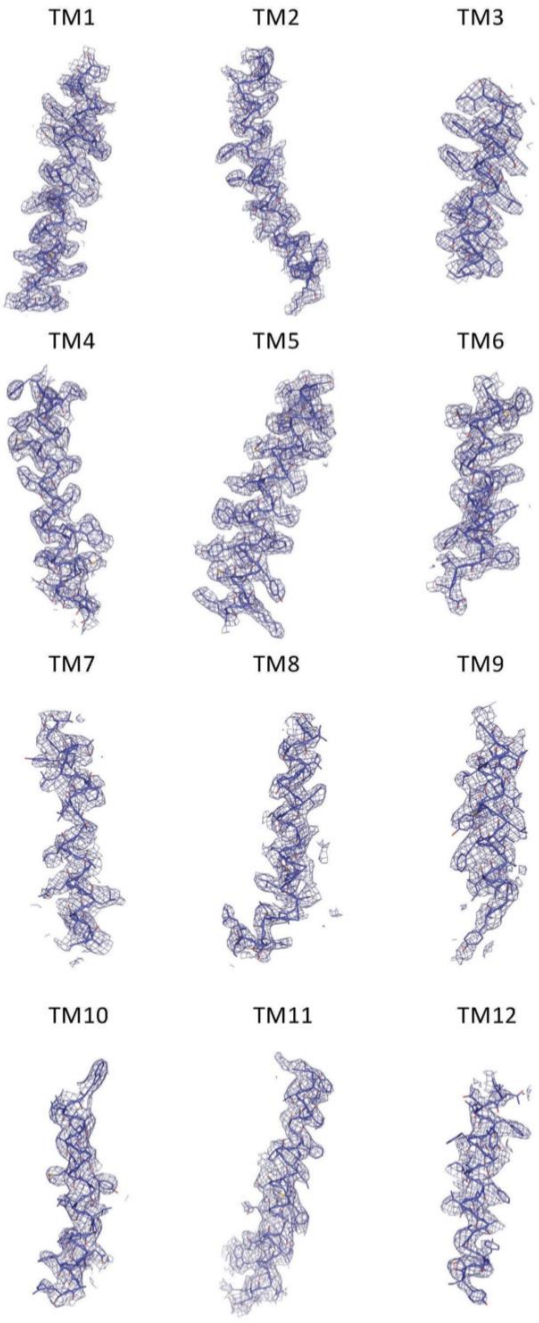

Extended Data Fig. 3 | 2Fo-Fc electron density map. Individual transmembrane segments of the 3.3Å structure of LtaA at 1.0σ level are shown.

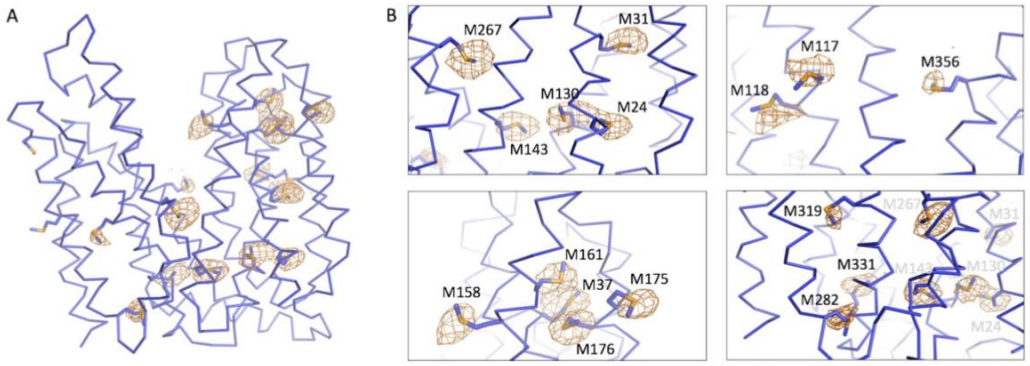

Extended Data Fig. 4 | Validation of side-chain register of LtaA model. a and **b**, Anomalous electron density map define selenomethionine (SeMet) sites. Contour levels is 4.0σ. Anomalous density was observed for 16 out of 19 SeMet residues in LtaA.

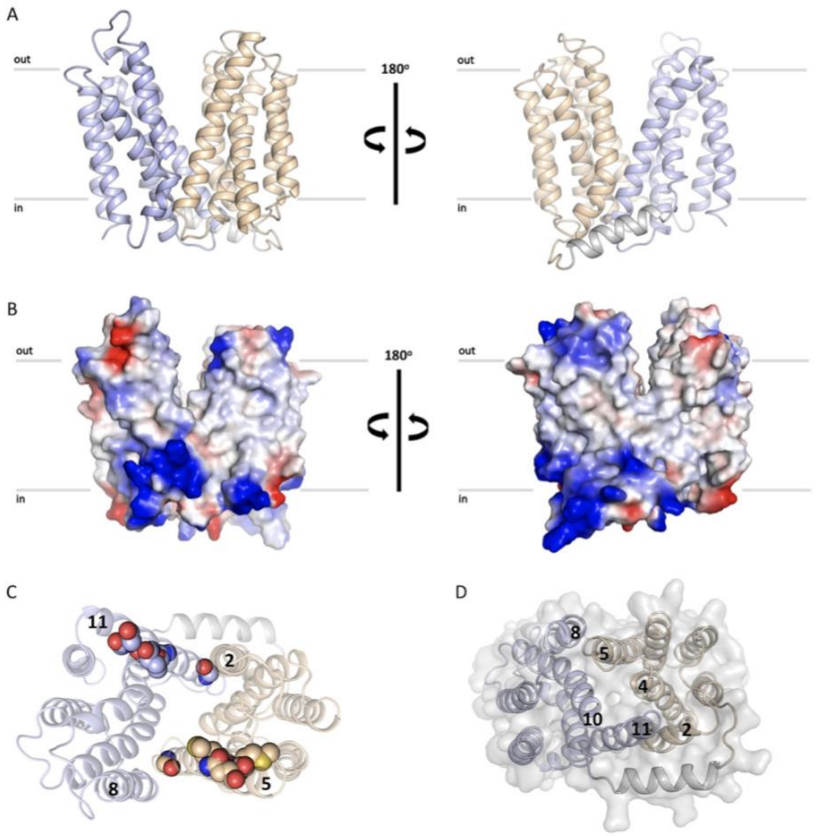

Extended Data Fig. 5 | LtaA structure analysis. a, Overall structure of LtaA. The N-terminal domain is shown in light-orange, C-terminal domain is shown in light-blue, the cytoplasmic helical loop connecting the N-terminal and C-terminal domains is shown in gray. **b**, Vacuum electrostatic surface representation of LtaA showing side views of the protein. **c**, Top view of LtaA showing residues participating in the motif-G sequence ($G^{345}(X)_8G(X)_3GP(X)_2GG^{363}$) in TM11 and motif-G-like sequence in TM5.**d**, Cytoplasmic view of LtaA showing TMs and loops blocking the access to the central cavity.

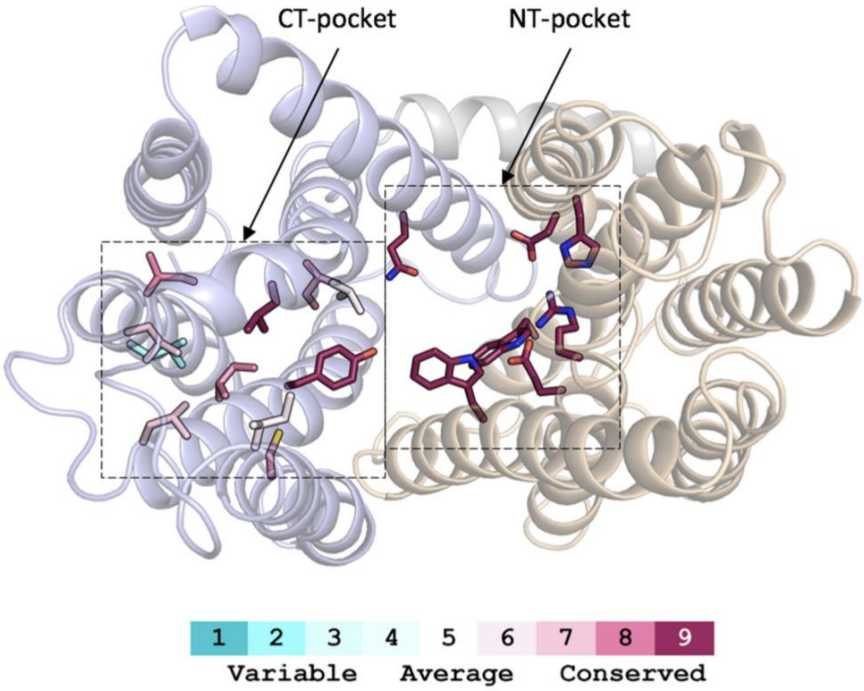

Extended Data Fig. 6 | Sequence conservation analysis. A multiple sequence alignment of 76 LtaA homologues found in related *Staphylococcus* species or other Gram-positive bacteria was generated. Top view of LtaA, residues in N-terminal and C-terminal cavity are colored by sequence conservation (ConSurf server).

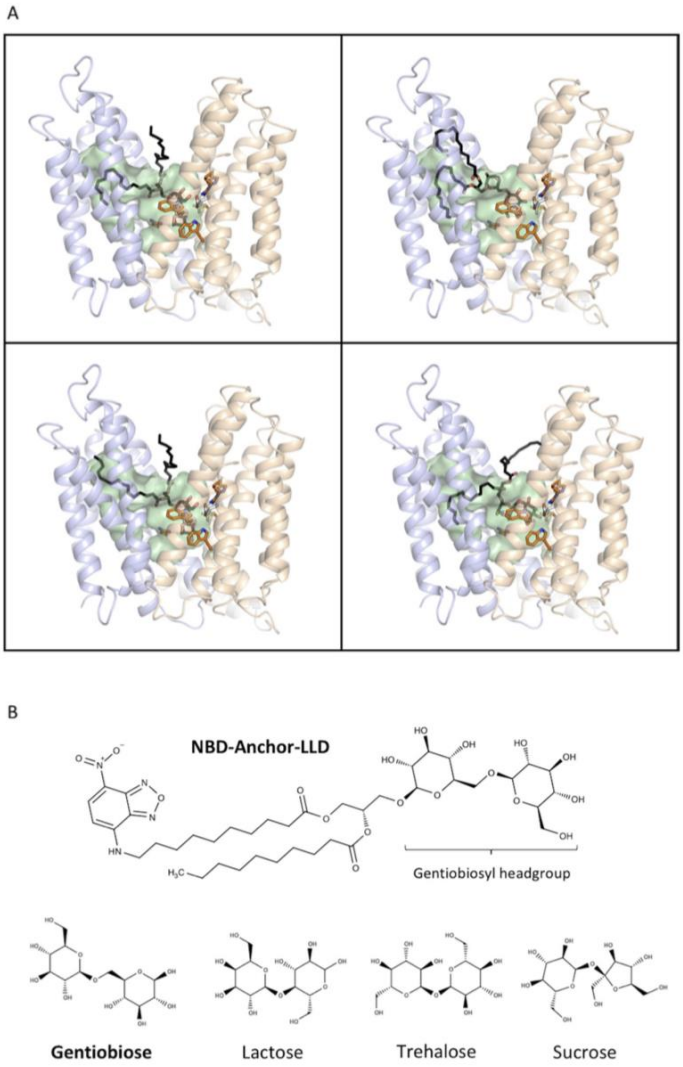

Extended Data Fig. 7 | Docking analysis and structures of compounds used in this study. a, Models of lipid-linked-disaccharide docked into the amphiphilic cavity of LtaA. Lipid-linked-disaccharide is shown in black and red sticks. Green surface shows the amphiphilic central cavity of LtaA. **b**, Structures of disaccharides and Anchor-LLD (β-D-Glc-(1→6)-β-D-Glc-(1→3)-diacylglycerol).

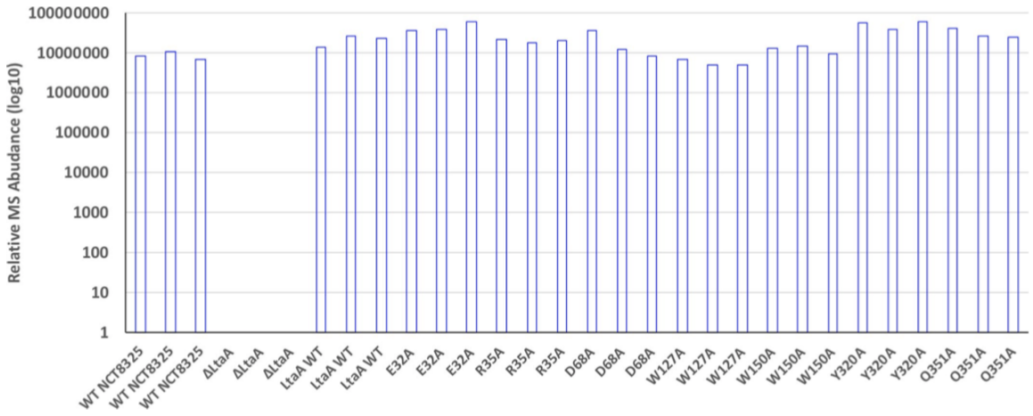

Extended Data Fig. 8 | Liquid chromatography mass spectrometry (LC-MS) analysis of relative abundance of LtaA and variants in S. aureus membranes. Chromatographic separation of peptides was carried out using an EASY nano-LC 1000 system. Mass spectrometry analysis was performed on a Q-Exactive mass spectrometer equipped with a nanoelectrospray ion source. Three peptides ions of LtaA, LTNYNTRPVK (2+ and 3+ ion) and MQDSSLNNYANHK (2+) could be confidently identified and were used for label-free parallel reaction monitoring (PRM) quantification. The integrated peak areas of the 3 peptide ions quantified by PRM were summed and employed for LtaA quantification. The histogram shows relative abundances of LtaA and variants from independent experiments (n = 3).

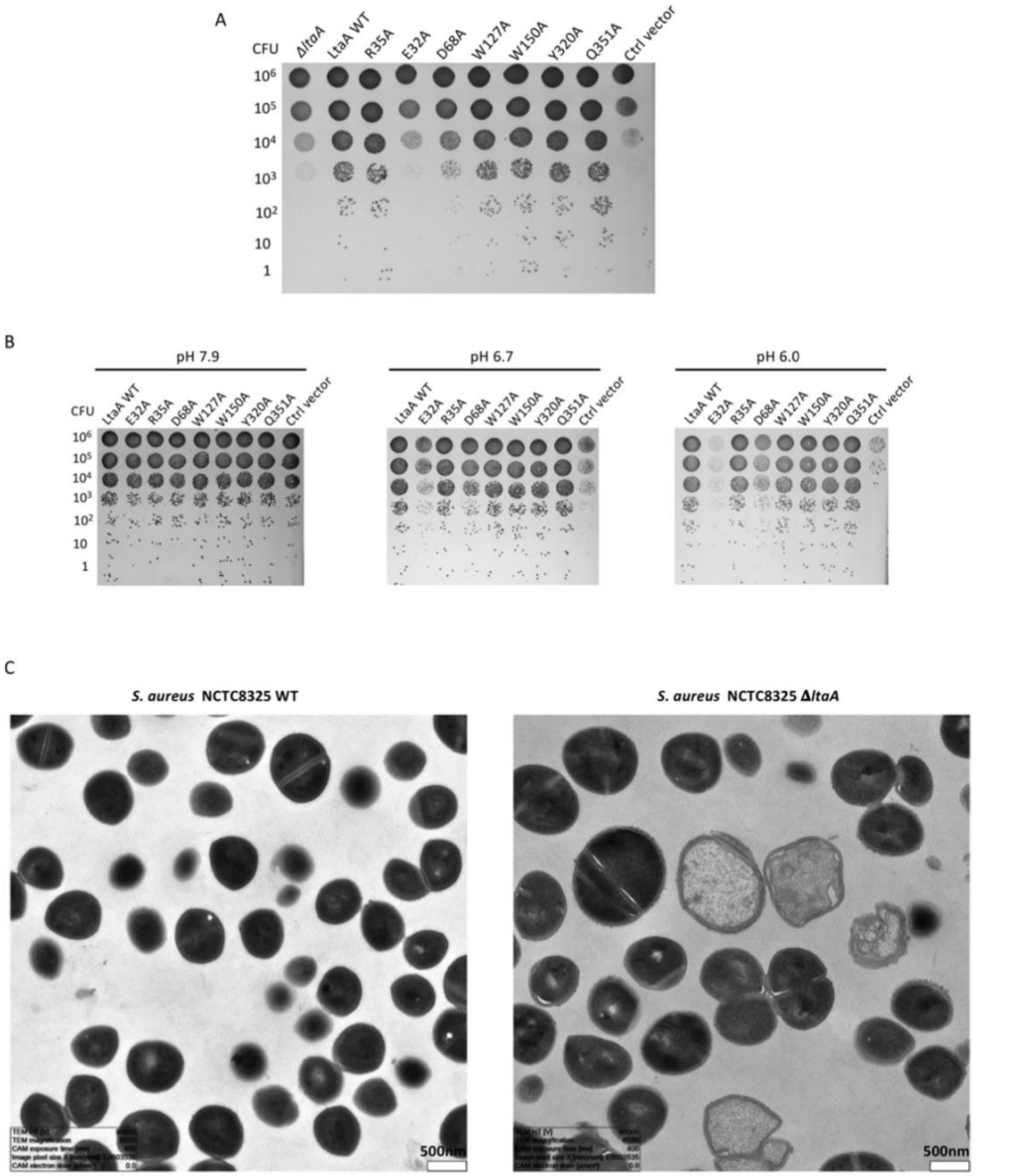

Extended Data Fig. 9 | Phenotypes of S. aureus WT, ΔltaA, and LtaA mutants. a, Over-expression of LtaA mutants. *S. aureus* strain NCTC8325 growth on C+Y agar plates in the presence of 0.1 mM IPTG incubated at 37 °C and 5% CO_2. **b**, Over-expression of LtaA mutants. *S. aureus* strain NCTC8325 growth on C+Y agar plates in the presence of 0.1 mM IPTG incubated at 37 °C under different pH conditions. LtaA WT represents Δ*ltaA* mutant complemented with wild type *ltaA* on pLOW vector; Ctrl vector indicates Δ*ltaA* mutant complemented with pLOW carrying a functionally unrelated gene as vehicle control; the other labels represent Δ*ltaA* mutant complemented with *ltaA* with corresponding point mutations. **c**, Transmission electron microscopy (TEM) images at low magnification showing the morphology of *S. aureus* NCTC8325 WT and Δ*ltaA* mutant.

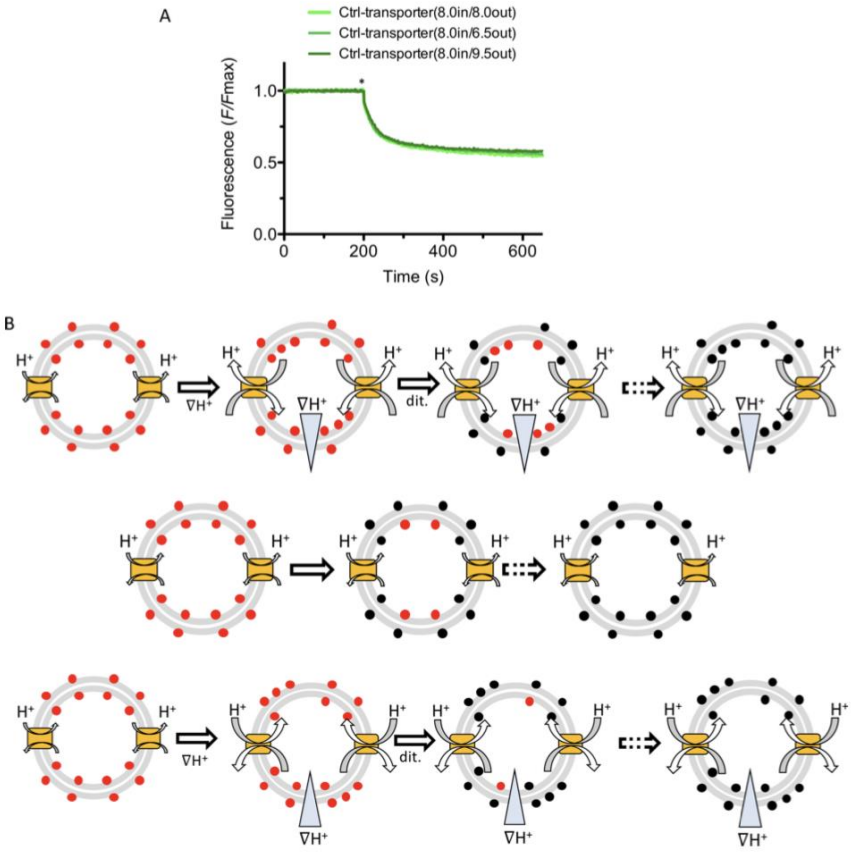

Extended Data Fig. 10 | LtaA-catalyzed lipid-linked-disaccharide flipping and proton gradients. a, Representative traces of flipping assays with a control transporter (bacterial choline transporter) in the presence of different proton gradients, *in* and *out* denote pH of buffer inside and outside of liposomes, respectively ($n \geq 3$). Asterisk marks addition of dithionite. *F* correspond to the fluorescence intensity measured for each time point. F_{max} is the average fluorescence measured during the first 200 seconds. **b**, Scheme of LtaA-catalyzed lipid-linked-disaccharide flipping under an outward proton gradient (*top*), no gradient (*center*), and an inward proton gradient (*bottom*). Under application of a pH gradient (∇H^+), LtaA (yellow boxes) translocates NBD-anchor-LLD (red spheres) contrary to the proton gradient. Addition of dithionite (dit.) then reduces exposed and exchanged NBD-anchor-LLD (black spheres). The extent of quenching is in accordance to the direction of the pH gradient. Full fluorescence quenching will be achieved after prolonged incubation (dashed arrows).

4 Discussion

4.1 Stabilization and Crystallization of a Membrane Protein Involved in Lipid Transport

X-ray crystallography is a robust technique to obtain the atomic structure of proteins and has been applied to solve 89% of the structures deposited in the PDB database (https://www.rcsb.org/stats/summary). However, only around 2% of them are membrane proteins and only 27 are MFS transporters (https://blanco.biomol.uci.edu/mpstruc/). By applying several tips, we successfully obtained high-quality LtaA crystals which were suitable for structure determination via vapor diffusion.

Poly-His tag is a common affinity tag, applied in nearly 60% of solved protein structures[177]. Generally, the cleavage of the His-tag is a trivial factor to the final structure determination, because this small tag does not influence the native structure in general[178]. However, in the case of LtaA, N-terminal His_{10}-tag cleavage led to a dramatic improvement of protein stability and mono-dispersity during the purification process, thus promoting the formation of high-quality crystals. Indeed, the length of His-tag was proposed to influence the oligomeric state and the chromatographic behavior of some membrane proteins[179]. The improvement of LtaA mono-dispersity might be due to the decrease of unspecific interactions between LtaA monomers through the His-tag.

One of the reasons for low-resolution X-ray diffraction is radiation damage. Cryogenic data collection has been commonly applied to reduce the radical damage to protein crystals caused by X-ray[180]. However, flash-cooling of protein crystals is believed to cause heterogeneous thermal contractions of crystal contents, thus increasing the orientational misalignment of molecular arrays and contributing to the dispersion of the Bragg diffraction peaks and low quality of diffraction data, specifically for crystals with large pores containing bulk-solution component[181–183]. "*In situ* annealing" that includes warming the flash-cooled crystal and flash cooling it again on the goniometer[184], was demonstrated to be an effective way to reduce the crystal mosaicity caused by the flash-cooling process via allowing the reorder of mosaic blocks inside the crystalline, improving the data quality, such as obtaining better shaped, well ordered

and high-resolution spots and getting rid of ice rings[185,186]. According to the thermal contraction theory, the LtaA crystal, packaged in an orthorhombic space group with 71.94% solvent content, most likely would undergo the mismatch of the molecular arrays during flash-cooling, resulting in diffractions only to a low-resolution range. Indeed, although LtaA crystals were formed by high-quality protein in a well-defined shape, the highest resolution of diffraction went to a low range (>7 Å). By applying the annealing, disordered molecular arrays might be realigned and diffract to a high-resolution range. Indeed, LtaA crystals diffracted to 3-4 Å with better-defined patterns, dramatically promoting the final structure determination. Notably, the volume of the unit cell shrank 18% after annealing on average, indicating the protein molecules were packed tighter. Flash-cooling, as well as annealing, may change the unit cell size, varying from 1%-7%, partially contributed by the thermal expansion/contraction of the solvent content[182,186,187]. This significant contraction of the unit cell of LtaA might result from its high solvent content (71.94%), while the solvent content of former reported cases normally ranged from 20%-60%[182–184,186]. However, the effect of "*in situ* annealing" is also case-dependent[186]. Therefore, we recommend checking crystals case by case. Notably, the dramatic change of unit cell will introduce difficulties in applying the isomorphous replacement, due to different shrinking levels of native crystals and derivative crystals.

4.2 Structure of a proton-dependent lipid transporter involved in lipoteichoic acids

In this part of the project, we elucidated the structure of LtaA. The canonical MFS fold was observed, in agreement with other known MFS structures[120]. LtaA showed a large amphiphilic cavity formed by a hydrophilic half pocket (with an overall negative electrostatic surface potential) of N-domain and a hydrophobic half pocket of C-domain. MFS transporters were believed to evolve through multiple rounds of the duplication event, from the 6-TMs bundle to a further 12-TMs transporter[119]. The amphipathic property suggested the heterogeneous duplication through TMs bundles with different properties (such as a combination of a hydrophobic bundle and a hydrophilic bundle) to fit the requirement of amphiphilic substances translocation. This feature may help in identifying MFS transporters dealing with amphiphilic substances *in silico*. Although no typical amphipathic cavity of an MFS transporter that flips glycolipids has been elucidated, the amphipathic feature of the binding pocket was reported in

MFS transporters, such as GluP[135] that transfers glucose and FucP[188] mediating fucose transport. Notwithstanding that the binding cavity is amphiphilic, both glucose and fucose were proposed to interact with the hydrophilic part of the cavity[135,188]. This feature highlighted the importance of the hydrophilic half pocket in sugar moiety recognition, which was reminiscent of the potential interaction between the glucosyl group of Glc_2-DAG and the hydrophilic half pocket of LtaA. We performed the docking analysis *in silico* and found that the disaccharide group could be indeed accommodated by the hydrophilic half pocket. Thus, we further conducted flipping assays with the addition of different disaccharides as competitors of Glc_2-DAG. The inhibition effect of the gentiobiose but not the lactose, fructose or trehalose clearly pointed out that LtaA recognized the di-glucosyl moiety of Glc_2-DAG precisely and specifically. The inhibition effect also suggested that the di-glucosyl moiety might serve as a template for the design of potential inhibitors of LtaA, providing a concept of drug design.

We selected residues including E32, R35, D68, W127 and W150 showed potential interactions with the di-glycosyl region, mutated to alanine and subjected to flipping assays. However, these mutants did not show a big change in the flipping ability. It might be that the single-point mutation was not enough to interrupt the recognition and loading since the substrate is big and may form multiple interactions with LtaA. Several double-point mutations including E32A/D68A, R35A/D68A, W150A/D68A were further investigated, and we found that they displayed a significant reduction of their flipping activity, which was consistent with our structural analysis. Our data supported a model in which LtaA loads the Glc_2-DAG to its central cavity from lipids pool through the recognition of the di-glucosyl moiety by hydrophilic residues including E32, R35, D68 and W150 in the N-domain. This brought insights into the recognition mechanism of other MFS transporters mediating glycolipid flipping.

Notably, three charged residues, E32, R35 and D68 were positioned in proximity of the binding pocket. They might undergo protonation/deprotonation during conformational shifts of LtaA, fitting the typical feature of MFS proton-dependent transporters[142,146,148,149,156,160,163]. We verified this hypothesis by performing flipping assays under different pH gradients. We observed that the flipping activity of LtaA responded to different pH gradients. When an inward proton gradient (lower pH outside the liposome) appeared, more Glc_2-DAG molecules

were transported to the outside of the liposome compared to the one without a proton gradient. Correspondingly, an outward proton gradient (higher pH outside the liposome) led to less Glc_2-DAG transported to the outside of the liposome. Based on this, we demonstrated that LtaA behaves as a proton-dependent antiporter. To identify which residues carry on the proton transfer, we calculated the theoretical pKa value of E32, R35 and D68 under the current outward-facing conformation, with 7.8, 14, 3.4 respectively. We postulated that E32 was most likely the protonation/deprotonation site, which was verified in the flipping assay where the E32A mutant lost the response to pH gradients. Herein, a proton-coupling mechanism of LtaA was proposed that after the release of the Glc_2-DAG, E32 would be protonated, facilitating the transition from the outward-facing stage to an inward-facing state, where it would undergo deprotonation.

However, whether other residues participate in the proton transfer is not known. The trait of the proton-coupling of LtaA also highly resembles proton-dependent MFS sugar transporters[135,161,188,189], even though they are all symporters. An interesting fact is that MFS glucose transporters of bacteria are often proton-coupled, while their homologs in humans are commonly uniporters[135], even though both of them contain a conserved Glu residue serving as the primary protonation/deprotonation site[135]. The loss of proton-coupling in many human glucose uniporters was attributed to the substitution of a critical Asp residue to an Asn near Glu, which disrupted the proton-coupling environment[135]. In our docking model, an Asp residue (D68) was close to the protonation/deprotonation site E32, indicating D68 might also participate in the proton-coupling mechanism. Indeed, we observed impaired growth of the D68A mutant under the acidic condition in *S.aureus*, implicating D68 involves in the proton-coupling network.

The aliphatic tails were proposed to fit into the hydrophobic pocket formed by the C-terminal domain. This showed similarities to the interaction between MurJ and the lipid moiety of lipid II[111,190] (Fig. 4.1). In MurJ, a hydrophobic groove formed by TM 13 and 14 contributed to accommodating the lipid tails[191]. The specific hydrophobic region might be a general feature of secondary transporters to accommodate the hydrophobic moieties of amphiphilic molecules, which might be exerted to identify new secondary transporters dealing with amphiphilic substrates in *silico*.

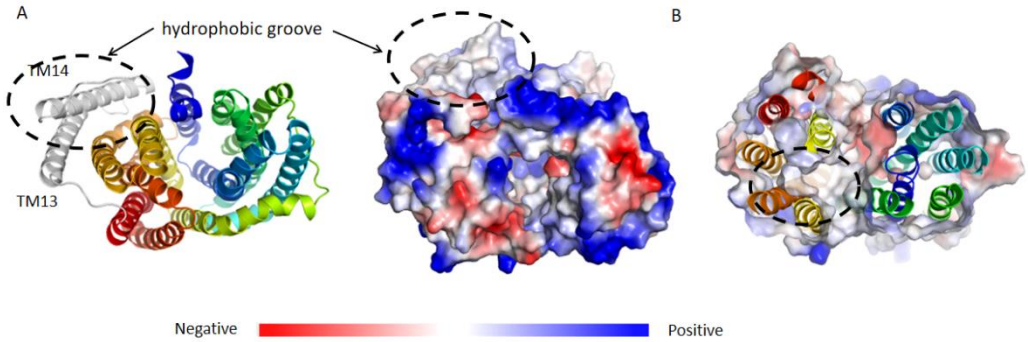

Fig. 4.1 Electrostatic potential surface representatives of MurJ (A) and LtaA (B). A. Hydrophobic extended groove formed by TM13 and TM14 of MurJ highlighted by black circles. PDB: 6CC4. Adapted from[191] B. The hydrophobic half pocket highlighted by a black circle of LtaA. Transporters are colored in rainbow.

Overall, our structural and biochemical characterization on LtaA established a framework for understanding the mechanism of proton-dependent MFS antiporters and MFS glycolipid transporters.

ABC-transporters are frequently involved in glycolipid transport[100]. The structures of known ABC-transporter flippases show that sometimes lipid moieties of substrates are bound in the internal cavity of the transporter, but in other cases, they were proposed to stay in the membrane rather[104,106,107]. A similar question remains in the case of LtaA. It was suggested that one of the lipid tails might be left in the membrane from the docking analysis. Capturing other states (such as the inward-facing and the occluded conformation), as well as a substrate-bound structure, will provide direct evidence to clarify whether a "credit card" or "trap and flip" model is applied by LtaA.

It's mentioned above that glucose transporters of humans are often uniporters while the ones from bacteria tend to couple with protons. Human glucose transporters were hypothesized to lose their proton coupling ability because they are always exposed to sufficient glucose, while bacteria glucose transporters are coupled with protons to enhance their utility of the low concentration of glucose in the environment[135]. This difference highlights the biological relevance of the proton-coupling mechanism. In *S.aureus*, the natural substrate Glc_2-DAG is synthesized inside the cytoplasm by YpfP constantly, followed by the export to extracellular[45]. This can set up an outward Glc_2-DAG gradient which can be applied as the energy source for its movement[45]. Indeed, we observed that the E32A mutant maintained a base level of the flipping activity which was comparable to the WT LtaA without a proton gradient. Therefore,

we were wondering about the physiological relevance of the proton-coupling of LtaA.

S.aureus can colonize acidic niches including the skin, nasal mucus and host macrophages[192–194]. An acidic environment is harmful to *S.aureus* cells, leading to the acidification of the cytoplasm, therefore affecting the activity of enzymes, the electron transport chain as well as the DNA structure due to the protonation of nitrogenous bases[195]. Therefore, *S.aurues* possess specific genes to confer acidic resistance. Suggested by the proton coupling of LtaA and the colonization of *S.aureus* under acidic environments, we speculated that the proton coupling mechanism might of LtaA contribute to the acidic resistance of *S.aureus*. To figure it out, intrinsic *ltaA* was knocked out in *S.aureus* NCTC 8325 and complementary plasmids carrying WT or mutant *ltaA* were transformed to *S.aureus*, followed by inspections on the growth state and the cell morphology under acidic environments, either by adjusting the pH value of medium or providing 5% CO_2 (acidify the medium to around pH 6). LtaA could work as a "pH-sensing" transporter in the presence of low external pH, flipping Glc_2-DAG at a higher rate by utilizing the energy generated by the pH gradient. More Glc_2-DAG flipped to the outer leaflet of the plasma membrane leads to an enhanced level of LTA assembly. Extra LTA molecules form a stronger mesh that can enhance the mechanical rigidity of the cell wall. Meanwhile, the newly formed LTA molecules increase the overall negative charge and protect *S.aureus* from acidic harm probably owing to a "buffering effect". Our results, for the first time, provided strong evidence that the Glc_2-DAG flippase LtaA contributes to the acidic resistance of *S.aureus*.

The acidic tolerance mechanism of *S.aureus* has been studied for many years. Two major classes of genes are involved in developing acidic tolerance. One type is responsible for sensing the acidic stimulus, including two-component system GraXRS[194], cytoplasmic regulators such as sigma factor *sigB* and *sarA* from the SarA family[196–198], GdpP from the additional signal transduction protein system and its downstream target second messenger c-di-AMP[197,199]. The other cluster serves as the response apparatus. At least four categories of genes have been identified to respond to acidic tolerance in at least two ways. The first way is to consume excess protons via metabolic reactions in the cytoplasm, and related genes are upregulated, including genes involved in urease function[200,201], acetolactate synthase/decarboxylase function[202,203] and the arginine deiminase pathway[195,204]. The second way is to promote the excretion of protons. ATP can be generated in the arginine deiminase

pathway, then taken by specific ATPases to expel protons from the cell[195,204]. Besides, many other factors also have been reported to involve in the acidic resistance, such as the reactive oxygen species (ROS) clusters[195] and superoxide dismutase *sodA*[205].

Different from all types of genes proposed, LtaA is the first identified glycolipid flippase involved in acidic tolerance among bacteria to our knowledge, hinting at the complexity and diversity of the acidic resistance regulatory network of bacteria. Another striking feature is that LtaA combines the stimuli-sensing and the effectuating modules, which are generally implemented by different proteins. The proton coupling of the transporter acts as the "sensing module" and the response module is achieved by accelerating the flipping activity which leads to the enhanced LTA assembly level. This combination of "sensing" and "effectuating" allows a fast and potent response to combat the acidic stress. Our research brought new insights into understanding the mechanism of the acidic resistance.

During the growth state investigation of the LtaA knockout strain, several simultaneous suppressors that could rescue the growth defects were identified. A *gdpP* mutant partly rescued the growth defect of *S.aurues* under acidic stress, in agreement with a previous report[199]. This *gdpP* mutant allowed an enhanced level of cellular c-di-AMP and contributed to cell wall integrity[206–208]. Our result indicated that LtaA cooperates with other acidic-resistant proteins but the mechanism is not known. If there are interactions between LtaA and other factors involved in the acidic resistance also remains an attractive question.

Both acidic resistance and antibiotic resistance render *S.aureus* a versatile human pathogen. The cross-talking between mechanisms of acidic tolerance and antibiotic resistance has been observed. The exposure to the acidic environment (pH<5.5) enhanced the susceptibility of MRSA strains to antibiotics such as benzylpenicillin, Methicillin, meropenem and cloxacillin[27,209,210]. An enhanced level of Glc_2-DAG in the membrane was reported in clinical isolates with antibiotic resistance compared to antibiotics susceptible strains[211].

In a previous study, the growth arrest was not observed in the LtaA knockout strain under standard laboratory conditions[44]. Our result highlighted a pivotal condition, the acidic environmental pH, making LtaA a decisive factor for *S.aureus* viability. Our study suggested that for bacteria colonizing an acidic environment, such as *S.aureus*, a standard culturing

protocol might conceal the specific feature of the target and underestimate its physiological significance. Our findings would encourage additional studies on proton-coupled antiporters of other human pathogens that can survive under acidic niches. This eventually will help in identifying new potential anti-bacterial targets.

5 Conclusion and outlook

In this project, we determined the atomic structure of LtaA at 3.3Å (PDB code: 6S7V), investigated the molecular basis of the recognition of the substrate Glc_2-DAG and proposed a proton-coupled flipping mechanism. Furthermore, we revealed an unprecedented function of LtaA in *S.aureus* acidic resistance and figured out its regulatory mechanism. Our results set a framework for understanding the mechanism of MFS glycolipid transporters, contributed to the comprehension of *S.aureus* pathogenesis and provided a novel target for anti-*S.aureus* therapeutics.

One of the crucial questions of flippase research is to illustrate the mechanism of substrate recognition and binding. We have already identified crucial residues involved in Glc_2-DAG-LtaA interaction by performing *in vitro* biochemical assays. However, how does LtaA flip the lipid tails, such as by a "credit card" model or a "trap and flip" model, remains enigmatic. Solving substrate-bound structures would provide direct evidence to address this question. A co-crystallization or a soaking strategy can be applied to get the substrate-bound complex. Besides obtaining this structure, flipping assays with different lengths of Glc_2-DAG as competitors will also contribute to illustrate whether the lipid tails are enclosed by the binding pocket from a biochemical perspective. Another question is to figure out the molecular basis of conformational changes. Obtaining an inward-facing state of LtaA would help with the analysis of local rearrangements of residues involved in conformational changes. LtaA with gating residues cross-linked on the extracellular side would help to lock the inward-facing during the crystallization. As mentioned above, D68 might participate in proton-coupling. To verify it, a neutral mutation to Asn can be constructed and subjected to flipping assays under different pH gradients.

The substrate Glc_2-DAG is synthesized by a membrane-associated protein YpfP, whose coding sequence overlaps to the start of LtaA[44]. Expression of YpfP in *E.coli* produced Glc_2-DAG and triglucosyl-diacylglycerol (Glc_3-DAG)[212], while co-expression of LtaA and YpfP only produced Glc_2-DAG[44,212], indicating a function of LtaA in regulating the number of sugars added by YpfP. Thus, we assumed that there might be physical contacts between LtaA and

YpfP. A pull-down assay can be carried out first to see if there are interactions. To further clarify it, LtaA and YpfP can be co-purified, followed by the crystallography or cryo-EM study.

Abbreviations

3D	three-dimensional
Å	Angstrom(s)
ATP	adenosine triphosphate
ABC transporters	ATP-binding cassette transporters
CAMPs	cationic antimicrobial peptides
c-di-AMP	cyclic-di-adenosine monophosphate
DAG	diacylglycerol
Glc_2-DAG	diglucosyl-diacylglycerol
E. coli	*Escherichia coli*
et al.	et alia
etc.	et cetera
LPS	lipopolysaccharide
LTA	lipoteichoic acids
LtaA	lipoteichoic acid protein A
MFS	major facilitator superfamily
MRSA	methicillin-resistant *S. aureus*
NBDs	nucleotide-binding domains
PDB	protein data base
PG	peptidoglycan
PBPs	penicillin-binding proteins
S.aureus	*Staphylococcus aureus*
TM	transmembrane
TMDs	transmembrane domains
TMs	transmembrane helices
TLR2	Toll-like receptors 2
UDP-Glc	uridine diphosphate glucose
Und-PP	undecaprenol pyrophosphate
VRSA	vancomycin-resistant *S. aureus*
WTA	wall teichoic acids
WT	wildtype
µm	micro meter

Amino acid	One-letter code	Three-letter code
Alanine	A	Ala
Aspartate	D	Asp
Cysteine	C	Cys
Glutamate	E	Glu
Phenylalanine	F	Phe
Glycine	G	Gly
Histidine	H	His
Isoleucine	I	Ile
Lysine	K	Lys
Leucine	L	Leu
Methionine	M	Met
Asparagine	N	Asn
Proline	P	Pro
Glutamine	Q	Gln
Arginine	R	Arg
Serine	S	Ser
Threonine	T	Thr
Valine	V	Val
Tryptophan	W	Trp
Tyrosine	Y	Tyr

References

1. Götz, F., Bannerman, T. & Karl-Heinz, S. *The genera staphylococcus and macrococcus*. *Prokaryotes* (2006). doi:10.1007/0-387-30744-3
2. Xia, G., Kohler, T. & Peschel, A. The wall teichoic acid and lipoteichoic acid polymers of Staphylococcus aureus. *Int. J. Med. Microbiol.* **300**, 148–154 (2010).
3. Ogston, A. 'On Abscesses'. *Clin. Infect. Dis.* **6**, 122–128 (1984).
4. Wertheim, H. F. L. *et al.* The role of nasal carriage in Staphylococcus aureus infections. *Lancet Infect. Dis.* **5**, 751–762 (2005).
5. Lowy, F. staphylococcus aureus infections. *N. Engl. J. Med.* **339**, 520–532 (1998).
6. Toshkova, K., Annemuller, C., Akineden, O. & Lammler, C. The significance of nasal carriage of Staphylococcus aureus as risk factor for human skin infections. *FEMS Microbioloy Lett.* **202**, 17–24 (2001).
7. Lee, A. S. *et al.* Methicillin-resistant Staphylococcus aureus. *Nat. Rev. Dis. Prim.* **4**, 1–23 (2018).
8. Turner, N. A. *et al.* Methicillin-resistant Staphylococcus aureus: an overview of basic and clinical research. *Nat. Rev. Microbiol.* **17**, 203–218 (2019).
9. Arciola, C. R., Campoccia, D. & Montanaro, L. Implant infections: Adhesion, biofilm formation and immune evasion. *Nat. Rev. Microbiol.* **16**, 397–409 (2018).
10. Tong, S. Y. C., Davis, J. S., Eichenberger, E., Holland, T. L. & Fowler, V. G. Staphylococcus aureus infections: Epidemiology, pathophysiology, clinical manifestations, and management. *Clin. Microbiol. Rev.* **28**, 603–661 (2015).
11. Boutin, C., Guerin, J. C., Viallat, J. R., Astoul, P. & Bejui-Thivolet, F. Methicillin-Resistant Staphylococcus aureus:AConsensus Review ofthe Microbiology, Pathogenesis, and Epidemiology With Implications for Prevention and Management. *Am. J. Med.* **94**, 81–97 (1992).
12. Weinstein, R. A. & Fridkin, S. K. Vancomycin-Intermediate and -Resistant Staphylococcus aureus: What the Infectious Disease Specialist Needs to Know. *Clin. Infect. Dis.* **32**, 108–115 (2001).
13. Livermore, D. M., Macgowan, A. P. & Wale, M. C. J. *Surveillance of antimicrobial resistance in Europe 2018*. *British Medical Journal* **317**, (2018).
14. Köck, R. *et al.* Methicillin-resistant Staphylococcus aureus (MRSA): Burden of disease and control challenges in Europe. *Eurosurveillance* **15**, 1–9 (2010).
15. Cassini, A. *et al.* Attributable deaths and disability-adjusted life-years caused by infections with antibiotic-resistant bacteria in the EU and the European Economic Area in 2015: a population-level modelling analysis. *Lancet Infect. Dis.* **19**, 56–66 (2019).
16. Bagnoli, F. & Rappuoli, R. *Staphylococcus aureus Microbiology, Pathology, Immunology, Therapy and Prophylaxis*. *Springer Nature* (2017). doi:10.1016/B978-0-12-386454-3.00539-X
17. Boudjemaa, R., Steenkeste, K., Canette, A., Briandet, R. & Marlière, C. Direct observation of the cell-wall remodeling in adhering Staphylococcus aureus 27217_ An AFM study supported by SEM and TEM. *Cell Surf.* **5**, 100018 (2019).
18. Joon, S., Chang, J. & Singh, M. Peptidoglycan architecture of Gram-positive bacteria by solid-state NMR. *Biochim. Biophys. Acta* **1848**, 350–362 (2015).
19. Silhavy, T. J., Kahne, D. & Walker, S. The Bacterial Cell Envelope. *Cold Spring Harb. Perspect. Biol.* **2**, a000414 (2010).
20. Neuhaus, F. C. & Baddiley, J. A Continuum of Anionic Charge : Structures and Functions of D -Alanyl-Teichoic Acids in Gram-Positive Bacteria. *Microbiol. Mol. Biol. Rev.* **67**, 686–723 (2003).
21. Arciola, C. R., Campoccia, D., Ravaioli, S. & Montanaro, L. Polysaccharide intercellular adhesin in biofilm : structural and regulatory aspects. *Front. celluar Infect. Microbiol.* **5**, 1–10 (2015).
22. Bagnoli, F. & Rappuoli, R. *Protein and Sugar Export and Assembly in Bacteria*. (2017).

23. Bush, K. & Bradford, P. A. b -Lactams and b -Lactamase Inhibitors: An Overview. *Cold Spring Harb. Perspect. Med.* (2016).
24. Fleming, A. On the antibacterial action of cultures of a penicillium, with special reference to their use in the isolation of B. influenzae. *Br. J. Exp. Pathol.* **10**, 226 (1929).
25. Hiramatsu, K. Vancomycin-resistant Staphylococcus aureus : a new model of antibiotic. *Lancet Infect. Dis.* **1**, 147–155 (2001).
26. Walsh, C. Molecular mechanisms that confer antibacterial drug resistance. *Nature* **406**, 775–781 (2000).
27. Hartman, B. J. & Tomasz, A. Low-Affinity Penicillin-Binding Protein Associated with β-Lactam Resistance in Staphylococcus aureus. *J. Bacteriol.* **158**, 513–516 (1984).
28. Kim, C. *et al.* Properties of a Novel PBP2A Protein Homolog from Staphylococcus aureus Strain LGA251 and Its Contribution to the -Lactam-resistant Phenotype * □. *J. Biol. Chem.* **287**, 36854–36863 (2012).
29. Rubinstein, E. & Keynan, Y. Vancomycin revisited - 60 years later. *Front. Public Heal.* **2**, 1–7 (2014).
30. Cong, Y., Yang, S. & Rao, X. Vancomycin resistant Staphylococcus aureus infections : A review of case updating and clinical features. *J. Adv. Res.* **21**, 169–176 (2020).
31. Hu, Q., Peng, H. & Rao, X. Molecular Events for Promotion of Vancomycin Resistance in Vancomycin Intermediate Staphylococcus aureus. *Front. Microbiolgy* **7**, (2016).
32. Armstrong, J. J., Baddiley, J., Buchanan, J. G., Carss, B. & Greenberg, G. R. Isolation and structure of ribitol phosphate derivatives (teichoic acids) from bacterial cell walls. *J. Chem. Soc.* (1958).
33. Percy, M. G. & Gr, A. Lipoteichoic Acid Synthesis and Function in Gram-Positive Bacteria. *Annu. Rev. Microbiol.* **68**, 81–100 (2014).
34. Fischer, W. Lipoteichoic acid and lipids in the membrane of Staphylococcus aureus. *Med. Microbiol. Immunol.* **183**, 61–76 (1994).
35. Fischer, W. *Physiology of Lipoteichoic Acids in Bacteria*. *Advances in Microbial Physiology* **29**, (1988).
36. Schneewind, O. & Missiakas, D. Lipoteichoic Acids, Phosphate-Containing Polymers in the Envelope of Gram-Positive Bacteria. *J. Bacteriol.* **196**, (2014).
37. KOCH, H. U., HAAS, R. & FISCHER, W. The role of lipoteichoic acid biosynthesis in membrane lipid metabolism of growing Staphylococcus aureus. *Eur. J. Biochem.* **138**, 357–363 (1984).
38. Duckworth, M., Archibald, A. R. & Baddiley, J. Lipoteichoic acid and lipoteichoic acid carrier in Staphylococcus aureus H. *FEBS Lett.* **53**, 176–179 (1975).
39. Kho, K. & Meredith, T. C. Salt-Induced Stress Stimulates a Lipoteichoic Acid-Specific Three-Component Glycosylation System in Staphylococcus aureus. *J. Bacteriol.* **200**, 1–16 (2018).
40. Weidenmaier, C. & Peschel, A. Teichoic acids and related cell-wall glycopolymers in Gram-positive physiology and host interactions. *Nat. Rev. Microbiol.* **6**, 276 (2008).
41. Fournier, B. & Philpott, D. J. Recognition of Staphylococcus aureus by the Innate Immune System. *Clin. Microbiol. Rev.* **18**, 521–540 (2005).
42. Young, S. A., Desbois, A. P., Coote, P. J. & Smith, T. K. Characterisation of Staphylococcus aureus lipids by nanoelectrospray ionisation tandem mass spectrometry (nESI-MS/MS). *bioRxiv* 593483 (2019). doi:10.1101/593483
43. Schneewind, O. & Missiakas, D. Lipoteichioc Acid Synthesis and Function in Gram-Positive Bacteria. in *Biogenesis of Fatty Acids, Lipids and Membranes* 1–18 (2017). doi:10.1007/978-3-319-43676-0
44. Gründling, A. & Schneewind, O. Genes required for glycolipid synthesis and lipoteichoic acid anchoring in Staphylococcus aureus. *J. Bacteriol.* **189**, 2521–2530 (2007).
45. Kiriukhin, M. Y., Debabov, D. V., Shinabarger, D. L. & Neuhaus, F. C. Biosynthesis of the glycolipid anchor in lipoteichoic acid of Staphylococcus aureus RN4220: Role of YpfP, the diglucosyldiacylglycerol synthase. *J. Bacteriol.* **183**, 3506–3514 (2001).
46. Lu, D. *et al.* Structure-based mechanism of lipoteichoic acid synthesis by Staphylococcus aureus LtaS. *Proc. Natl. Acad. Sci.* **106**, 1584–1589 (2009).
47. Grundling, A. & Schneewind, O. Synthesis of glycerol phosphate lipoteichoic acid in Staphylococcus

aureus. *Proc. Natl. Acad. Sci.* **104**, 8478–8483 (2007).
48. Taron, D. J., Childs, W. C. & Neuhaus, F. C. Biosynthesis of D-alanyl-lipoteichoic acid: Role of diglyceride kinase in the synthesis of phosphatidylglycerol for chain elongation. *J. Bacteriol.* **154**, 1110–1116 (1983).
49. Fischer, W. & P, R. The alanine ester substitution of lipoteichoic acid (lta) in Staphylococcus aureus. *FEBS Lett.* **119**, 224–226 (1980).
50. Neuhaus, F. C. & Baddiley, J. A Continuum of Anionic Charge: Structures and Functions of D-Alanyl-Teichoic Acids in Gram-Positive Bacteria. *Microbiol. Mol. Biol. Rev.* **67**, 686–723 (2003).
51. Percy, M. G. & Gründling, A. Lipoteichoic Acid Synthesis and Function in Gram-Positive Bacteria. *Annu. Rev. Microbiol.* **68**, 81–100 (2014).
52. Oku, Y. *et al.* Pleiotropic roles of polyglycerolphosphate synthase of lipoteichoic acid in growth of Staphylococcus aureus cells. *J. Bacteriol.* **91**, 141–151 (2009).
53. Corrigan, R. M., Abbott, J. C., Burhenne, H., Kaever, V. & Gründling, A. C-di-amp is a new second messenger in staphylococcus aureus with a role in controlling cell size and envelope stress. *PLoS Pathog.* **7**, (2011).
54. Karinou, E., Schuster, C. F., Pazos, M., Vollmer, W. & Gründling, A. Inactivation of the monofunctional peptidoglycan glycosyltransferase sgtb allows staphylococcus aureus to survive in the absence of lipoteichoic acid. *J. Bacteriol.* **201**, 1–18 (2019).
55. Hesser, A. R., Matano, L. M., Vickery, C. R. & Wood, B. M. The length of lipoteichoic acid polymers controls Staphylococcus aureus cell size and envelope integrity. *bioRxiv* 1–38 (2020).
56. Yamada, S. *et al.* An autolysin ring associated with cell separation of Staphylococcus aureus. *J. Bacteriol.* **178**, 1565–1571 (1996).
57. Lutkenhaus, J., Pichoff, S. & Du, S. Bacterial cytokinesis: From Z ring to divisome. *Cytoskeleton* **69**, 778–790 (2012).
58. Schirner, K., Marles-Wright, J., Lewis, R. J. & Errington, J. Distinct and essential morphogenic functions for wall- and lipo-teichoic acids in Bacillus subtilis. *EMBO J.* **28**, 830–842 (2009).
59. Bæk, K. T. *et al.* The Cell Wall Polymer Lipoteichoic Acid Becomes Nonessential in Staphylococcus aureus Cells Lacking the ClpX Chaperone. *MBio* **7**, 1–11 (2016).
60. Zoll, S. *et al.* Ligand-binding properties and conformational dynamics of autolysin repeat domains in staphylococcal cell wall recognition. *J. Bacteriol.* **194**, 3789–3802 (2012).
61. Fedtke, I. *et al.* A Staphylococcus aureus ypfP mutant with strongly reduced lipoteichoic acid (LTA) content: LTA governs bacterial surface properties and autolysin activity. *Mol. Microbiol.* **65**, 1078–1091 (2007).
62. Bierbaum, G. & Sahl, H. Autolytic System of Staphylococcus simulans 22 : Influence of Cationic Peptides on Activity of N-Acetylmuramoyl- L-Alanine Amidase. *J. Bacteriol.* **169**, 5452–5458 (1987).
63. Lambert, B. P. A., Hancock, I. A. N. C. & Baddiley, J. Influence of Alanyl Ester Residues on the Binding of Magnesium Ions to Teichoic Acids. *Biochem. J.* 671–676 (1975).
64. Peschel, A., Vuong, C., Otto, M. & Götz, F. The D -Alanine Residues of Staphylococcus aureus Teichoic Acids Alter the Susceptibility to Vancomycin and the Activity of Autolytic Enzymes. *Antimicrob. Agents Chemother.* **44**, 2845–2847 (2000).
65. Akira, S., Uematsu, S. & Takeuchi, O. Pathogen recognition and innate immunity. *Cell* **124**, 783–801 (2006).
66. Takeuchi, O. & Akira, S. Pattern Recognition Receptors and Inflammation. *Cell* **140**, 805–820 (2010).
67. Takeda, K., Kaisho, T. & Akira, S. Toll-like receptors. *Annu. Rev. Immunol.* **21**, 335–376 (2003).
68. Morath, S. *et al.* Lipoteichoic Acid (LTA) of Streptococcus pneumoniae and Staphylococcus aureus Activates Immune Cells via Toll-like Receptor (TLR) -2 , Lipopolysaccharide-binding Protein (LBP), and CD14 , whereas TLR-4 and MD-2 Are Not Involved *. *J. Biol. Chem.* **278**, 15587–15594 (2003).
69. Nilsen, N. J. *et al.* Cellular trafficking of lipoteichoic acid and Toll-like receptor 2 in relation to signaling; role of CD14 and CD36. *J. Leukoc. Biol.* **84**, 280–291 (2008).

70. Morath, B. S., Geyer, A. & Hartung, T. Structure – Function Relationship of Cytokine Induction by Lipoteichoic Acid from Staphylococcus aureus. *J. Exp. Med.* **193**, 393–397 (2001).
71. Lynch, N. J. *et al.* L-Ficolin Specifically Binds to Lipoteichoic Acid, a Cell Wall Constituent of Gram-Positive Bacteria, and Activates the Lectin Pathway of Complement. *J. Immunol.* **172**, 1198–1202 (2004).
72. Greenberg, J. W., Fischer, W. & Joiner, K. A. Influence of lipoteichoic acid structure on recognition by the macrophage scavenger receptor. *Infect. Immun.* **64**, 3318–3325 (1996).
73. Hoebe, K. *et al.* CD36 is a sensor of diacylglycerides. *Nature* **433**, 523–527 (2005).
74. Naclerio, G. A., Onyedibe, K. I. & Sintim, H. O. Lipoteichoic acid biosynthesis inhibitors as potent inhibitors of S. Aureus and E. Faecalis Growth and Biofilm Formation. *Molecules* **25**, (2020).
75. Sheen, T. R. *et al.* Penetration of the blood – brain barrier by Staphylococcus aureus : contribution of membrane-anchored lipoteichoic acid. *J Mol Med* **88**, 633–639 (2010).
76. Flemming, H. C. *et al.* Biofilms: An emergent form of bacterial life. *Nat. Rev. Microbiol.* **14**, 563–575 (2016).
77. Scherr, T. D. *et al.* Staphylococcus aureus Biofilms Induce Macrophage Dysfunction Through Leukocidin AB and Alpha-Toxin. *MBio* **6**, e01021-15 (2015).
78. Savage, V. J., Chopra, I. & O'Neill, A. J. Staphylococcus aureus biofilms promote horizontal transfer of antibiotic resistance. *Antimicrob. Agents Chemother.* **57**, 1968–1970 (2013).
79. Peschel, A. *et al.* Inactivation of the dlt Operon in Staphylococcus aureus Confers Sensitivity to Defensins , Protegrins , and Other Antimicrobial Peptides *. *J. Biol. Chem.* **274**, 8405–8410 (1999).
80. Oku, Y. *et al.* Pleiotropic Roles of Polyglycerolphosphate Synthase of Lipoteichoic Acid in Growth of Staphylococcus aureus Cells. *J. Bacteriol.* **191**, 141–151 (2009).
81. Fischer, W., Koch, H. U., Rosel, P., Fiedler, F. & Schmuck, L. Structural Requirements of Lipoteichoic Acid Carrier for Recognition by the Poly (ribitol Phosphate) Polymerase from Staphylococcus aureus H. *J. Biol. Chem.* **255**, 4550–4556 (1980).
82. Joo, H. & Otto, M. Mechanisms of resistance to antimicrobial peptides in staphylococci. *Biochim Biophys Acta.* **1848**, 3055–3061 (2016).
83. Coe, K. A. *et al.* Multi-strain Tn-Seq reveals common daptomycin resistance determinants in Staphylococcus aureus. *PLoS Pathog.* 1–25 (2019).
84. Pader, V. *et al.* Staphylococcus aureus inactivates daptomycin by releasing membrane phospholipids. *Nat. Microbiol.* **16194**, (2016).
85. Richter, S. G. *et al.* Small molecule inhibitor of lipoteichoic acid synthesis is an antibiotic for Gram-positive bacteria. *Proc. Natl. Acad. Sci. U. S. A.* **110**, 3531–3536 (2013).
86. Naclerio, G. A., Karanja, C. W., Opoku-Temeng, C. & Sintim, H. O. Antibacterial Small Molecules That Potently Inhibit Staphylococcus aureus Lipoteichoic Acid Biosynthesis. *ChemMedChem* **14**, 1000–1004 (2019).
87. Weisman, L. E. *et al.* A randomized study of a monoclonal antibody (pagibaximab) to prevent staphylococcal sepsis. *Pediatrics* **128**, 271–279 (2011).
88. Chen, Q. *et al.* Novel Synthetic (Poly)Glycerolphosphate-Based Antistaphylococcal Conjugate Vaccine. *Infect. Immun.* **81**, 2554–2561 (2013).
89. Yi, X. *et al.* Immunization with a peptide mimicking Lipoteichoic acid protects mice against Staphylococcus aureus infection. *Vaccine* **37**, 4325–4335 (2019).
90. Theilacker, C. *et al.* Protection Against Staphylococcus aureus by Antibody to the Polyglycerolphosphate Backbone of Heterologous Lipoteichoic Acid. *J. Infect. Dis.* **205**, (2012).
91. Simons, K. & Vaz, W. L. C. Model systems, lipid rafts, and cell membranes. *Annu. Rev. Biophys. Biomol. Struct.* **33**, 269–295 (2004).
92. Mitchell, P. Translocations Through Natural Membranes. *Adv. Enzymol. Relat. Areas Mol. Biol.* **29**, 33–87 (1976).
93. Saier, M. H. A Functional-Phylogenetic Classification System for Transmembrane Solute Transporters.

Microbiol. Mol. Biol. Rev. **64**, 354–411 (2000).
94. Shi, Y. Common Folds and Transport Mechanisms of Secondary Active Transporters. *Annu. Rev. Biophys.* **42**, 51–72 (2013).
95. Dimroth, P. Primary sodium ion translocating enzymes. *Biochim. Biophys. Acta - Bioenerg.* **1318**, 11–51 (1997).
96. Mitchell, P. & Moyle, J. Respiration-driven proton translocation in rat liver mitochondria. *Biochem. J.* **105**, 1147–1162 (1967).
97. Maloney, P. C. Bacterial transporters. *Curr. Opin. Cell Biol.* **6**, 571–582 (1994).
98. Law, C. J., Maloney, P. C. & Wang, D.-N. Ins and Outs of Major Facilitator Superfamily Antiporters. *Annu. Rev. Microbiol.* **62**, 289–305 (2008).
99. De Carvalho, C. C. C. R. & Caramujo, M. J. The various roles of fatty acids. *Molecules* **23**, (2018).
100. Liston, S. D., Mann, E. & Whitfield, C. Glycolipid substrates for ABC transporters required for the assembly of bacterial cell-envelope and cell-surface glycoconjugates. *Biochim. Biophys. Acta - Mol. Cell Biol. Lipids* **1862**, 1394–1403 (2017).
101. Kleinfeld, A. M., Chu, P. & Romero, C. Transport of long-chain native fatty acids across lipid bilayer membranes indicates that transbilayer flip-flop is rate limiting. *Biochemistry* **36**, 14146–14158 (1997).
102. Locher, K. P. Mechanistic diversity in ATP-binding cassette (ABC) transporters. *Nat. Struct. Mol. Biol.* **23**, 487–493 (2016).
103. Ward, A., Reyes, C. L., Yu, J., Roth, C. B. & Chang, G. Flexibility in the ABC transporter MsbA: Alternating access with a twist. *Proc. Natl. Acad. Sci. U. S. A.* **104**, 19005–19010 (2007).
104. Perez, C. *et al.* Structure and mechanism of an active lipid-linked oligosaccharide flippase. *Nature* **524**, 433–438 (2015).
105. Bi, Y. & Zimmer, J. Structure and Ligand-Binding Properties of the O Antigen ABC Transporter Carbohydrate-Binding Domain. *Structure* **28**, 252-258.e2 (2020).
106. Bi, Y., Mann, E., Whitfield, C. & Zimmer, J. Architecture of a channel-forming O-antigen polysaccharide ABC transporter. *Nature* (2018). doi:10.1038/nature25190
107. Chen, L. *et al.* Cryo-electron microscopy structure and transport mechanism of a wall teichoic acid ABC transporter. *MBio* **11**, 1–13 (2020).
108. Mi, W. *et al.* Article Structural basis of MsbA-mediated lipopolysaccharide transport. *Nat. Publ. Gr.* **549**, 233–237 (2017).
109. Padayatti, P. S. *et al.* Structural Insights into the Lipid A Transport Pathway in MsbA. *Struct. Des.* **27**, 1114-1123.e3 (2019).
110. Caffalette, C. A., Kuklewicz, J., Spellmon, N. & Zimmer, J. Biosynthesis and Export of Bacterial Glycolipids. *Annu. Rev. Biochem.* **89**, 741–768 (2020).
111. Kuk, A. C. Y., Mashalidis, E. H. & Lee, S. Y. Crystal structure of the MOP flippase MurJ in an inward-facing conformation. *Nat. Struct. Mol. Biol.* **24**, 171–176 (2017).
112. Hao, A., Guan, Z. & Lee, S. Visualizing conformation transitions of the Lipid II fl ippase MurJ. *Nat. Commun.* doi:10.1038/s41467-019-09658-0
113. Rubino, F. A., Kumar, S., Ruiz, N., Walker, S. & Kahne, D. E. Membrane Potential Is Required for MurJ Function. *J. Am. Chem. Soc.* **140**, 4481–4484 (2018).
114. Bi, Y., Mann, E., Whitfield, C. & Zimmer, J. Architecture of a channel-forming O-antigen polysaccharide ABC transporter. *Nature* **553**, 361–365 (2018).
115. Finn, R. D., Mistry, J., Schuster-Bockler, B. & Griffiths-Jones, S. Pfam: clans, web tools and services. *Nucleic Acids Res.* **34**, D247–D251 (2006).
116. Saier, M. H. *et al.* The Transporter Classification Database (TCDB): Recent advances. *Nucleic Acids Res.* **44**, D372–D379 (2016).
117. Henderson, P. J. F. Proton-linked sugar transport systems in bacteria. *J. Bioenerg. Biomembr.* **22**, 525–569 (1990).
118. Marger, M. D. & Saier, M. H. A major superfamily of transmembrane facilitators that catalyse uniport,

symport and antiport. *Trends Biochem. Sci.* **18**, 13–20 (1993).
119. Reddy, V. S., Shlykov, M. A., Castillo, R., Sun, E. I. & Saier, M. H. The major facilitator superfamily (MFS) revisited. *FEBS J.* **279**, 2022–2035 (2012).
120. Yan, N. Structural Biology of the Major Facilitator Superfamily Transporters. *Annu. Rev. Biophys.* **44**, 257–283 (2015).
121. Yan, N. Structural advances for the major facilitator superfamily (MFS) transporters. *Trends Biochem. Sci.* **38**, 151–159 (2013).
122. Quistgaard, E. M., Löw, C., Guettou, F. & Nordlund, P. Understanding transport by the major facilitator superfamily (MFS): Structures pave the way. *Nat. Rev. Mol. Cell Biol.* **17**, 123–132 (2016).
123. Henderson, P. J. F. The 12-transmembrane helix transporters. *Curr. Opin. Cell Biol.* **5**, 708–721 (1993).
124. Chang, A. B., Lin, R., Studley, W. K., Tran, C. V. & Saier, M. H. Phylogeny as a guide to structure and function of membrane transport proteins. *Mol. Membr. Biol.* **21**, 171–181 (2004).
125. Saier, M. H. *et al.* The major facilitator superfamily. *J. Mol. Microbiol. Biotechnol.* **1**, 257–279 (1999).
126. Paulsen, I. T., Brown, M. H. & Skurray, R. A. Proton-dependent multidrug efflux systems. *Microbiol. Rev.* **60**, 575–608 (1996).
127. Zhao, Y. *et al.* Substrate-bound structure of the E. coli multidrug resistance transporter MdfA. *Cell Res.* **25**, 1060–1073 (2015).
128. Kakarla, P., KC, R., Shrestha, U. & Ranaweera, I. Functional Roles of Highly Conserved Amino Acid Sequence Motifs A and C in Solute Transporters of the Major Facilitator Superfamily. in *Drug Resistance in Bacteria, Fungi, Malaria, and Cancer* 1–629 (2017). doi:10.1007/978-3-319-48683-3
129. Pasrija, R., Banerjee, D. & Prasad, R. Structure and function analysis of CaMdr1p, a major facilitator superfamily antifungal efflux transporter protein of Candida albicans: Identification of amino acid residues critical for drug/H+ transport. *Eukaryot. Cell* **6**, 443–453 (2007).
130. Abramson, J. *et al.* Structure and Mechanism of the Lactose Permease of Escherichia coli. *Science (80-.).* **301**, 610–615 (2003).
131. Huang, Y., Lemieux, M. J., Song, J., Auer, M. & Wang, D. Structure and Mechanism of the Glycerol-3-Phosphate Transporter from Escherichia coli. *Science (80-.).* **301**, 616–621 (2003).
132. Dang, S. *et al.* Structure of a fucose transporter in an outward-open conformation. *Nature* **467**, 734–738 (2010).
133. Ethayathulla, A. S. *et al.* Structure-based mechanism for Na + / melibiose symport by MelB. *Nat. Commun.* (2014). doi:10.1038/ncomms4009
134. Sun, L. *et al.* Crystal structure of a bacterial homologue of glucose transporters GLUT1-4. *Nature* **490**, 361–366 (2012).
135. Iancu, C. V, Zamoon, J., Bum, S., Aleshin, A. & Choe, J. Crystal structure of a glucose / H + symporter and its mechanism of action. *Proc Natl Acad Sci* **110**, 17862–17867 (2013).
136. Deng, D. *et al.* Crystal structure of the human glucose transporter GLUT1. *Nature* **510**, 121–125 (2014).
137. Deng, D. *et al.* Molecular basis of ligand recognition and transport by glucose transporters. *Nature* **526**, 391–396 (2015).
138. Nomura, N. *et al.* Structure and mechanism of the mammalian fructose transporter GLUT5. *Nature* **526**, 397–401 (2015).
139. Paulsen, P. A., Custódio, T. F. & Pedersen, B. P. Crystal structure of the plant symporter STP10 illuminates sugar uptake mechanism in monosaccharide transporter superfamily. *Nat. Commun.* **10**, (2019).
140. Qureshi, A. A. *et al.* The molecular basis for sugar import in malaria parasites. *Nature* **578**, 321–325 (2020).
141. Newstead, S. *et al.* Crystal structure of a prokaryotic homologue of the mammalian oligopeptide – proton symporters ,. *EMBO J.* **30**, 417–426 (2010).
142. Solcan, N. *et al.* Alternating access mechanism in the POT family of oligopeptide transporters. *EMBO J.* **31**, 3411–3421 (2012).

143. Doki, S. *et al.* Structural basis for dynamic mechanism of proton-coupled symport by the peptide transporter POT. *Proc. Natl. Acad. Sci. U. S. A.* **110**, 11343–11348 (2013).
144. Zhao, Y. *et al.* Crystal structure of the E. coli peptide transporter YbgH. *Structure* **22**, 1152–1160 (2014).
145. Boggavarapu, R., Jeckelmann, J. M., Harder, D., Ucurum, Z. & Fotiadis, D. Role of electrostatic interactions for ligand recognition and specificity of peptide transporters. *BMC Biol.* **13**, 1–10 (2015).
146. Parker, J. L. *et al.* Proton movement and coupling in the POT family of peptide transporters. *Proc. Natl. Acad. Sci. U. S. A.* **114**, 13182–13187 (2017).
147. Minhas, G., Bawdon, D., Herman, R. & Rudden, M. Structural basis of malodour precursor transport in the human axilla. *Elife* **7**, (2018).
148. Yin, Y., He, X., Szewczyk, P., Nguyen, T. & Chang, G. Structure of the Multidrug Transporter EmrD from Escherichia coli. *Science (80-.).* **741**, 741–744 (2011).
149. Jiang, D. *et al.* Structure of the YajR transporter suggests a transport mechanism based on the conserved motif A. *Proc. Natl. Acad. Sci. U. S. A.* **110**, 14664–14669 (2013).
150. Pedersen, B. P. *et al.* Crystal structure of a eukaryotic phosphate transporter. *Nature* **496**, 533–536 (2013).
151. Yan, H. *et al.* Structure and Mechanism of a Nitrate Transporter. *Cell Rep.* **3**, 716–723 (2013).
152. Zheng, H., Wisedchaisri, G. & Gonen, T. Crystal structure of a nitrate/nitrite exchanger. *Nature* **497**, 647–651 (2013).
153. Parker, J. L. & Newstead, S. Molecular basis of nitrate uptake by the plant nitrate transporter NRT1.1. *Nature* **507**, 68–72 (2014).
154. Taniguchi, R. *et al.* Outward-and inward-facing structures of a putative bacterial transition-metal transporter with homology to ferroportin. *Nat. Commun.* **6**, 1–10 (2015).
155. Hvorup, R. N. & Jr, M. H. S. Sequence similarity between the channel- forming domains of voltage-gated ion channel proteins and the C- terminal domains of secondary carriers of the major facilitator superfamily. *Microbiology* **148**, 3755–3756 (2002).
156. Yan, N. Structural investigation of the proton-coupled secondary transporters. *Curr. Opin. Struct. Biol.* **23**, 483–491 (2013).
157. Guettou, F. *et al.* Selectivity mechanism of a bacterial homolog of the human drug-peptide transporters PepT1 and PepT2. *Nat. Struct. Mol. Biol.* **21**, 728–731 (2014).
158. Martinez Molledo, M., Quistgaard, E. M., Flayhan, A., Pieprzyk, J. & Löw, C. Multispecific Substrate Recognition in a Proton-Dependent Oligopeptide Transporter. *Structure* **26**, 467-476.e4 (2018).
159. Fukuda, M. *et al.* Structural basis for dynamic mechanism of nitrate/nitrite antiport by NarK. *Nat. Commun.* **6**, 1–12 (2015).
160. Zhao, Y. *et al.* Substrate-bound structure of the E. coli multidrug resistance transporter MdfA. *Cell Res.* **25**, 1060–1073 (2015).
161. Wisedchaisri, G., Park, M., Iadanza, M. G., Zheng, H. & Gonen, T. Proton-coupled sugar transport in the prototypical major facilitator superfamily protein XylE. *Nat. Commun.* **5**, 1–11 (2014).
162. Du, D. *et al.* Multidrug efflux pumps: structure, function and regulation. *Nat. Rev. Microbiol.* **16**, 523–539 (2018).
163. Newstead, S. *et al.* Crystal structure of a prokaryotic homologue of the mammalian oligopeptide-proton symporters, PepT1 and PepT2. *EMBO J.* **30**, 417–426 (2011).
164. Mirza, O., Guan, L., Verner, G., Iwata, S. & Kaback, H. R. Structural evidence for induced fit and a mechanism for sugar/H+ symport in LacY. *EMBO J.* **25**, 1177–1183 (2006).
165. Kumar, H., Kasho, V., Smirnova, I., Finer-moore, J. S. & Kaback, H. R. Structure of sugar-bound LacY. *Proc Natl Acad Sci* **111**, 1784–1788 (2013).
166. Grytsyk, N., Sugihara, J., Kaback, H. R. & Hellwig, P. pKa of Glu325 in LacY. *Proc. Natl. Acad. Sci. U. S. A.* **114**, 1530–1535 (2017).
167. Grytsyk, N., Seiça, A. F. S., Sugihara, J., Kaback, H. R. & Hellwig, P. Arg302 governs the pK a of Glu325 in LacY. *Proc. Natl. Acad. Sci. U. S. A.* **116**, 4934–4939 (2019).

168. Drew, D. & Boudker, O. Shared Molecular Mechanisms of Membrane Transporters. *Annu. Rev. Biochem.* **85**, 543–572 (2016).
169. Abramson, J. *et al.* Structure and mechanism of the lactose permease of Escherichia coli. *Science (80-.).* **301**, 610–615 (2003).
170. Kumar, H., Finer-moore, J. S., Kaback, H. R. & Stroud, R. M. Structure of LacY with an α -substituted galactoside : Connecting the binding site to the protonation site. *Proc Natl Acad Sci* **112**, 9004–9009 (2015).
171. Kumar, H. *et al.* Crystal structure of a ligand-bound LacY–Nanobody complex. *Proc. Natl. Acad. Sci. U. S. A.* **115**, 8769–8774 (2018).
172. Jiang, X. *et al.* Crystal structure of a LacY-nanobody complex in a periplasmic-open conformation. *Proc. Natl. Acad. Sci. U. S. A.* **113**, 12420–12425 (2016).
173. Sun, L. *et al.* Crystal structure of a bacterial homologue of glucose transporters GLUT1-4. *Nature* **490**, 361–366 (2012).
174. Quistgaard, E. M., Löw, C., Moberg, P., Trésaugues, L. & Nordlund, P. Structural basis for substrate transport in the GLUT-homology family of monosaccharide transporters. *Nat. Struct. Mol. Biol.* **20**, 766–769 (2013).
175. Andersson, M. *et al.* Proton-coupled dynamics in lactose permease. *Structure* **20**, 1893–1904 (2012).
176. Ethayathulla, A. S. *et al.* Structure-based mechanism for Na(+)/melibiose symport by MelB. *Nat. Commun.* **5**, 3009 (2014).
177. Heras, B. & Martin, J. L. Post-crystallization treatments for improving diffraction quality of protein crystals. *Acta Crystallogr. Sect. D Biol. Crystallogr.* **61**, 1173–1180 (2005).
178. Carson, M., Johnson, D. H., Mcdonald, H. & Lawrence, J. His-tag impact on structure research papers. *Acta Crystallogr. Sect. D Biol. Crystallogr.* **63**, 295–301 (2007).
179. Mohanty, A. K. & Wiener, M. C. Membrane protein expression and production: Effects of polyhistidine tag length and position. *Protein Expr. Purif.* **33**, 311–325 (2004).
180. Garman, E. F. & Schneider, T. R. Macromolecular Cryocrystallography. *J. Appl. Crystallogr.* **30**, 211–237 (1997).
181. Hanson, B. L., Schall, C. A. & Bunick, G. J. New techniques in macromolecular cryocrystallography : macromolecular crystal annealing and cryogenic helium. *J. Struct. Biol.* **142**, 77–87 (2009).
182. Kriminski, S., Caylor, C. L., Nonato, M. C., Finkelstein, K. D. & Thorne, R. E. Flash-cooling and annealing of protein crystals. *Acta Crystallogr. Sect. D Biol. Crystallogr.* **58**, 459–471 (2002).
183. Juers, D. H. *et al.* The impact of cryosolution thermal contraction on proteins and protein crystals: Volumes, conformation and order. *Acta Crystallogr. Sect. D Struct. Biol.* **74**, 922–938 (2018).
184. Hanson, B. L. & Bunick, G. J. Annealing macromolecular crystals. in *Methods in Molecular Biology* **364**, 31–41 (2007).
185. Harp, J. M., Timm, D. E. & Bunick, G. J. Macromolecular crystal annealing: Overcoming increased mosaicity associated with cryocrystallography. *Acta Crystallogr. Sect. D Biol. Crystallogr.* **54**, 622–628 (1998).
186. Stevenson, C. E. M., Mayer, S. M., Delarbre, L. & Lawson, D. M. Crystal annealing - Nothing to lose. *J. Cryst. Growth* **232**, 629–637 (2001).
187. Juers, D. H. & Matthews, B. W. Reversible lattice repacking illustrates the temperature dependence of macromolecular interactions. *J. Mol. Biol.* **311**, 851–862 (2001).
188. Dang, S. *et al.* Structure of a fucose transporter in an outward-open conformation. *Nature* **467**, 734–738 (2010).
189. Mirza, O., Guan, L., Verner, G., Iwata, S. & Kaback, H. R. Structural evidence for induced fit and a mechanism for sugar / H þ symport in LacY. *EMBO J.* **25**, 1177–1183 (2006).
190. Kumar, S., Rubino, F. A., Mendoza, A. G. & Ruiz, N. The bacterial lipid II flippase MurJ functions by an alternating-access mechanism. *J. Biol. Chem.* **294**, 981–990 (2019).
191. Zheng, S. *et al.* Structure and mutagenic analysis of the lipid II flippase MurJ from Escherichia coli. *Proc*

Natl Acad Sci 201802192 (2018). doi:10.1073/pnas.1802192115
192. England, R. J. A., Homer, J. J., Knight, L. C. & Ell, S. R. Nasal pH measurement: A reliable and repeatable parameter. *Clin. Otolaryngol. Allied Sci.* **24**, 67–68 (1999).
193. Lambers, H., Piessens, S., Bloem, A., Pronk, H. & Finkel, P. Natural skin surface pH is on average below 5, which is beneficial for its resident flora. *Int. J. Cosmet. Sci.* **28**, 359–370 (2006).
194. Flannagan, R. S., Kuiack, R. C., McGavin, M. J. & Heinrichs, D. E. Staphylococcus aureus uses the GraXRS regulatory system to sense and adapt to the acidified phagolysosome in macrophages. *MBio* **9**, 1–20 (2018).
195. Zhou, C. & Fey, P. D. The acid response network of Staphylococcus aureus. *Curr. Opin. Microbiol.* **55**, 67–73 (2020).
196. Clements, M. O. & Foster, S. J. Stress resistance in Staphylococcus aureus. *Trends Microbiol.* 458–462 (1999).
197. Jenul, C. & Horswill, A. R. Regulation of Staphylococcus aureus Virulence. in *Gram Positive Pathogens Third Edition* **6**, (2018).
198. Chan, P. A. N. F., Foster, S. J., Ingham, E. & Clements, M. O. The Staphylococcus aureus Alternative Sigma Factor B Controls the Environmental Stress Response but Not Starvation Survival or Pathogenicity in a Mouse Abscess Model. *J. Bacteriol.* **180**, 6082–6089 (1998).
199. Bowman, L., Zeden, M. S., Schuster, C. F., Kaever, V. & Gründling, A. New insights into the cyclic di-adenosine monophosphate (c-di-AMP) degradation pathway and the requirement of the cyclic dinucleotide for acid stress resistance in Staphylococcus aureu. *J. Biol. Chem.* **291**, 26970–26986 (2016).
200. Weinrick, B. *et al.* Effect of Mild Acid on Gene Expression in Staphylococcus aureus. *J. Bacteriol.* **186**, 8407–8423 (2004).
201. Zhou, C. *et al.* Urease is an essential component of the acid response network of Staphylococcus aureus and is required for a persistent murine kidney infection. *PLoS Pathog.* **15**, 1–23 (2019).
202. Yang, S. J., Dunman, P. M., Projan, S. J. & Bayles, K. W. Characterization of the Staphylococcus aureus CidR regulon: Elucidation of a novel role for acetoin metabolism in cell death and lysis. *Mol. Microbiol.* **60**, 458–468 (2006).
203. Haag, A. F. & Bagnoli, F. The Role of Two-Component Signal Transduction Systems in Staphylococcus aureus Virulence Regulation. in *Current Topics in Microbiology and Immunology* **409**, 145–198 (2017).
204. Grosser, M. R. *et al.* Genetic requirements for Staphylococcus aureus nitric oxide resistance and virulence. *PLoS Pathog.* **14**, 1–27 (2018).
205. Clements, M. O., Watson, S. P. & Foster, S. J. Characterization of the major superoxide dismutase of Staphylococcus aureus and its role in starvation survival, stress resistance, and pathogenicity. *J. Bacteriol.* **181**, 3898–3903 (1999).
206. Kim, H. *et al.* Structural Studies of Potassium Transport Protein KtrA Regulator of Conductance of K ⁺ (RCK) C Domain in Complex with Cyclic Diadenosine Monophosphate (c-di-AMP) *. *J. Biol. Chem.* **290**, 16393–16402 (2015).
207. Commichau, F. M., Gibhardt, J., Halbedel, S., Gundlach, J. & Stülke, J. Opinion A Delicate Connection : c-di-AMP Affects Cell Integrity by Controlling Osmolyte Transport. *Trends Microbiol.* **26**, 175–185 (2018).
208. Schuster, C. F. *et al.* The second messenger c-di-AMP inhibits the osmolyte uptake system OpuC in Staphylococcus aureus. *Sci. Signal.* **9**, 1–14 (2016).
209. Sabath, L. D., Wallace, S. J. & Gerstein, D. A. Suppression of Intrinsic Resistance to Methicillin and Other Penicillins in Staphylococcus aureus. *Antimicrobal agents Chemother.* **2**, 350–355 (1972).
210. Lemaire, S., Van Bambeke, F., Mingeot-Leclercq, M. P., Glupczynski, Y. & Tulkens, P. M. Role of acidic pH in the susceptibility of intraphagocytic methicillin-resistant Staphylococcus aureus strains to meropenem and cloxacillin. *Antimicrob. Agents Chemother.* **51**, 1627–1632 (2007).
211. Hewelt-Belka, W. *et al.* Untargeted Lipidomics Reveals Differences in the Lipid Pattern among Clinical Isolates of Staphylococcus aureus Resistant and Sensitive to Antibiotics. *J. Proteome Res.* **15**, 914–922

(2016).

212. Jorasch, P., Warnecke, D. C., Lindner, B., Zähringer, U. & Heinz, E. Novel processive and nonprocessive glycosyltransferases from Staphylococcus aureus and Arabidopsis thaliana synthesize glycoglycerolipids, glycophospholipids, glycosphingolipids and glycosylsterols. *Eur. J. Biochem.* **267**, 3770–3783 (2000).

Curriculum Vitae

Personal information

Surname	Zhang
Given name	Bing
Gender	Female
Date of Birth	15.01.1992
Place of Birth	Xianyang, Shaanxi Province, China

Education

University of Basel, Basel, Switzerland **08/2017-12/2020**

Ph.D. student in Structural biology and biophysics
Project: Structural and mechanistic insights of a proton-dependent lipid transporter involved in lipoteichoic acids biosynthesis

Xi'an Jiaotong University, Xi'an, China **09/2014 -07/2017**

M.E. in Biomedical Engineering**,** School of Life Science and Technology
Project I: Mechanisms of Action of Human beta-Defensin 3 in the Promotion of Cervical Cancer
Project II: Characterize surface targets of human defensin 5 on *Shigella flexneri* 2a

Xi'an Jiaotong University, Xi'an, China **09/2010 -07/2014**

B.E. in Biomedical Engineering, School of Life Science and Technology
Project: Design peptide inhibitor that targets the HPV16 E6-E6AP interaction

Conferences and Ph.D. retreats

Biozentrum Symposium 2020, Basel, Switzerland 2020
Oral talk and poster presentation:
Structure and mechanism of a pH-sensing lipid flippase

GRC and GRS: Mechanisms of Membrane Transport, New London, NH, US 2019
Oral talk at GRS and poster presentation:
Structure and mechanism of a cell wall teichoic acids flippase

7th Murnau Conference, Murnau, Gemany 2018

Biozentrum Symposium 2018, Basel, Switzerland 2018
Poster presentation: Mechanism of lipoteichoic acids assembly *in Staphylococcus aureus*

10th Ph.D. retreat, Engelberg, Switzerland 2017
Poster presentation: Mechanism of lipoteichoic acids assembly *in Staphylococcus aureus*

Publications

[1] **Zhang, B.*,** Liu, X.*, Lambert, E.*, Mas, G., Hiller, S., Veening, J. W., & Perez, C. (2020). Structure of a proton-dependent lipid transporter involved in lipoteichoic acids biosynthesis. *Nature Structural & Molecular Biology*, 27(6), 561-569.

[2] **Zhang, B.**, & Perez, C. (2020). Stabilization and crystallization of a membrane protein involved in lipid transport. In *Expression, Purification, and Structural Biology of Membrane Proteins* (pp. 283-292). Humana, New York, NY.

[3] Xu, D.*, **Zhang, B.***, Liao, C., Zhang, W., Wang, W., Chang, Y., & Shao, Y. (2016). Human beta-defensin 3 contributes to the carcinogenesis of cervical cancer via activation of NF-κB signaling. Oncotarget, 7(46), 75902.

[4] Liao, C., Fang, K., Xiao, J., Zhang, W., **Zhang, B.**, Yuan, W., ... & Xu, D. (2019). Critical determinants of human neutrophil peptide 1 for enhancing host epithelial adhesion of *Shigella flexneri*. Cellular Microbiology, 21(10), e13069.

[5] Xu, D.*, Liao, C.*, **Zhang, B.**, Tolbert, W. D., He, W., Dai, Z., ... & Yu, J. (2018). Human enteric α-defensin 5 promotes *Shigella* infection by enhancing bacterial adhesion and invasion. Immunity, 48(6), 1233-1244.

[6] Xu, D.*, Zhang, W.*, **Zhang, B.**, Liao, C., & Shao, Y. (2016). Characterization of a biofilm-forming Shigella flexneri phenotype due to deficiency in Hep biosynthesis. PeerJ, 4, e2178.

* shared authorship

[1] and [2] are academic achievements during the Ph.D. stage